ISSN 1000-9620

Marine Science Bulletin

海洋通报

Volume 8 • Number 1 2006

ISSN 1000-9620

NATIONAL MARINE DATA AND
INFORMATION SERVICE OF CHINA

MARINE SCIENCE BULLETIN

Vol.8 No.1 May, 2006

LIBRARY
Pacific Islands Fisheries Science Center
NOAA Fisheries
Honolulu, Hawai'i

CONTENTS

Deep-sea Pollen Record during 3.0 - 2.0 Ma B.P. from ODP Site 1143 and
Its Response to Global Climate Changes ····· YUAN Jinhong (袁金红) et al. (1)
Coastal Erosion Feature and Mechanism at Feiyantan
in the Yellow River Delta ····· CHEN Shenliang (陈沈良) et al. (11)
Coastal Current Systems and the Movement and Expansion of Suspended Sediment
from Changjiang River Estuary ····· LI Sihai (李四海) et al. (22)
Inactivation Kinetics of β-N-Acetyl-D-Glucosaminidase from
Prawn (*Penaeus vannamei*) by Formaldehyde ····· XIE Xiaolan (谢晓兰) et al. (34)
Isolation of Denitrifying Bacteria in Sea Sediment and Simulated Experiment
of Removing Nitrate-N from Seawater ····· QUAN Weimin (全为民) et al. (46)
Optimization of Fermentation and Product Collection Process of the Functional Bacteria
for Bioremediation of Shrimp Culture Environment ····· LI Qiufen (李秋芬) et al. (53)
Sea Surface Roughness Derivation from Wind Speed Estimated
by Satellite Altimeter ····· ZHOU Liangming (周良明) et al. (61)
Distribution Characteristics of COD in the Waters of Pearl River Estuary
····· YANG Meilan (杨美兰) et al. (68)
Fluorescence-assisted Image Analysis of Harmful Microalgae
····· WANG Xuemin (王学民) et al. (75)
Research on Prediction of Red Tide Based on Fuzzy Neural Network
····· ZHANG Rong (张 容) et al. (83)
Nontoxic Marine Anti-fouling Coating Containing Capsaicin
····· SHI Hang (史 航) et al. (92)

Deep-sea Pollen Record during 3.0 - 2.0 Ma B.P. from ODP Site 1143 and Its Response to Global Climate Changes

YUAN Jinhong (袁金红)[1*], LUO Yunli (罗运利)[1], XU Zhaoliang (徐兆良)[1], SUN Xiangjun (孙湘君)[1, 2]

1. *Laboratory of Systematic and Evolutionary Botany, Institute of Botany, Chinese Academy of Sciences, Beijing* 100093, *China*

2. *Key Laboratory of Marine Geology, Ministry of Education, Tongji University, Shanghai* 200092, *China*

Abstract: In order to study vegetation evolution and environmental changes around 2.5 Ma B.P., a total of 146 pollen samples with an average time resolution of 7 000 years were analyzed in the deep-sea record at the depth of 135 - 95 m (in composition depth) from ODP Site 1143 (9° 22′ N, 113° 17′ E) in the southern South China Sea. The results show that the pollen influx has a distinct change. During 2.6 - 2.0 Ma B.P., the average value of pollen influx increased evidently compared with that of 3.0 - 2.6 Ma B.P. It shows that the sea level of SCS dropped dramatically around 2.6 Ma B.P., corresponding to the formation of the Northern Hemisphere ice-sheets and the enhancement of the East Asian Monsoon. The pollen influx variations reflect the glacial-interglacial cycles corresponding with the deep-sea oxygen isotope curve and indicate that the sea level of SCS rose and dropped many times after 2.6 Ma B.P. The spectrum analysis results of pollen influx show that there are cycles at 0.1Ma (eccentricity) and 46.9 ka (obliquity) during 3.0 - 2.0 Ma B.P.

Keywords: pollen influx; 3.0 - 2.0 Ma B.P.; ODP Site 1143; the South China Sea

3.0 - 2.0 Ma B.P. is an important period of global climate changes. During this period, both Arctic and Antarctic ice-sheets formed, and the global climate turned to the glacial climate of late Pliocene-Pleistocene from the Pliocene warmth. Around 2.5 Ma B.P., a series of events led to the changes of global climate patterns, such as the formation of the Northern Hemisphere ice-sheets [1]; the rapid uplift of Tibet Plateau which changed the general circulation model and the ground surface structure [2]; the uplift and closure of Panama isthmus and the variations in oceanic circulation [3].

This period is a focus of global climate research. Former researches were mainly in mid- and high-latitude regions with scarce low-latitude records [4-5]. Recent researches showed that tropical oceans especially the west Pacific warm pool plays a key role in global climatic variations [6-7]. The semi-closed South China Sea (SCS) is one of the biggest marginal seas of west Pacific. The sediments of SCS with continuous and high accumulation rates provided ample information good for studying paleoenveronment, paleoclimate and paleovegetation changes [8-9]. In this paper, the pollen record during

Received on Sept. 29, 2005

* Corresponding author. E-mail: yuanjinhong@ibcas.ac.cn

3.0 - 2.0 Ma B.P. from Site 1143 in the southern SCS was analyzed to study the evolution of East Asian paleo-Monsoon and the response of vegetation around the southern SCS to climatic variations around 2.5 Ma B.P.. Located in the "West Pacific Warm Pool", Core 1143 was taken by ODP Leg 184 in the spring of 1999.

1 Material and methods

The deep-sea sediments from ODP Site 1143 (9° 21.72′N, 113° 17.11′E), located in the northwest Nansha sea areas the at water depth of 2 772 m (Fig. 1), are continuous, complete and undisturbed. The sediments at the depth of 135 - 95 m (in composite depth) consist mostly of olive, greenish, and light gray green and greenish gray clayey nannofossil mixed sediment, clay with nannofossils, and clay. The key stratigraphic ages are provided by the benthic foraminifer oxygen isotope chronostratigraphy from ODP Site 1143 [9]. The corresponding age for each pollen sample is linearly interpolated owing to the continuity and stability of sediments (See the sedimentation rate curve in Fig. 2). A total of 146 pollen samples at the depth of 135 - 95 m were analyzed with an average time resolution of 7 ka.

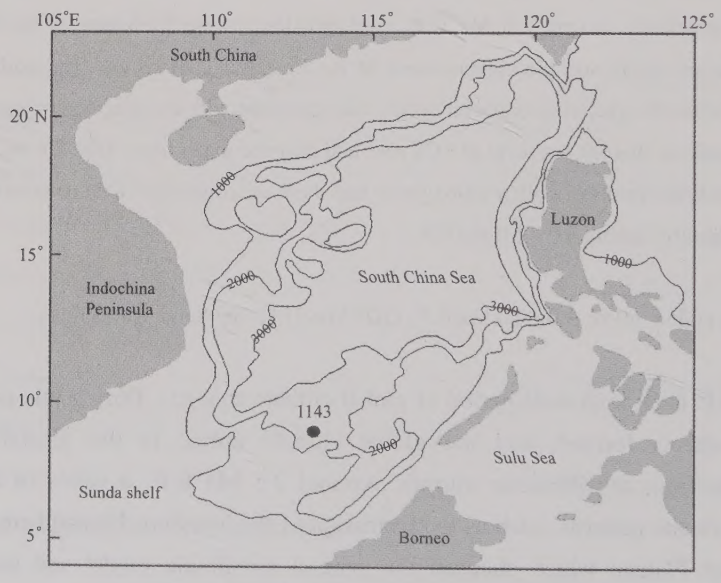

Fig. 1 Location of ODP Site 1143 in the southern South China Sea

Pollen samples were prepared at Tongji University using hydrochloric and hydrofluoric acids to remove carbonates and silicates. To concentrate pollen and spores, the remaining material after acid reactions was sieved through a 7 μm mesh in an ultrasonic bath. A *Lycopodium* tablet was added to each pollen sample of 6 - 26 mL. More than 200 pollen grains of land seed plants per sample were counted (i.e. excluding fern spores and pollen of aquatics). If the pollen of land seed plants is scarce, the exotic

Lycopodium spores are calculated up to 1 000 per sample. The influx values were calculated by the adding exotic *Lycopodium* spore method as the number of pollen grains accumulated on 1 cm^{-2} during a thousand years (grains·cm^{-2}·ka^{-1}).

2 The source areas of pollen and modern vegetation

ODP 1143 is located north of Borneo and its southwest is the famous Sunda Shelf. Pollen distribution patterns in modem surface sediments from the SCS indicate that the pollen and spores of the southern SCS are mainly from the surrounding islands south of Sunda Shelf [10]. Borneo is the main source area of deep-sea pollen for ODP Site 1143 [11-12].

Tropical rainforest is the major vegetation type of Borneo. Distributing under 1 200 m a.s.l., the lowland rainforest is represented by Dipterocarpaceae, Sapindaceae, Meliaceae, Moraceae, Rubiaceae and Rutaceaece. The tropical low montane rainforest composed chiefly of *Castanopsis*, *Quercus*, Theaceae, Myrtaceae and Elaeocarpaceae grows on the belt between 1 200 and 1 500 m a.s.l. The tropical middle montane rainforest represented by *Podocarpus* and *Dacrydium* covers the land between 1 500 and 3 000 or 3350 m a.s.l. Above 3 000 m it is replaced by the tropical subalpine vegetation with *Phyllocladus*, *Dacrycarpus*, *Myrica*, and *Rhododendron*. Mangroves, represented often by *Bruguiera*, *Avicennia*, *Rhizopohra* and *Sonneratia*, are found along the southeast coast of Borneo [13-15].

3 Results and analyses

A total of 88 pollen types were identified. To make the influx pollen diagram easier to interpret, several groups of taxa according to the plant ecology of pollen and spores besides *Pinus* are represented as follows.

Upper montane rainforest (*Podocarpus*, *Dacrycarpus*, *Dacrydium* etc.);

Lower montane rainforest (*Castanopsis*, *Quercus* evergreen, Elaeocarpaeae, etc.);

Tropical lowland rainforest (*Mallotus/Macaranga*, Euphorbiaceae, Palmae, Oleaceae, Melastomataceae, Meliaeae, Moraceae, etc., a large number of taxa, with a few pollen grains in each taxon);

Mangroves (*Rhizophora*, Sonneratia, etc);

Temperate taxa (*Alnus*, *Betula*, *Salix*, etc.);

Herbs (Cyperaceae, Graminaeae, etc.).

In addition there were many types of ferns represented by *Stenochlaena*, *Pteridaceae*, Gleicheniaceae, *Ploypodium*, *Pyrriosia* and Davaliaceae.

The pollen assemblages in the section of 135 - 95 m (3.0 - 2.0 Ma B.P.) are characterized by high influxes of Pinus, upper montane rainforest and lower montane rainforest pollen and low influx of herbaceous, mangroves and aquatic pollen. Based on the downcore variations in different ecological

groups, the pollen influx diagram is divided into two zones.

Zone P1: 135 - 120.8 m, 3.0 - 2.6 Ma B.P. In this zone, the total pollen influx is quite low with an average value of 102.5 grains·cm^{-2}·ka^{-1} (the following is the same). Thereinto, *Pinus* pollen influx is 44.2, upper montane forest pollen influx is 26.7, lower montane forest pollen influx is 14.3, lowland tropical rainforest pollen influx is 7.8 and herbaceous pollen influx is 7.0. The pollen influxes of temperate forest, mangroves and aquatic taxa are low, respectively 1.5, 1.0 and 0. The fern spore influx is 454.8 on the average.

Zone P2: 120.8 - 95 m, 2.6 - 2.0 Ma B.P. Compared with the zone P1, the pollen influx increased distinctly. The average total pollen influx reaches 208(twice of P1) and the spores influx arrives at 1 108.5 on the average (2.4 times that of P1). Thereinto, *Pinus* pollen influx is 82.8, 1.9 times that of P1, upper montane rainforest pollen influx is 51.5, 1.9 times that of P1, lower montane rainforest pollen influx is 29.5, 2 times that of P1, lowland tropical rainforest pollen influx is 25.7, 3.3 times that of P1. Herbaceous pollen influx is 9.5, 1.4 times that of P1. The pollen influxes of temperate rainforest, mangroves and aquatic taxa reach 5.8, 3.1 and 0.7 respectively.

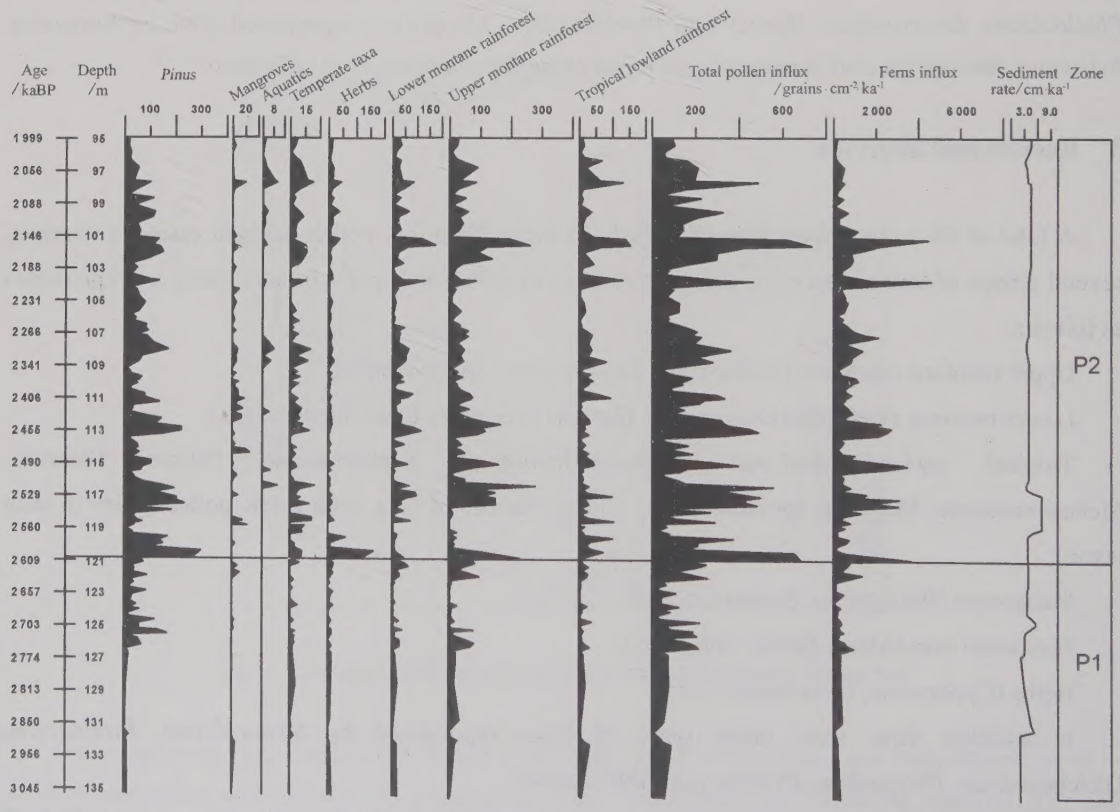

Fig. 2 Pollen influx diagram of 135 – 95 m (3.0 - 2 .0 Ma B.P.) deep-sea record from ODP Site 1143, Leg 184, in the southern South China Sea

4 Discussion

4.1 Pollen influx diagram reveals the sea level drop and the enhancement of East Asian monsoon around 2.6 Ma B.P.

Pollen influx diagram shows that the average value of pollen influx during 2.6 - 2.0 Ma B.P. was different from that during 3.0 - 2.6 Ma B.P. and increased notably. Thereinto, the influxes of pollen transported mainly by windy force such as *Pinus*, *Podocarpus*, *Darcrycarpus* and *Darcrydium* increased by 0.9 times and the influxes of other pollen and spores transported by river runoff increased by 1.4 times. The pollen distribution patterns in the modem surface sediments from the SCS revealed the pollen source areas, the dispersal routes and the transport mechanism [10]. It is showed that the concentrations of the majority of pollen and spores types from the southern SCS decreased from the continental shelf to the deep-sea, indicating that the pollen is dispersed from the coastal areas of south China mainly by the river runoff.

The pollen influxes began to increase around 2.6 Ma B.P. On the one hand, the monsoon enhancement had probably contributed to the influx increase of pollen transported mainly by wind. On the other hand, since pollen and spores transported by fluvial runoff largely increased, it might be concluded that due to the sea level lowering during the Northern Hemisphere ice-sheet growth period, the continental shef emerged, the pollen source area enlarged and the transport distance was shortened.

The researches in the SCS show that the Northern Hemisphere ice-sheets formed and the East Asian monsoon intensified around 2.6 Ma BP. Analysis on the benthic foraminiferal $\delta^{18}O$ value from Site 1143 revealed that the Atlantic-Pacific benthic $\delta^{18}O$ difference ratio increased during 3.6 - 2.7 Ma B.P. and during 2.7 - 2.1 Ma B.P., corresponding to the growth of the Northern Hemisphere ice-sheet [9]. The benthic foraminiferal $\delta^{18}O$ value from ODP Site 1148, northern SCS became heavy during 3.1 - 2.5 Ma B.P., indicating the formation of boreal ice-sheets at that time. Furthermore, the $\delta^{18}O$ value around 2.7 Ma B.P. was very heavy and reached that of Holocene. It is indicated that around 2.7 Ma B.P. the Northern Hemisphere ice-sheetshad reached the size at present [16]. During 3.2 - 2.0 Ma B.P., both the increase of phytolith contents and the rapid increase of the grain size of terrigenous clastic sediments from Site 1143 around 2.5 Ma B.P. indicate the enhancement of winter monsoon [17-18]. Researches on planktonic foraminifers from ODP Site 1148 showed the distinct drop of $\delta^{13}C$ value of *Globigerinoides rubber* and the notable increase of *Neogloboquadria dutertrei* relative abandance, indicating the intensification of winter monsoon [19]. Analysis on foraminifer assemblages and shells from ODP Site 1146 showed that abundance of mixed layer and thermocline species, high productivity species of planktonic foraminifera and infaunal species of benthic foraminifera changed around 2.7 Ma B.P., and the carbon isotope difference ratio varied distinctly around 2.4 Ma B.P. [20]. This indicated the enhancement of the East Asian winter monsoon around 2.7 Ma B.P., which in turn is associated with the progressive intensification of glaciation in the Northern Hemisphere.

The SCS level drop and the East Asian monsoon intensification around 2.6 Ma B.P. indicated by the

deep-sea pollen record from Site 1143 are supported by other researches on global climate changes.

Past researches showed that the global climate was changed from Pliocene warmth to Quaternary glacier climate with critical cold and ice-sheet mass around 2.6 Ma B.P. Most benthic $\delta^{18}O$ records indicate that the global ice-sheets grew rapidly during 3.0 - 2.5 Ma B.P. [1, 16, 21-23]. For example, Chinese loess began to deposit around 2.47 Ma B.P. [25], indicating the intensification of the East Asian monsoon [26]. The dust fluxes both in the red clay and deep-sea aeolian sediments increased rapidly during 3.6 - 2.6 Ma B.P., indicating the intensification of the East Asian winter monsoon [27]. Around 2.5 Ma B.P., the East Asia turned into the Quaternary monsoon climate with the alternation of winter and summer monsoon dominance [27].

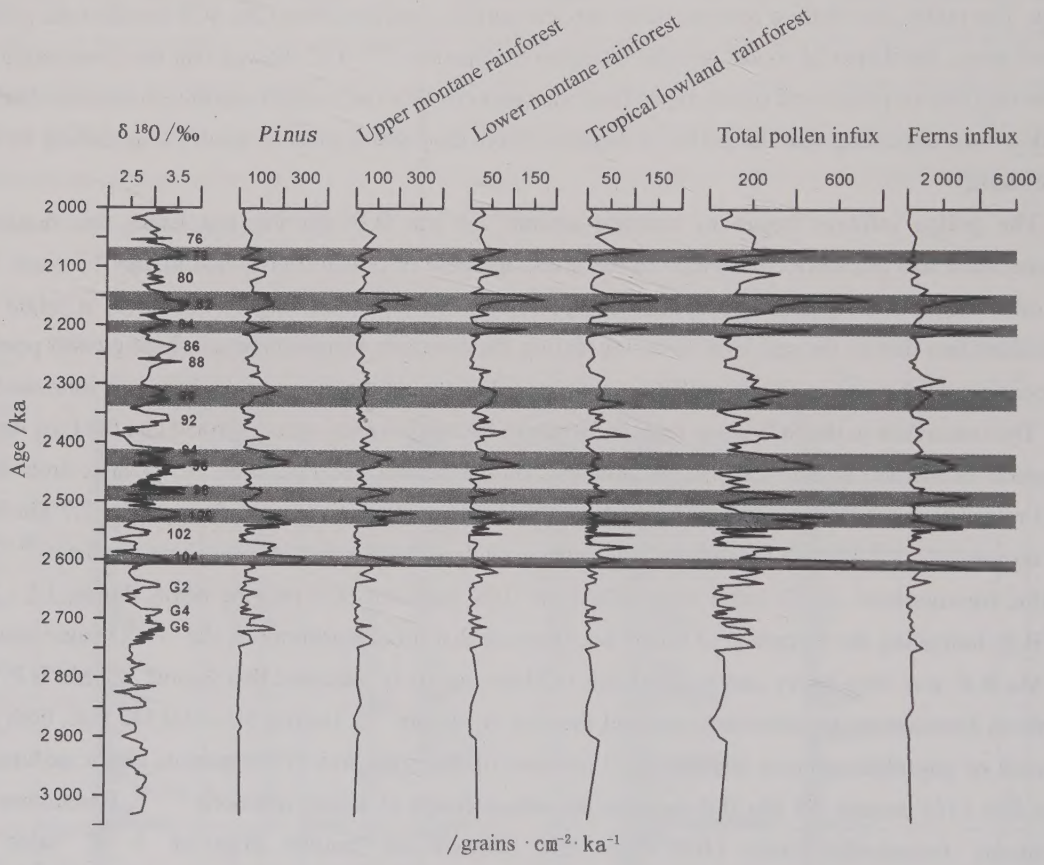

Fig. 3 Comparison of pollen influx curve with that of $\delta^{18}O$ from ODP Site 1143

4.2 Glacial-interglacial cycles after 2.6 Ma B.P.

The detailed comparison of the pollen influx with the benthic $\delta^{18}O$ value from Site 1143 indicates that the pollen influx diagram might be subdivided further into many subzones and exhibits the same variation trends as that of $\delta^{18}O$ curve from Site 1143. The downcore variations of the pollen influxes (Fig. 3) show that the higher values occur in the even Marine Isotope stages (glacial periods) while the

lower values occur in odd stages (interglacials), which indicates the intensification of winter monsoon in the glacial periods and the weakening in the interglacials. During the glacial periods the SCS level dropped and the tropical rainforest vegetation grew on the exposed Sunda Shelf. Since the pollen source areas were enlarged and the transport distance from the pollen source area to the deposition site was shortened, more pollen and spores were carried to the research site, and vice versa, the further distance and smaller source areas in interglacials because of the SCS level rising contributed less pollen and spores that were transported to the research site. After 2.6 Ma B.P., corresponding to the $\delta^{18}O$ value curve, the pollen influx diagram presented many cycles, implying that the sea level rose and dropped many times.

4.3 Analysis of climatic cyclicity during 3.0 - 2.0 Ma B.P.

As showed from Fig. 3, pollen subzones during 3.0 - 2.0 Ma B.P. are well correlated with Marine Isotope Stages. In search for a variation pattern in the pollen record, univariate spectrum analysis from the SPECTRUM program [28] is used to perform spectrum analysis of the upper montane rainforest, Pinus and the lower montain rainforest pollen influxes during 3.0 - 2.0 Ma B.P.. The results display two Milankovitch cycles (Fig. 4) characterized by strong eccentricity-dominance (~ 105 ka cycles) and notable obliquity-relation (~ 46.9 ka cycles). Besides, there seemingly exist a 287 ka cycle. The reason for such a cycle is unclear yet.

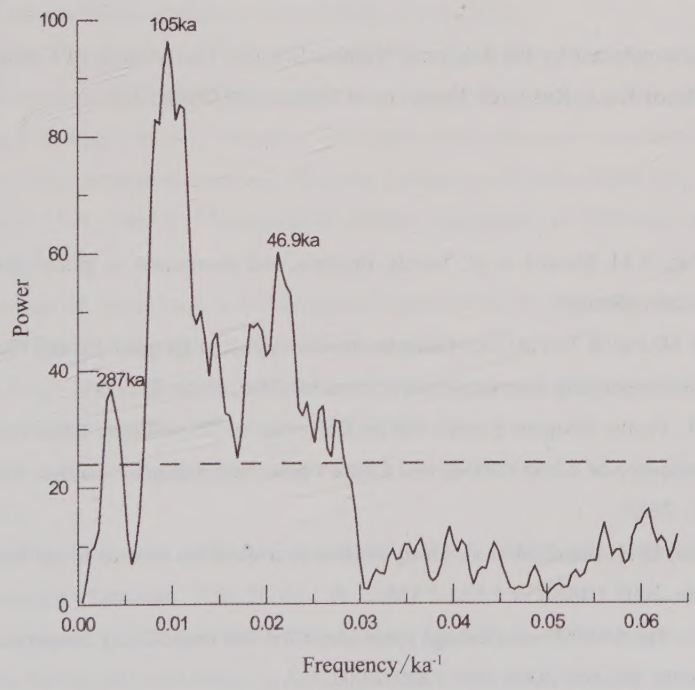

Fig. 4 Spectrum analysis of pollen influx during 3.0 - 2.0Ma B. P. showing presence of 0.1 Ma and 46.9 ka cycles

(The dashed line indicates 95 % level of significance.)

5 Conclusion

Due to the global cooling, the Northern Hemisphere ice-sheets initiated and enlarged during the late Cenozoic, which is a very important period for climate system research. Deep-sea sediments, Chinese loess deposits and polar ice-cores are the three important kinds of records of global climate changes. The ODP Site 1143 provided good materials for research on the global climate change and filled in the gap that there is lack of deep-sea pollen records during 3.0 - 2.0 Ma B.P. in the SCS.

The research on the deep-sea pollen record during 3.0 - 2.0 Ma B.P. from Site 1143 in the southern SCS shows that during 2.6 - 2.0 Ma B.P. pollen influxes increased largely. It reveals the formation of Northern Hemisphere ice-sheets, the fall of sea level of SCS, the intensification of East Asian monsoon and the transition of global climate at 2.6 Ma B.P, corresponded to the records in other global areas and to the Tibet uplift during that period. In correspondence with the deep-sea δ18O curve from Site 1143, the pollen influx variations showed the glaclial-interglacial cycles, which indicates that the sea level of SCS rose and dropped many times after 2.6 Ma B.P. Spectrum analysis results show that there exist orbital cycles at 0.1 Ma and at 46.9 ka during 3.0 - 2.0 Ma B.P..

Acknowledgements

This work was supported by the National Natural Science Foundation of China projects (40371116) and the National Major Basic Research Program of China (G200078502).

References

[1] Zachos J S, Pagani M, Sloan L et al. Trends, rhythms, and aberrations in global climate 65 Ma to present. Science, 2001, 292: 686-693.

[2] Li J J, Fang X M, Pan B T et al. Late Cenzoic intensive uplift of Qinghai-Xizang Plateau and its impacts on environments in surrounding area. Quaternary Sciences, 2000, 21(5): 381-391.

[3] Duque-Caro H.. Pacific Neogene Events. Tokyo: University of Tokyo Press. 1990, 101-113.

[4] Liu T S. Significance of ocean drilling and China's paleooceanographic studies. Chinese Science Bulletin, 2003, 048(023): 2523.

[5] Wang P X, Zhao Q H, Jian Z M et al. Thirty million year deep-sea records in the South China Sea. Chinese Science Bulletin, 2003, 048(023): 2 524-2 535.

[6] Shackleton N J. The 100,000-year ice-age cycle identified and found to lag temperature, carbon dioxide, and orbital eccentricity. Science, 2000, 289: 1 897-1 902.

[7] Kerr R A. The tropics return to the climate system. Science, 2001, 292: 660-661.

[8] Wang P X. Marine Quaternary research in China and sea-land interaction in environmental changes.Quaternary Sciences, 2001, 21(3): 218-222.

[9] Tian J, Wang P X, Cheng X R et al.. Astronomically tuned Plio-Pleistocene benthic δ18O record from South China Sea and Atlantic-Pacific comparison. Earth and Planetary Science Letters, 2002, 203: 1 015-1 029.

[10] Sun X J, Li X. Different dynamics and routes of modern pollen transport in the northern and southern parts of the South China Sea. Science in China (Series D), 1998, 41(1): 57-61.

[11] Sun X J, Li X, Luo Y L. Vegetation and climate on the Sunda Shelf of the South China Sea during the Last Glaciation-pollen results from station 17962. Acta Botanica Sinica, 2002, 44(6): 746-752.

[12] Li X, Sun X J. Palynological records since Last Glacial Maximum from a deep sea core in southern South China Sea. Quaternary Sciences, 1999, 19(6): 526-535.

[13] Whitmore T C. Tropical rain forests of the Far East. Oxford: Claerndon Press. 1975: 155-253.

[14] Kitayama K. An altitudinal transect study of the vegetation on Mount Kinabalu. Vegetation, 1992, 102: 149-171.

[15] Whitmore T C. Tropical Rain Forests. Oxford: Claerndon Press. 1990: 1-226.

[16] Jian Z M, Cheng X R, Zhao Q H et al. Oxygen isotope stratigraphy and events in the northern South China Sea during the last 6 million years. Sciences in China(series D), 2001, 44(10): 952-960.

[17] Li J R, Wang R J, Li B H. Variations of opal accumulation rates and paleoproductivity over the past 12 Ma at ODP Site 1143, southern South China Sea. Chinese Science Bulletin, 2002, 47(7): 596-598.

[18] Wang P. X., Jian Z. M., Zhao Q. H.. Evolution of the South China Sea and monsoon history revealed in deep-sea records. Chinese Science Bulletin, 2003, 048(023): 2549-2561.

[19] Jian Z M, Wang P X, Zhao Q H et al.. Late Paleocene enhanced east Asian winter monsoon: evidence of isotope and foraminifers from the northern South China Sea. Quaternary Siences, 2001, 21(5): 461-469.

[20] Huang B Q, Cheng X R, Jian Z M et al. Variations and upper ocean structure in the South China Sea and the evolution of the east Asian monsoons since Late Pliocene. Quaternary Sciences, 2004, 24(1): 110-115.

[21] Shackleton N J, Hall M A, Pate D. Pliocene stable isotope stratigraphy of ODP site 846. Proc ODP Sci Results, 1995, 138: 337-355.

[22] Tiedemann R, Sarnthein M, Shackleton N J. Astronomic timescale for the Pliocene Atlantic δ18O and dust flux records of Ocean Drilling Program site 659. Paleoceanography, 1994, 9(4): 619-638.

[23] Mix A, Pisias N G, Rugh W et al. Benthic foraminifer stable isotope record from Site 849(0～5Ma): local and global climate changes. Pro. ODP. Sci. Results, 1995, 138: 371-412.

[24] Ding Z L, Liu T S, Liu X M et al.. Thirty-seven climatic cycles in the last 2.5Ma. Chinese Science Bulletin, 1990, 35(8): 667-671.

[25] Liu T S, Shi Y F, Wang R J et al.. Table of Chinese Quaternary stratigraphic correlation remarked with climate change. Quaternary Sciences, 2000, 20(2): 108-128.

[26] Liu T S, Zheng M P, Guo Z T. Initiation and evolution of the Asian monsoon system timely coupled with the ice-sheet growth and the tectonic movements in Asia. Quaternary Sciences, 1998, 18(3): 194-204.

[27] Cao J J, Zhang X Y, An Z S et al. Variations of dust flux in the Loess Plateau during 6.5~2.2 Ma B.P.: implications for east Asian winter monsoon evolution and Asian aridity. Marine Geology and Quaternary Geology, 2003, 23(3): 97-101.

[28] Schulz M, Stattegger K. Spectrum analysis of uneven spaced paleoclimatic time series. Computers and Geosciences, 1997, 23: 929-945

3.0～2.0 MaBP 南海南部深海沉积物孢粉记录及其对全球气候变化的响应

袁金红[1]，罗运利[1]，徐兆良[1]，孙湘君[1,2]

（1. 中国科学院植物研究所系统与进化植物学重点实验室，北京 100093；2. 同济大学海洋地质教育部重点实验室，上海 200092）

摘 要：为了探索和揭示 2.5 MaBP 前后东亚季风演变历史及植被演替对气候演化的响应，对南海南部大洋钻探 ODP1143 站（9° 22'N、113° 17'E）深海柱状样的上部 135 ～ 95 m（3.0～2.0 MaBP）共 146 个孢粉样品进行了分析研究，时间分辨率为 7 ka/样，孢粉谱显示沉积率变化显著，以 2.6 MaBP 为界可明显分为两个阶段，与前一阶段 3.0～2.6 MaBP 相比，2.6～2.0 MaBP 时段各类型花粉及孢子沉积率均有显著提高。该结果表明 2.6 MaBP 南海海平面有显著下降，可与北半球冰盖形成、东亚季风增强相对应。2.6 MaBP 以后，各类型孢粉沉积率高低变化揭示南海海平面有多次上升和下降，代表了多次冰期-间冰期旋回。该结果与深海氧同位素分期相对应。频谱分析表明 3.0～2.0 MaBP 存在 0.1 Ma（偏心率）和 46.9 ka（斜率）的周期。

关键词： 孢粉沉积率；3.0～2.0 MaBP；ODP1143 站；南海南部

Coastal Erosion Feature and Mechanism at Feiyantan in the Yellow River Delta

CHEN Shenliang (陈沈良)*, ZHANG Guoan (张国安), CHEN Xiaoying (陈小英)
State Key Laboratory of Estuarine and Coastal Research, East China Normal University, Shanghai 200062, *China*

Abstract: Feiyantan was the discharge area of Diaokou River distributary of the Yellow River during the period of 1964 to 1976. The coastal erosion feature and morphological evolution at the Feiyantan coast are studied in the light of the topography and section depth, and the corresponding dynamics of wave and current. Results indicate that the protruding topography left after the Diaokou River distributary was abandoned is the main cause of strong coastal erosion. Further research suggests that waves start up the sediment and the tidal current transports it, and the waves and tidal current are combined to be the dominant dynamic mechanism of coastal erosion, in which the tidal residual current takes and transports the sediment outward, thus causing the sediment to wane in the coast.

Keywords: coastal erosion; waves; tidal current; Feiyantan coast; Yellow River delta

Introduction

Coastal erosion problems are widespread throughout the world [1], especially those of some great river deltas are remarkable, i.e. Nile Delta in Egypt [2], Ebro River Delta in Spain [3], Yellow River Delta and Luanhe River Delta in China [4-6]. In particular, the whole Yellow River Delta has a tendency to retreat, because riverine water discharge and sediment load into the sea decrease remarkably, resulting in slow accumulation even near the current river mouth [7]. The Yellow River is a well-known sediment laden river throughout the world. Since the Tongwaxiang dike breaching in Henan province in 1855, the Yellow River migrated towards north, flowing into the Gulf of Baohai after crossing the Daqinghe River, the new delta land had been created at a rate of 26.8 km^2/a during the period of 1855 to 2001 [8]. However, due to the terminal channel of the Yellow River shifting frequently, the abandoned delta lobes have been eroded all the time. In the past, people paid more attention to the rapid accumulation and progressive development of delta land near the flowing estuary than the erosion of some other areas. At present, coastal erosion of the Yellow River Delta has become a very serious problem with decreased sediment load of the Yellow River in recent years.

The Feiyantan coast studied in this paper, which is about 37 km long, is located in the north of the Yellow River delta coast from 118° 38′ E to 118° 55′ E (Fig. 1). The coast formed resulting from the

Received on Sept. 30, 2005

* Corresponding author. E-mail: slchen@sklec.ecnu.edu.cn

rapid accumulation near the estuary at the stage of Diaokou River distributary from January 1964 to May 1976. However, since the Yellow River was diverted to the Qingshuigou River distributary emptying into sea in May 1976, the sediment supply of Diaokou River distributary has been cut off, and the Feiyantan coast has been abandoned. Additionally, Feiyantan is situated in the north of the Yellow River Delta where ocean dynamics is very strong, which results in the serious coastal erosion and has a great effect on the exploitation of the local oilfield. Based on the analyses of the coastal erosion feature and morphological evolution at the Feiyantan coast, together with the corresponding dynamics of wave and current, this paper reveals the mechanism of coastal erosion and offers scientific gist for the protection of this coast.

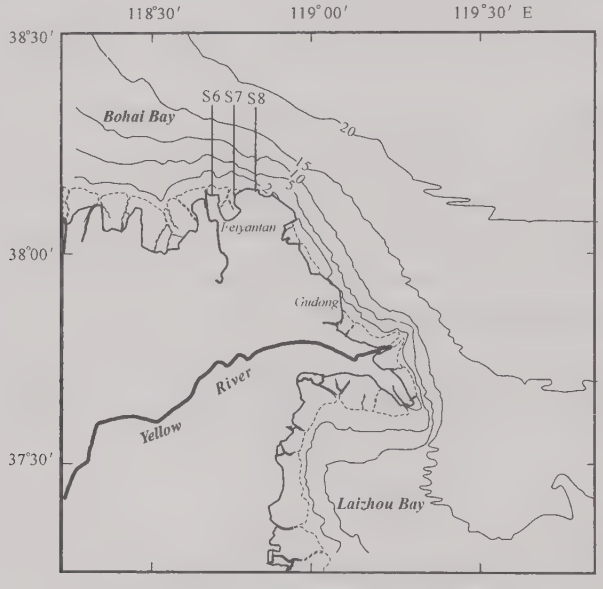

Fig. 1 Location of the studied coast and profiles

1 Coastal erosion of Feiyantan

1.1 The erosion characteristics of Feiyantan coast

Feiyantan coast belongs to the coast of Diaokou River delta lobe. It has been formed since the Yellow River's terminal course was diverted to the Diaokou River distributary to flow to the sea in January 1964. Due to the rapid accumulation, the sediment of coast was so loose during the flowing stage of Diaokou River distributary. However, the coast has been eroded strongly by wave and tidal current after the Diaokou River distributary was abandoned in May 1976. The protruding mouth spit suffers from the most serious erosion with an erosional depth of -15 m.

The formation of mouth spit is associated with the levee along both banks of the estuary which stretch out towards the sea and protrude from the shoreline. The front of mouth spit protruding from the seabed can get to the intertidal zone or subtidal zone, so the energy of wave is easily focused and the

velocity of tidal current is increased immediately there. This means that if the distributary is abandoned and the riverine sediment supply ceases, the protruding mouth spit will suffer from quite serious erosion and retreat. Figure 2 shows shoreline changes of the Feiyantan coast from 1975 to 2000. The mouth spit stretched out from 1975 to 1976 when the Diaokou River distributary was in the mature stage, and then retreated 3.2 km with a rate of 0.4 km/a from 1976 to 1984. Thereafter, the retreat rate decreased gradually, with a rate of 0.2 km/a from 1984 to 1986 [9].

The retreat rate of the subaqueous slope (0 to -15 m), less than that of the mouth spit, was 0.254 km/a. Due to the differentiation of the dynamics conditions at different parts of the slope profile, the retreat rates are not the same, decreasing with the increase of water depth of the subaqueous slope (Table 1). For the 0 m isobath, it retrograded most rapidly with a rate of 0.437 km/a, a little more quickly than the mouth spit. The causes lie in that the zone near 0 m isobath is also located at the front of the mouth spit where waves frequently break.

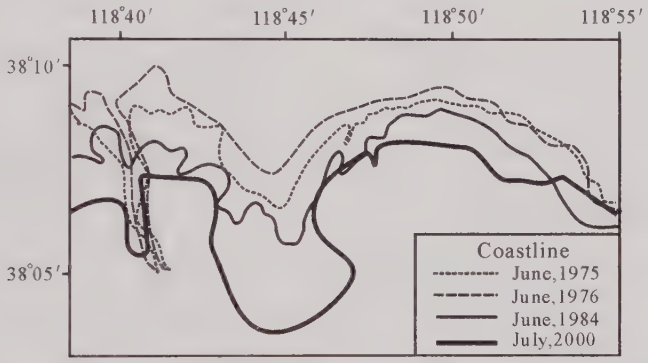

Fig. 2 Shoreline changes of the Feiyantan coast from 1975 to 2000

Tab. 1 Retreat rates for different isobaths along the Feiyantan coast

Isobath / m	Period	Duration / a	Retreat distance /km	Retreat rate / km • a^{-1}
0	1976 −2000	24	10.500	0.437
-2	1976 −1999	23	7.890	0.343
-5	1976 −1999	23	4.180	0.182
-10	1976 −1999	23	1.239	0.054
-15	stable			

Shoreline retreated gradually since the Diaokou River distributary was abandoned in 1976. According to the comparison and computation of the positions of shorelines for different periods from 1976 to 2000, the results showed that the retreat rate for shoreline was 0.233 km/a, and the land area has been eroded for 207 km^2 with a retreat rate of 8.63 km^2/a (Table 2). As time went, the retreat rate tended to decrease, however, still remained at a high level in recent years.

In conclusion, the erosion feature of Feiyantan coast was concluded as follows: (1) the coast has suffered from the continual erosion since the Diaokou River distributary was abandoned. Retreat rates were in order of mouth spit > shoreline > subaqueous slope. (2) As time went, retreat rates tended to decrease, in other words, the coast was eroded quickly at the beginning and then gradually slowly. But the coastal erosion was still intense at the end of the stage. (3) Mouth spit was eroded so quickly that its shoreline tended to be leveled after the Diaokou River distributary was abandoned about 10 years ago. (4) Retreat rates apparently decreased outside the 10 m isobath of the subaqueous slope, which became tiny and kept stable relatively at approximately the 15 m isobath of the subaqueous slope.

Tab. 2 Shoreline retreat for different periods along the Feiyantan coast from 1976 to 2000

Period	Duration / a	Retreat distance of shoreline / km	Retreat rate of shoreline / km • a^{-1}	Retreat area / km^2	Eroded area rate /km^2 • a^{-1}
1976 —1988	12	4.000	0.333	148.00	12.23
1988 —1991	4	0.890	0.223	32.92	8.23
1992 —2000	8	0.710	0.089	26.27	3.28
1976 —2000	24	5.600	0.233	207.00	8.63

1.2 Evolution of nearshore profiles

On account of large amounts of sediment accumulating quickly, the Feiyantan coast formed the accumulated geomorphology of subdelta which was characterized by steep convex slope profiles, during the flowing stage of the Diaokou River distributary. Since the Diaokou River was abandoned after May 1976, the kinetic balance between ocean dynamics and coastal topography has been destroyed and coastal profiles rapidly retreated, especially, erosion was most intense above the 12 m isobath of the subaqueous slope (Fig. 3). We took the 5 m isobath for example. During 25 years from 1975 to 2000, the maximum of retreat rate was 240 m/a for Profile S8, the minimum was 110 m/a for Profile S6, and the average was 170 m/a. The seabed, which was deeper than -12 m, was slightly eroded from 1976 to 2000, accumulated slightly after 1980, and then got back to the level of 1975 up to 2000. This indicated that since the Diaokou River distributary was abandoned, continual erosion of Feiyantan coast generally occurred near the shore, which was shallower than -12m, where combined action of waves and currents was very intense. As nearshore topography was eroded and retreated continually, the seabed of deep waters was accumulated slightly. The underwater slope profiles tended to be convex and gentle.

2 Mechanism of coastal erosion

Stability of coast rests with the kinetic balance among sediment supply, hydrodynamics and coastal topography. Since the Diaokou River distributary was abandoned, the sediment supply of Feiyantan coast has been cut off, and the ocean dynamics has become stronger relatively. Due to the wave stirring

sediment and the current transporting sediment, the loss of coastal sediment resulted in intense coastal erosion.

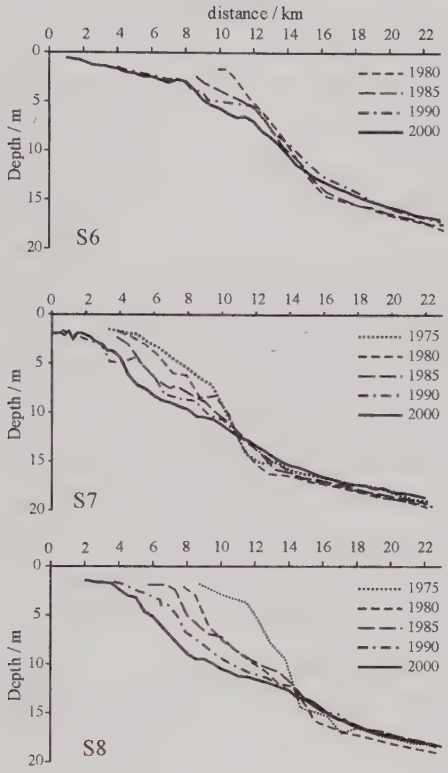

Fig. 3 Profile erosion for the S6, S7, S8 along the Feiyantan coast

2.1 Wave stirring sediment

The wave stirs the sediment mainly by means of wave breaking and disturbance. Wave disturbance means that the wave can stir the sediment of seabed though the wave has not gotten to the depth of wave breaking. Generally speaking, like the depth for wave breaking, the depth for wave disturbance increases with wave height increasing. If a certain grade of wave occurs frequently, the frequency of wave breaking in response to the wave breaking zone is high, and, accordingly, the wave stirs the sediment of seabed intensely. In brief, the wave stirring the sediment is associated with wave breaking, disturbance and frequency of wave occurrence, which dominate the coastal erosion. In addition, the relation between directions of wave and coast has influenced greatly the coastal erosion. Based on the local measured data (Table 3), we can conclude that wind waves prevail, the prevailing direction of waves was NE and the frequency of wave occurrence was 10.3 %. Strong waves were mainly from NNE-ENE in which waves from NE were the strongest, waves from aside NW were secondary. During the observation period, the measured utmost wave height was 5.2 m, the corresponding H1/10 was 3.1 m, and the average period of waves was 8.2 s. For Feiyantan, the trend of the coastline located to the east of

118° 50′ E is WNW-ESE, turned into WSW—ENE from 118° 50′ E to 118° 44′ E, and then WNW-ESE again for the coasts located to the west of 118° 44′ E. It was obvious that the whole Feiyantan coasts showed the trend of E-W, which intersected the directions of strong waves and frequent waves, thus strengthening the coastal erosion from wave action.

The depth of wave breaking is calculated by 1.28 times the wave height approximately [10]. The depth of wave disturbance, which is regarded as the critical depth where the sediment at seabed can be mostly moved by wave, is worked out according to Sato Formula [11]. In addition, frequencies of wave breaking and wave disturbance can be worked out based on frequencies for all grades of waves. Table 4 shows the results of wave breaking depths, wave disturbance depths and corresponding frequencies of various grades of waves in the subaqueous slope of Feiyantan. It can be seen that the wave breaking mostly existed in the water area which was shallower than -6.5 m, while the wave wouldn't break in the water area which was deeper than -6.5 m unless the wave height was larger than 5 m. The frequency of wave breaking decreased with the increase of water depth. According to the wave breaking depth and corresponding frequency, coasts where the depth range varied from 0 m to -2 m were called the wave breaking zone of high frequency. Additionally, the wave breaking frequency for the shallow zone which varied from 0 m to -0.64 m was the highest, getting to 51.1 %. Therefore, the coastal zone near the 0 m isobath suffered from the strongest erosion. Coasts where the depth range varied from -2 m to -6.5 m belonged to the wave breaking zone of low frequency, what's more, the wave breaking frequency was about 12 % and retreat rates of subaqueous slope tended to decrease. The wave breaking frequency decreased to below 0.5 % in the water area which was shallower than -6.5 m.

Tab.3 Wave feature in the offshore of Feiyantan

Item	Dir																Total
	N	NNE	NE	ENE	E	ESE	SE	SSE	S	SSW	SW	WSW	W	WNW	NW	NNW	
0≤H<0.5	2.3	1.8	2.7	1.5	2.4	3.5	3.5	3.5	3.7	4.6	4.3	3.3	3.9	3.1	5.2	1.8	51.1
0.5≤H<1.5	2.1	1.9	4.0	2.5	4.1	2.3	3.8	2.1	1.4	1.7	0.9	0.9	1.0	1.4	2.5	2.7	35.3
1.5≤H<3.0	0.4	1.4	3.4	3.0	1.2	0.7	0.8	0.2	0.2	0.7	0.1	0.1				0.2	11.8
3.0≤H<5.0	0.1		0.2	0.1		0.1											0.5
Total frequency	4.9	5.1	10.3	7.1	7.7	6.6	8.1	5.8	5.3	6.4	5.3	4.3	4.9	4.5	7.7	4.7	98.7
Max $H_{1/10}$ height / m	3.0	2.5	3.1	3.3	2.5	3.0	2.8	2.6	0.8	2.0	1.5	2.4	1.1	1.0	1.4	2.1	
Max average period / s	7.4	7.5	8.2	7.4	6.0	5.8	6.7	6.3	5.2	6.4	6.0	5.1	6.5	5.7	5.8	6.4	
Max wave height / m	4.6	3.8	5.2	4.1	3.6	4.7	4.5	3.4	2.1	2.7	2.0	3.4	2.7	2.2	3.0	3.5	

Tab. 4 Wave breaking depth, disturbing depth and their corresponding frequency

Wave grade / m	Breaking depth / m	Breaking frequency / %	Disturbance depth / m	Disturbance frequency / %
0≤H<0.5	0 - 0.64	51.1	0 - 1.56	98.7
0.5≤H<1.5	0.64 - 1.92	35.3	1.56 - 6.59	47.6
1.5≤H<3.0	1.92 - 3.84	11.8	6.59 - 13.10	12.3
3.0≤H<5.0	3.84 - 6.44	0.5	13.10 - 15.30	0.5

Compared with the wave breaking for the same grade of waves, the depths of wave disturbance were larger and the influenced areas by wave disturbance were wider. As the wave height increased, the depths of wave disturbance increased. For example, the disturbance depth for 1.5 m wave height is -6.5 m where all of disturbance frequencies got to 47.6 %. It could reach 100 % in the underwater area which was shallower than -1.5 m where wave breaking or wave disturbance occurred as long as waves existed. The frequency of wave disturbance fell to 12 % in the underwater area where the depth was larger than 13 m, which coincided with the fact that retreat rates decreased obviously at the slope outside the 12 m isobath.

Wave breaking and disturbance stirred the sediment of seabed. Like frequencies of wave breaking and wave disturbance, retreat rates decreased with the increase of water depth. Wave breaking zones of high frequency were correlated with the coasts which were eroded intensely, which suggested that wave breaking plays an important role in the erosion of Feiyantan coast. Sediment of loose density was stirred and washed out firstly, and the close-grained sediment was left behind, causing the resistance to the coastal erosion to strengthen and the retreat rates to decrease gradually. This is the reason why the underwater slope was eroded quickly at the beginning, and then slowly as time went after Feiyantan coast was abandoned.

2.2 Tidal currents transporting sediment

The Yellow River delta is located near the amphidromic point of M2 tidal component (119° 03′ 57″ E, 38° 08′ 41″ N). Including the amphidromic point, tides of the limited areas around it belong to the regular diurnal tide, and then show a transition to the semi-diurnal tide towards south or west. In response to the complex tides, two areas of high current velocity, which are located in the north and the south along the Yellow River delta coast respectively, also exist (Fig. 4). The Feiyantan coast is just close to the northern area of high current velocity.

The measured data on the two northern areas with high current velocity are studied. For the northern measured area in December, 1999 where the depth was 18 m, the average velocity of flood current was 43 - 70 cm/s, with the maximum of 97 cm/s, and the direction was 301° ; the average ebb velocity was 43 - 73 cm/s, with the maximum of 65 cm/s, and the direction was 123° . For the eastern measured area in June 2000 where the depth was 10 - 15 m, the average velocity of flood current was 55

– 70 cm/s, with the maximum of 102 cm/s and the direction was 290—320° ; the average velocity of ebb current was 50 - 73 cm/s, with the maximum of 122 cm/s and the direction was 90—120° . Directions of flood current were mostly WNW and those of ebb current were mainly ESE, accordingly, current directions roughly paralleled the shoreline. The reciprocating semi-diurnal current prevailed in the study area where the ebb tide duration was 6 h 20 min and the flood tide duration was about 6 h. However, the diurnal inequality was conspicuous, what's more, velocities of ebb current and flood current were quite dissymmetric during a tidal period. Besides, current velocities at the bottom of the studied area were mainly 20 - 40 cm/s, which were smaller than those of middle layer and surface (Fig.5).

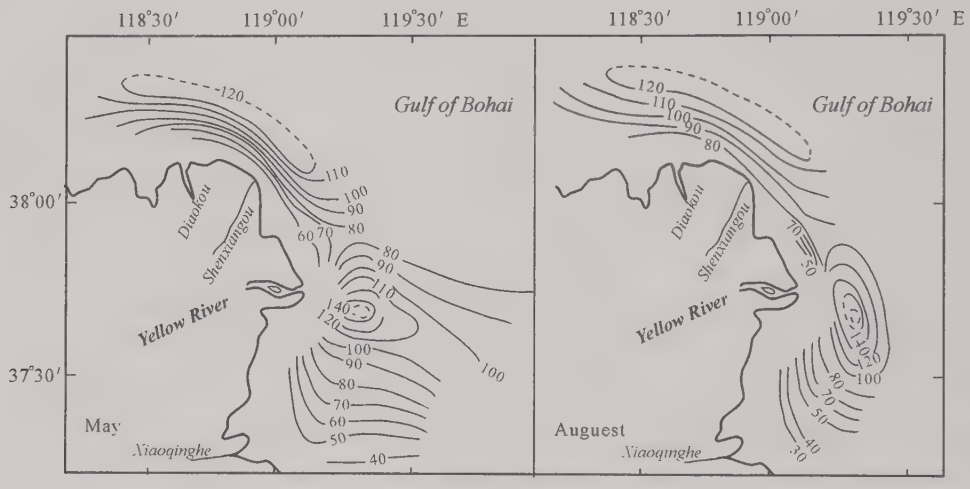

Fig. 4 Current field around the Yellow River delta (after reference 12)

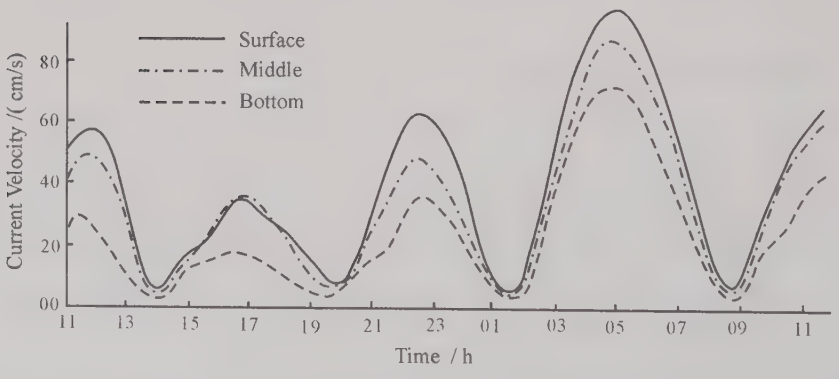

Fig. 5 Current velocity variations in the offshore of Feiyantan

According to the past researches [13], the fine sediment whose median diameter D50 was 0.0017 - 0.07 mm could appear an incipient motion only when the current velocity increased to 36 cm/s. The

statistical results showed that at the Feiyantan coast, the time periods with the bottom velocity larger than 30 cm/s accounted for 30 % of a tidal period, and the grain size of sediment was mainly 0.002 - 0.032 mm. Referring to the stated incipient velocity of sediment, time for current scouring bottom sediment was short. So currents transported mainly the sediment stirred by wave action.

Large current velocities were distributed in the water area from -1 m to -12 m where isobaths were dense and wave breaking or disturbance frequently occurs, which was helpful for tidal currents to transport the sediment stirred by wave. This indicated that the combined action of waves and tidal currents had a great effect on the coastal erosion of Feiyantan.

Asymmetry between ebb and flood currents results in a tide-induced residual current. Besides, residual currents result from various hydrometeorological factors such as winds, waves and currents, etc. Though velocities of residual currents are far smaller than those of tidal currents, they can induce net transportation of water, and, consequently, the fine sediment is transported for a long distance, resulting in the loss of coastal sediment. Calculating the measured data, residual currents of water area in the Feiyantan coast consist of tide-induced residual currents and wind currents. They belong to the offshore current whose velocities are 7 - 14 cm/s and the directions mostly focus on NW—N and aside E. Therefore, tidal currents transporting the sediment to distance mainly depends on residual currents, the coastal erosion is resulted from the loss of coastal sediment.

3 Conclusion

Coastal stability rests with the kinetic balance among sediment supply, hydrodynamics and coastal topography. Since the Diaokou River distributary was abandoned in May 1976, the supply of water and sediment has been cut off, however, ocean dynamics has been strengthened relatively. Accordingly, Feiyantan coast suffered from serious erosion. It was characterized by the following: Retreat rates were in order of mouth spit>shoreline>underwater slope. As time went, retreat rates decreased gradually, convex profiles showing transition to concave profiles. Retreat rates decreased obviously at the underwater slope outside the 10 m isobath, tending to be basically stable.

The dominant cause of the coastal erosion of Feiyantan is the combined action of the wave stirring the sediment and the tidal current transporting the sediment. The strong waves in the directions of NW and NE got to the coast and stirred large amounts of sediment. What's more, the residual currents transported the sediment towards NW—N which is offshore. So the coastal sediment loses, and the coast retreats continually. Considering the continuous strong erosion along the Feiyantan coast, the protection of the coast cannot be ignored.

Acknowledgements

This work was supported by the National Major Basic Research Program of China (grant no.

2002CB412408). The authors would like to acknowledge the contribution of Mr. Jianhua Zhang and Congliang Xu, Yellow River Estuary Survey Bureau of Hydrology and Water Resources, for their help in topographic data.

References

[1] Komar P D. Coastal erosion – underlying factors and human impacts. Shore & Beach, 2000, 68(1): 3-16.

[2] Stanley D J. Nile delta: extreme case of sediment entrapment on a delta plain and consequent coastal land loss. Marine Geology, 1996, 129: 189-195.

[3] Guillén J, Palanque A. A historical perspective of the morphological evolution in the lower Ebro river. Environmental Geology, 1997, 30 (3/4): 174-180.

[4] Yin Yanhong, Zhou Yongqing, Ding Dong. Evolution of modern Yellow River delta. Marine Science Bulletin, 2004, 23(2): 32-40.

[5] Wang Wenhai, Wu Sangyun, Xia Dongxing. The erosional process of the soft shore of China in the recent decades. Chinese Geographical Science, 1994, 4(2): 106-118.

[6] Qian Chunlin. Effects of the water conservancy projects in the Luanhe River basin on Luanhe River delta, Hebei Province. Acta Geographica Sinica, 1994, 4(2): 158-166.

[7] Yang Z S, Milliman J D, Galler J et al. Yellow River's water and sediment discharge decreasing steadily. Eos Transactions, 1998, 79: 589-592.

[8] Li Guang-xue, Yue Shu-hong, Zhao Dong-bo, et al. Rapid deposition and dynamic processes in the modern Yellow Rive mouth. MarineGeology & Quaternary Geology, 2004, 24(3): 29-36.

[9] Ji Zuwen, Hu Chunhong, Zeng Qinghua, et al. Analysis of recent evolution of the Yellow River estuary by landsat images. Journal of Sediment Research, 1994(3): 12-22.

[10] CERC (U S Army Coastal Engineering Research Center). Shore Protection Manual (3rd ed.). U S Government Printing Office, Wahington, D C, 1977.

[11] Li Ping, Zhu Dakui. The role of wave action on the formation of Yellow River delta. Marine Geology & Quaternary Geology, 1997, 17(2): 39-44.

[12] Chinese Editorial Group of Coastal Zone Hydrology. Coastal Zone Hydrology of China. Beijing: Ocean Press, 1995, 178-181.

[13] Sun Lian-cheng. Study on sediment movement at Bayuquan Port area of Yingkou Port. Port & Waterway Engineering, 2000, 317(6): 5-7.

黄河三角洲飞雁滩海岸的侵蚀与机理

陈沈良，张国安，陈小英

（华东师范大学河口海岸学国家重点实验室，上海 200062）

摘　要：飞雁滩海域是 1964—1976 年黄河刁口河流路入海区域。根据地形和断面水深监测资料，阐述了该岸段流路废弃后的岸滩侵蚀特征和地貌变化。研究结果表明，刁口河流路废弃后飞雁滩海岸向海凸出的地形特征，是造成该岸段强烈侵蚀的重要原因。进一步结合波、流动力的对应分析认为，波浪以掀沙为主，潮流以输沙为主，波浪和潮流的联合作用是飞雁滩海岸侵蚀的主要动力机制，其中潮流主要通过余流携沙外输，造成近岸泥沙亏损。

关键词：海岸侵蚀；波浪；潮流；飞雁滩；黄河三角洲

Coastal Current Systems and the Movement and Expansion of Suspended Sediment from Changjiang River Estuary

LI Sihai (李四海)[1,2*], YUN Caixing (恽才兴)[1]

1. *State Key Laboratory of Estuary and Coast Research, Shanghai* 200062, China

2. *National Marine Data and Information Service, Tianjin* 300171, *China*

Abstract: This paper , with NOAA/AHHRR data for 2 years, discusses the expanding path and extent of suspended sediment from the Changjiang River, and the relationship between the suspended sediment expanding and coastal current systems by analyzing the thermal infrared imagery with the sediment imagery, which is acquired by correlating the atmosphere corrected AVHRR imagery with in-situ suspended sediment data. The coastal current systems affecting the sediment dispersal mainly include: the Taiwan Warm Current (TWC), the Huanghai Sea Mixed Water (HSMW), North Jiangsu near-shore current, and Zhejiang near-shore current etc. In winter, the current systems are stable. Their distribution affects the sediment from north Jiangsu expanding toward the Changjiang estuary in some degree .The front between Zhejiang coastal current and TWC blocks the expanding of sediment toward the sea. In the flood season, apart from the limitation by coastal current systems, the spatial and temporal distribution of suspended sediment is also affected by the runoff, which shows as the jet stream and fresh water. Spring and autumn are the transitional periods of the forming of expanding patterns of flood season and winter respectively. In addition, the re-suspended sediment caused by the wind wave may make the expanding range of near-shore sediment larger.

Keywords: NOAA/AVHRR; Changjiang estuary; suspended sediment; coastal current systems

Introduction

The natural environment of Changjiang estuary is an important factor that affects the development of Shanghai, even the whole Changjiang delta. In recent years, with the construction of all kinds of coastal engineering, especially of the Changjiang deep waterway and the Shanghai deep-water harbor, the deposition and scouring of seabed nearby the Changjiang estuary is deeply concerned. Therefore, it is urgent to master the movement and expansion law of the suspended sediment of Changjiang estuary. There are many factors that affect the suspended sediment diffusion. Many scholars have done much

Received on Feb. 20, 2006

* Corresponding author.

study on them using in-situ data or numerical simulation methods, while, because of the difference of research methods and used data, they often got inconsistent conclusions. For example, Mao et al. (1963), LE(1984,1986), and ZHAO(1991) considered that the Changjiang runoff plays a significant role in the flood season. However, PU(1983), GU(1985), WANG et al.(1986), and YU et al.(1990) didn't think so. YUAN et al.(1982), PU(1983), GU(1985), WANG(1986), and ZHAO thought that the Taiwan Warm Current(TWC) is the main factor that influences the northeast turning direction of Changjiang River diluted water(CDW), while, ZHU et al.(1999) got the conclusion through numerical simulation that TWC has very little effect on the expansion of CDW; Additionally, as the impact of wind is concerned, different scholars also have different viewpoints (Mao et al., 1963; Zhao, 1991; GU, 1985; ZHU et al., 1999).

On the study of sediment dispersal,Cai Aizhi confirmed the sediment source of Changjiang estuary and its dispersal direction from a view of estuary morphology and coastal sediment features; Millicon et al., and Berdsley et al., by analyzing the field data, thought that the tide, the runoff , and the coastal circulations are important influencing factors, while, on the relationship between coastal current systems and the dispersal of sediment from Changjiang estuary, there is still lack of research, especially, with the method of remote sensing.

Satellite remote sensing has many advantages over other conventional means, such as wider view field, shorter repeated period, and lower cost etc., which make it suitable for the monitoring of ocean. If the satellite remotely sensed data are combined with the in-situ data, more reliable results can be obtained. In this paper, we, using NOAA/AVHRR data from April, 1997 to April, 1999, and the in-situ suspended sediment concentration in the surface layer of 4 fixed stations, obtained the sediment distribution map by a quantitative retrieved algorithm, and combined it with the temperature imagery to study the correlation between the dispersal of Changjiang suspended sediment and the coastal current systems. Figure 1 is the study area and the in-situ measurement sites.

1 Data and methods

1.1 In-situ data

Sediment water samples in the surface layer were got at 2:00 pm. every day from July 31, 1998 to August 1, 1999 at four fixed stations mentioned above, which were nearly synchronous with the NOAA/AVHRR data. Suspended sediment concentration is determined with filter method in laboratory.

1.2 Remotely sensed data

A set of 45 scenes AVHRR imagery of NOAA-14 were collected. In order to reduce the effect of cloud and atmosphere, some of them with good quality were analyzed and interpreted. AVHRR data includes 5 bands: visible (0.570 - 0.696 μm), NIR (0.716 - 0.986 μm), medium IR (3.0 - 3.5 μm), and thermal IR (10.5 - 11.5 μm, 11.5 - 12.5 μm).

Firstly, we convert the 1 A formatted data to 1B data which has longitude and latitude and other parameters; Secondly, we calibrate the gray values of the visible and NIR bands to reflectance, and do solar zenith correction; we calibrate the thermal IR values to radiance, do border darkening correction, and then convert it to the equivalent bright temperature; Thirdly, we make geometric rectification and projection transformation; At last, we get the reflectance imagery from visible and NIR bands, and the bright temperature imagery from thermal IR bands.

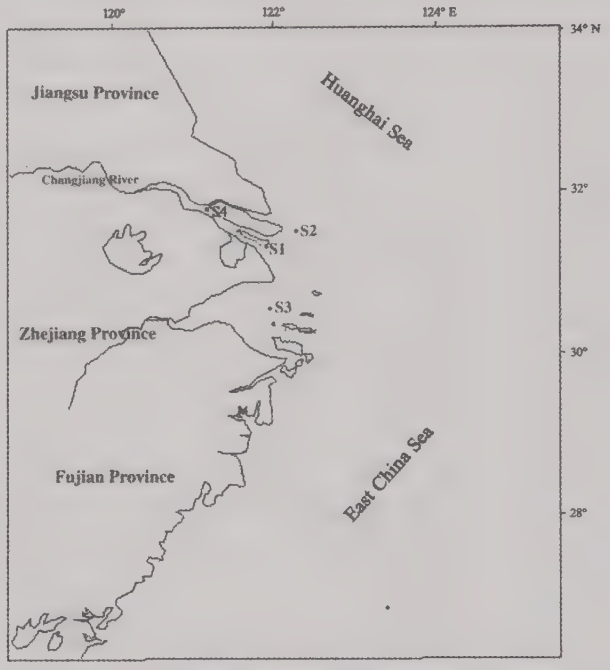

Fig. 1 The study area and in-situ measurement stations (from the map of 1986)

For lack of in-situ sea surface temperature data, we use the bright temperature instead of the sea surface temperature (SST) in the analysis. Because the bright temperature has a very good linear relation with SST, so we can use it to analyze the distribution and changes of SST.

1.3 Quantitative retrieval of suspended sediment concentration in the surface layer

We use the α R1-R2 algorithm based on the slope transmission of the spectral reflectance curve from ocean surface to remote sensor to correct the atmospheric effects on AVHRR visible and NIR bands (LI et al.,1998;1999), and correlate α with 14 in-situ sediment concentration values at 3 stations in 8 different dates (Fig. 2), and get the sediment quantitative retrieval model for the Changjiang estuary: $S < 200$ mg/L, $S = 387.68 \times \alpha + 30.737$, ($R^2 = 0.9177$); $S > 200$ mg/L, $S = 59.833 \times \exp(3.6735 \times \alpha)$, ($R^2 = 0.8357$). After the sediment concentration for each pixel is calculated, the suspended sediment image is output. Sample test shows that the relative error is about 12 %, as seen in Table 1.

Tab. 1 The comparison of suspended sediment concentration in the surface layer from in-situ and retrieval data

Date	Station	The curve of α of R2-R1	In-situ data / mg·L^{-1}	Retrieval data / mg·L^{-1}	Relative error / %
1998. 8. 4	S1	0.289	115.7	158.853	37.2973
	S3	0.341	154.7	197.233	27.4939
	S4	0.3	153	166.294	8.689
1998. 8. 6	S2	0. 3997	227. 8	251.811	7.154
	S3	0.55	470	470.681	0.145
	S4	0.4215	250	275.725	10.29
1998. 8. 9	S2	0. 3848	239. 1	236.67	1.39
	S3	0. 4568	327. 0	319.357	2.337
	S4	0. 1868	140.0	103.819	25.8436
1998.8.10 10	S1	0.333	171.9	190.774	10.9796
	S2	0. 3629	187. 6	216.054	11.945
	S4	0. 3426	265	198.551	25.075
1998. 8. 11	S1	0. 5158	370	408.238	10.335
	S2	0.33	200	188.407	5.796
	S3	0.418	329	271.737	17.405
	S4	0.3	142	180.117	26.843
1998. 8. 24	S2	0. 35	192. 7	216.433	8.76
	S3	0.3188	223.5	192.996	13.6483
	S4	0.4316	270	292.084	8.179
1998.12.21	S2	0.398	297.6	258.168	13.25
	S3	0.612	522	566.649	8.553
1999.1.29	S1	0.08	66	80.2733	21.6262
	S2	0.4842	370.2	354.343	4.2834
	S3	0.4311	361	291.548	19.239
1999.4.7	S1	0.068	59	76.812	30.19
	S2	0.5703	548.7	486.186	11.3931
	S3	0.5329	451	423.759	6.04

Note: Relative error= | Retrieval data−In-situ data | / In-situ data

2 The expansion features of suspended sediment from the Changjiang estuary

Changjiang estuary has 3 grades of branches, the suspended sediment is discharged into sea through

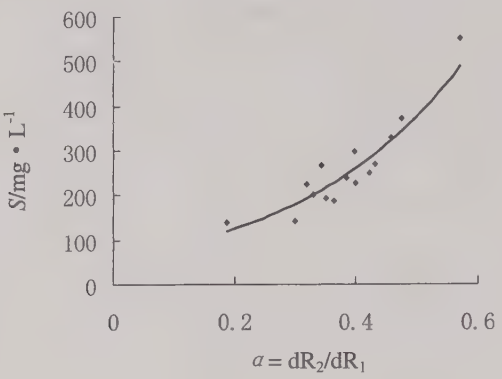

Fig. 2 The curve of α of R2-R1 and in-situ suspended sediment

north branch, north channel, north passage, and south passage (Fig.1). The suspended sediment forms a distinctly step-by-step diffusion and deposition, and the sediment may be divided into four stages: muddy stretch, turbid flow, plumes, and diluted water, in terms of the sediment concentration and expanding extent (YUN et al, 1981; Beardsley et al., 1985; Chente T. et al., 2000). The expansion extent and direction are different in dry and flood seasons. In general, the eastward expansion range doesn't exceed 122° 30′ E (YUN et al., 1981; Molliman et al., 1985; QIN et al., 1982; 1989). There are a lot of factors affecting the suspended sediment expansion. Here, we mainly discuss the effects of coastal current systems on it.

The coastal current systems affecting the sediment expansion mainly include: Taiwan Warm Current (TWC), Huanghai Sea Mixed Water (HSMW), North Jiangsu coastal current, and ZheJiang coastal current. Figure 3 is the typical distribution of coastal current systems outside the Changjiang estuary in winter.

2.1 In winter

The temperature field got from thermal IR bands of AVHRR shows the distribution of them. The relation between the coastal current systems and the suspended sediment expansion may be understood by analyzing the sediment and temperature imagery together. Figure 4-a, b are the processed sediment image and the quantitative sediment extraction result in Feb. 7, 1997. Figure 4-c, d are the temperature image and the extraction result.

As can be seen in Figure 4-c, d, the movement trend of TWC is consistent with the –50 m contour. The high temperature tongue extended to the east sea area of Chongming Island (about 121° 40′ E), a strong temperature front was formed between Jiangsu coastal current and TWC, where exists a bigger temperature and salinity gradient. The TWC with high temperature and salinity strongly blocks the expansion of Changjiang suspended sediment.

North of TWC is the HSCWM, which may extend southeastward to (126° 30′ E, 29° 50′ N), with a width of about 200 km. It has a larger sphere of influence in winter, and drives the suspended sediment to expand southeastward along the Jiangsu coast. YUN et al. (1981) mentioned that there

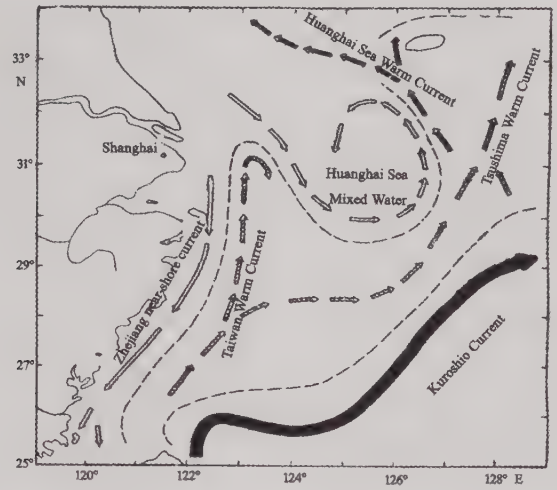

Fig. 3 The typical distribution of coastal current systems outside the Changjiang estuary in winter

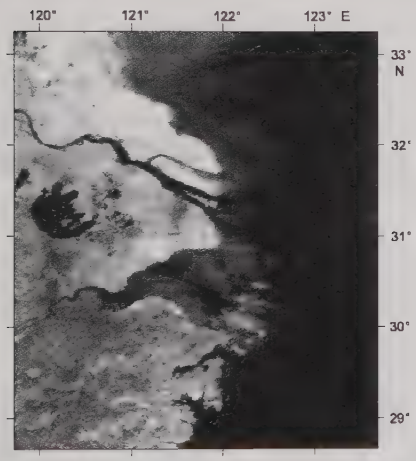

Fig. 4-a Sediment image of Feb.7, 1997

Fig. 4-b Quantitative sediment extraction result of Feb. 7, 1997

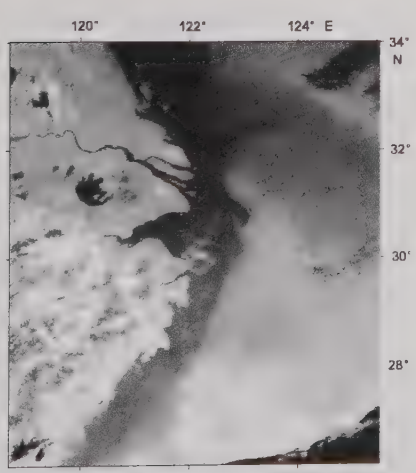

Fig. 4-c Temperature image of Feb.7, 1997

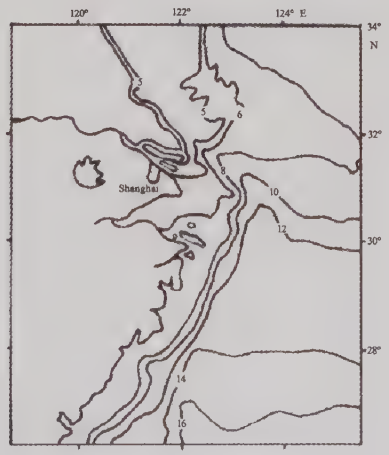

Fig. 4-d The extraction result of temperature of Feb. 7, 1997

existed a stripe of turbid water mass expanding eastward between 32° 00′ — 33° 00′ N, but its cause of formation was not very clear. This water can be found in many sediment images of January—March, 1998. Judging from the temperature imagery, we can conclude that it results from the expansion of north Jiangsu coastal sediment and part of Changjiang estuary sediment drived by the eastward flowing of the mixture of north Jiangsu coastal current, HSCWM, TWC, and Changjiang diluted water.

The confluence of north Jiangsu coastal current, HSCWM and TWC in the sea area east of Chongming Island near the –50 m contour confines the northeastward expansion of suspended sediment.

In winter, the stable coastal currents result in the southwestward diffusion of suspended sediment along the coast of east Zhejiang province.

Affected by the continuous north wind, the suspended sediment of Changjiang estuary may reach the Minjiang River mouth. As the sediment is stirred up by the wind wave, the sediment concentration of Changjiang estuary and Hangzhou Bay is higher in winter than in summer. As seen from Figures 4-b and 5-b, the sediment concentration along the front of turbid water is 170 mg/m^3 and 150 mg/m^3 respectively.

2.2 In Spring

Seen from AVHRR imagery, the power of TWC is gradually weakening. The stretch range has shrinked to the east of Zhoushan archipelago and the temperature fronts between HSCWM and TWC, and between Jiangsu coastal current and TWC are also weakened, while, the expansion extent and direction of Changjiang estuary suspended sediment change little. The turbid water generally begins to turn its direction in the sea area east of Hengsha Island in May—June.

2.3 In Summer

The runoff increases significantly in the flood season, and Changjiang estuary water generally forms a stripe of strong diluted water flow, called the "Changjiang diluted water". Because the density of seawater is greater than fresh water, the diluted water brings along the suspended water to expand seaward in floating form. In the flood season, the diluted water turns to northeast after flowing out of the estuary, and forms a tongue with low salinity. Some scholars have studied the expanding path and cause of the diluted water and put forth many ideas. The factors that have been studied mainly include the Changjiang runoff, coastal current, TWC, wind force, submarine topography, the Huanghai Sea eddy current etc.

After systematically analyzing serial NOAA images of August 1998 and other data(wind, runoff etc.), we consider that the runoff, the front between TWC and HSCWM, and the wind force are the important factors that affect the expanding path and extent. Figures 5-a, b are the processed sediment image and the quantitative sediment extraction result of August, 10, 1998. Figures 5-c, d are the temperature image and the extraction result.

In the summer of 1998, the largest scope of flood since 1954 took place in the whole Changjiang Valley. After the middle ten days of June, the lower reaches of Changjiang River entered the period of plum rain with high precipitation and long duration. After the beginning of August, the rate of discharge

of flood peak increased greatly. The water level of most segments of the river surpassed the historical highest one. There continually appeared the discharge rate larger than 80,000 m^3/s from 3—6 August at the Datong station (3 August, 8.04×10^4 m^3/s; 4 August, 8.15×10^4 m^3/s; 5 August, $8.13\times m^3/s$; 6 August, $8.13\times m^3/s$;XIE et al.,1999). The exceptionally large flood made the runoff increase significantly, and brought about a higher concentration of sediment, and a larger affecting extent of sediment. The turbid water may reach 123° 00′ E, while, judging from the temperature imagery, Changjiang diluted water may extend farther until 123° 58′ E.

We also find from many temperature images that there exist lots of little cold water eddy currents along the front between TWC and HSCWM, which strengthen the expanding ability of the diluted water. Whether the TWC is strong or week affects the intensity of the front between TWC and HSCWM, therefore, it also influences the existence and development of the eddy current. So we think the TWC plays an important role in the expansion of the diluted water. GUO et al., according to the in-situ data, found the cyclonic eddy formed by the cold ascending water. PAN et al. thought that the development of high density water circulation results in the expanding of the plume of the diluted water along the density front between the TWC and the East China Sea high density water. Figure 6 is the condition density distribution of surface and bottom water got from in-situ data, which shows the relation between the TWC and the movement trend of the diluted water. The TWC originating from the Taiwan Straits has a remarkable pushing power northward, the seaward slope is larger along the coast, which is helpful for the northeastward expanding. These conclusions have been verified by the information from remotely sensed data.

In addition, we consider that the wind force is an important factor that affects the turning direction of diluted water and the expansion of suspended sediment through the analysis of remotely sensed imagery. The direction and velocity of wind may cause a bigger change of turbid water range. Continuous strong southeast wind blew from 4-7 August, the velocity on August 6 reached 12m/s, the bottom sediment was strongly stirred, thus causing the sediment to resuspend. Under the action of wind, there appeared an obvious turning direction of turbid water. So the conclusion can be got that the wind force is an important factor for the turning direction of diluted water. Figures 7-a, b, c and figure 5-a are the sediment images of August 3, 6, 11, 10, Figure 7-d is the overlaying result of the front lines of the turbid water. We can see clearly the process of the turning direction from them. Here, we must point out: although the tide is different when the four remotely sensed images were received respectively, we can still discuss the effect of wind on the sediment expanding outside the Changjiang estuary. As the sediment expanding outside the Changjiang estuary is mainly controlled by coastal current systems, we may neglect the effects of the tidal current on it.

2.4 In Autumn

The power of HSCWM and north Jiangsu coastal current strengthen gradually, and the fronts between TWC and them become obvious little by little. The Changjiang runoff decreases. The expanding direction turns to southeast again, and the distribution pattern of winter is coming into being.

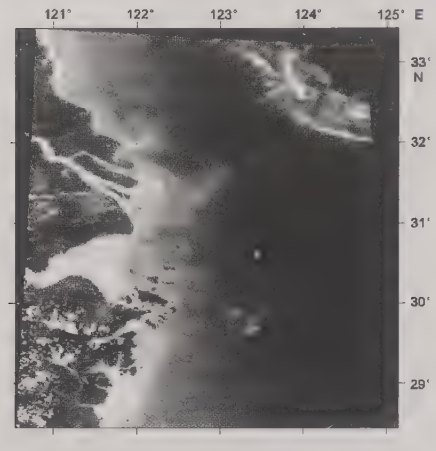

Fig. 5-a Sediment image of Aug.10, 1998

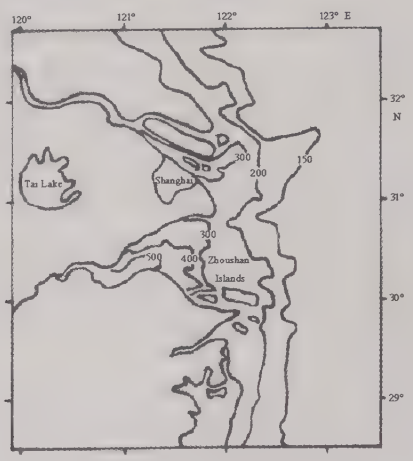

Fig. 5-b Quantitative sediment extraction result of Aug.10,1998

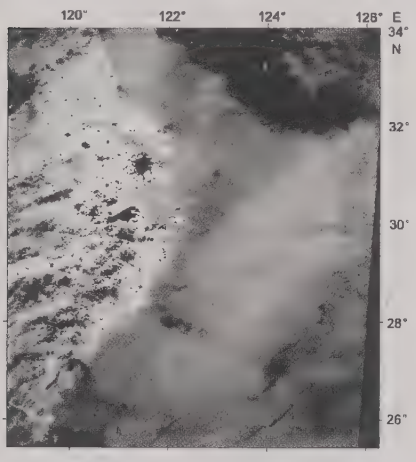

Fig. 5-c Temperature image of Aug.10, 1998

Fig. 5-d The extraction result of temperature of Aug.10, 1998

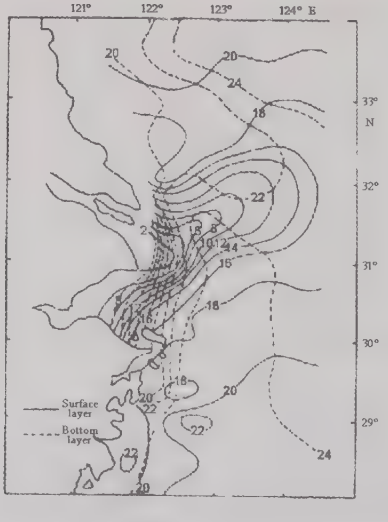

Fig. 6 The condition density distribution of surface and bottom water (PAN,1997)

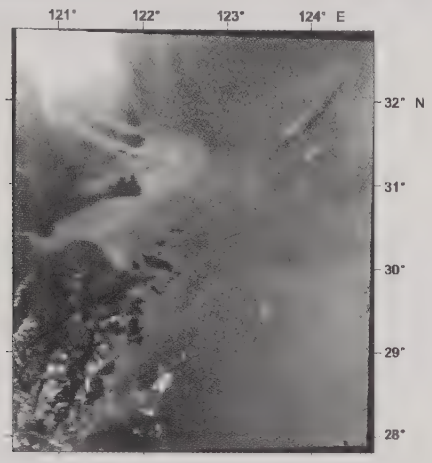

Fig. 7-a Sediment image of Aug.3, 1998

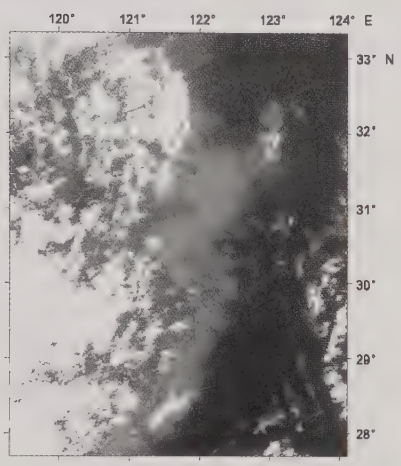

Fig. 7-b Sediment image of Aug.6, 1998

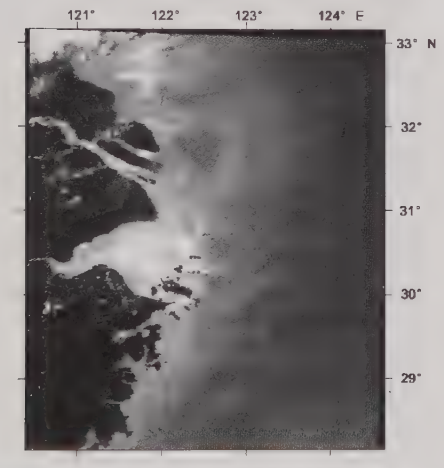

Fig. 7-c Sediment image of Aug.11, 1998

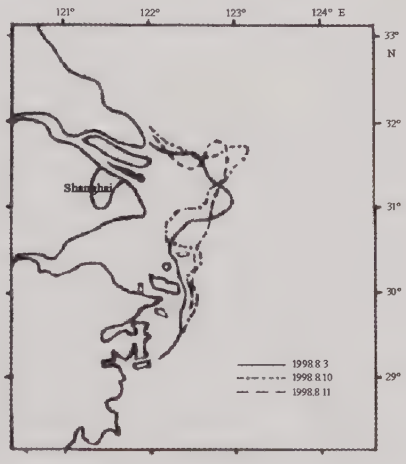

Fig. 7-d The overlaying of the front lines of Aug. 3, 10,11

3 Conclusions

This paper discusses the relation of the expansion of suspended sediment and coastal current systems, and we can get the following conclusions from the results of analysis:

In winter, the distribution of coastal current systems controls the expanding path and extent of the Changjiang suspended sediment. Under the action of partial north wind, the suspended sediment expands southwestward. In the meantime, the resuspending of sediment by the wind wave makes the expanding extent larger, and the concentration higher.

The runoff volume from the Changjiang River affects directly the expanding extent of turbid water and diluted water.

In the flood season, the power of TWC determines the front intensity between HSCWM and it, which influences the forming of eddy current near the boundary of them, so that the expanding path and

extent are also affected.

The wind force is an important factor affecting the suspended sediment expanding.

Acknowledgements

Thanks should go to Professor LIU Jianqiang, National Marine environment Forecast Center, and Professor YANG Xingwei, Meteorological Science Research Institute of Shanghai, for their satellite data. We also express our thanks to Professor LI Yan, the Second Institute of Oceanography, for his help and instructions.

References

[1] Gu Yuhe. A study on the cause of turning direction of Changjiang diluted water, Oceanologia et Limnologia Sinica, 1985, 16(5): 354-363.

[2] Guo Binghuo, Lu Jingming, Lin Kui *et al.* Some features of East China Sea circulation. In: Symposium of Kuroshio investigation and research, Beijing: Oceanography science press, 1987, 15-32.

[3] He Qing, Yun Caixing, Shi Weirong. Remote sensing analysis of surface suspended sediment concentration in the Changjiang estuary. Progress in natural science, 1999(6): 440-446.

[4] Le Kentang. A preliminary study on the path of Changjiang diluted water, I. Pattern. Oceanologia et Limnologia Sinica, 1984, 15(2): 157-167.

[5] Le Kentang. Several problems about the path of Changjiang diluted water. Symposium of oceanography science. Vol.27, Beijing: Science press, 1986, 221-228.

[6] Li Yan, HUANG Wei, FANG ming. An algorithm for the retrieval of suspended sediment in coastal waters of China from AVHRR data. Continental Shelf Research, 1998, 18: 487-500.

[7] Li Yan, Li Jing. An algorithm for the retrieval of suspended sediment from remotely sensed data based on the transmission of the spectral reflectance from ocean surface to remote sensor. Science bulletin, 1999, 44(17): 1 892-1 897.

[8] Mao Hanli, LAN Shufang. A preliminary research on the Changjiang diluted water and its mixture. Oceanologia et Limnologia Sinica, 1963, 5(3): 183-206.

[9] Milliman J D, Shen H, Yanf Z *et al.* Transport and deposition of river sediment in the Changjiang estuary and adjacent continental shelf. Continental Shelf Research, 1985, 4(1): 37-45.

[10] Pan Yuqiu, Wang Kangshan, HUANG Shusheng. An analysis of the transportation and expansion of Changjiang diluted water, Donghai marine science, 1997, 15(2): 25-34.

[11] Pu Yongxiu. A basic analysis of the expansion mechanism of Changjiang diluted water in summer, Donghai Marine Science, 1983, 1(1): 43-51.

[12] Qin Yunshan, Li Fan, Xu Shanmin. A study on the suspending substance in the south Yellow Sea. Oceanologia et Limnologia Sinica, 1989, 20(2): 101-111.

[13] Qin Yunshan, Zheng Tiemin. A preliminary study of the distribution features of depositions on the East China Sea shelf, Geology of Yellow Sea anf East China Sea, Beijing: Science press, 1982, 39-51.

[14] Wang Congmin, Wong Xuechuan. The affect of TWC on the expanding direction of Changjiang diluted water — an application of fuzzy equation, Oceanologia et Limnologia Sinica, 1986, (supplementary issue): 13-19.

[15] Xie Zhixiang, Zhong Xiaozhen. Three whole valley floods in the Changjiang River, Science, 1999, 51(2), 27-31.

[16] Yu Kejun. 2-dimensional numerical calculation of residual current and salinity. Oceanologia et Limnologia Sinica, 1990, 21(1): 92-96.

[17] Yuan Yaochu, SU Jilan, ZHAO Jinshan. A one-layer circulation model of the East China Sea. Acta Oceanologia Sinica, 1982, 4(1): 1-11.

[18] Yun Caixing, CAI Menyi, WANG Baoquang. An analysis of the diffusion of suspended sediment discharged from Changjiang Ruver based on the satellite images. Oceanologia et Limnologia Sinica, 1981, 12(5):392-401.

[19] Zhao Baoren. The mechanism of turning direction for Changjiang diluted water. Acta Oceanologia Sinica, 1991,13(5): 600-610.

[20] Zhao Changhai, YUN Caixing, ZHENG Xinjiang *et al*. A study on the sediment distribution in the Changjiang channel using meteorology satellite imagery. Land resource remote sensing, 1999, 10(1): 15-18.

[21] Zhu Jianrong, XIAO Chengyou, SHEN Huanting. Numerical model simulation of Changjiang diluted water in summer, Acta Oceanologia Sinica, 1998, 20(5): 13-22.

近岸流系与长江入海悬浮泥沙输移扩散

李四海[1, 2] 恽才兴[1]

（1. 华东师范大学河口海岸国家重点实验室，上海 200062；2. 国家海洋信息中心，天津 300171）

摘 要：通过两年较完整的序列 NOAA/AVHRR 数据和实测含沙量资料，利用考虑近岸 II 类水体大气校正的泥沙定量反演算法，获得了较高精度的河口高浓度泥沙遥感反演模式；利用泥沙浓度分级图和反映流系特征的温度图象，系统分析了长江口悬浮泥沙扩散途径、范围及其与近岸流系的关系。影响长江入海悬浮泥沙扩散的近岸流系主要包括台湾暖流、黄海混合水、苏北沿岸流及浙江沿岸流等。冬季，近岸流系比较稳定，其配置状况在一定程度上影响着苏北沿岸泥沙流向长江口的扩散，并制约着入海悬浮泥沙的扩散途径；洪季，长江入海径流量是影响悬浮泥沙扩散的重要因子。同时，长江冲淡水、浙江沿岸流共同形成的冷水区与台湾暖流水之间锋面的强度，也对悬浮泥沙和冲淡水的扩散方向和范围有重要影响；春、秋两季入海悬浮泥沙的扩散型式分别向夏、冬季的分布格局过渡。此外，风应力显著影响着浑水区的扩散方向和范围。风浪掀沙引起的河口泥沙再悬浮，可使近岸泥沙扩散范围增大。

关键词：NOAA/AVHRR；长江口；入海悬浮泥沙；近岸流系

Inactivation Kinetics of β-N-Acetyl-D-Glucosaminidase from Prawn (*Penaeus vannamei*) by Formaldehyde

XIE Xiaolan (谢晓兰)[1, 2], SHI Yan (石 艳)[1], HUANG Qiansheng (黄乾生)[1], CHEN Qingxi (陈清西)[1*]

1. *Key Laboratory of Ministry of Education for Cell Biology and Tumor Cell Engineering, School of Life Sciences, Xiamen University, Xiamen* 361005, *Fujian, China*

2. *Department of Chemistry, Quanzhou Normal University, Quanzhou* 362011, *Fujian, China*

Abstract: β-N-Acetyl-D-glucosaminidase (NAGase, EC.3.2.1.52) is a composition of chitinolytic enzymes and disintegrate dimmer and trimer oligomers of N-acetyl-β-D-glucosamine (NAG) into monomer. Prawn (*P. vannamei*) NAGase is involved in digestion and molting processes. Some pollutants in seawater affect the enzyme activity causing loss of the biological function of the enzyme, which affects the exuviating shell and threatens the survival of the animal. The effect of formaldehyde on prawn (*P. vannamei*) β-N-acetyl-D-glucosaminidase activity for the hydrolysis of pNP-NAG has been studied. The results show that formaldehyde, at appropriate concentrations, can lead to reversible inactivation of the enzyme, and the IC_{50} is estimated to be 1.05 mol • L^{-1}. The inactivation mechanism obtained from Lineweaver-Burk plots shows that the inactivation of the enzyme by formaldehyde belongs to the competitive type. The inactivation kinetics of the enzyme by formaldehyde has been studied using the progress-of-substrate-reaction method described by Tsou, and the rate constants have been determined. The results show that k_{+0} is much larger than k_{-0}, indicating the free enzyme molecule is fragile in the formaldehyde solution.

Keywords: *P. vannamei*; β-N-acetyl-D-glucosaminidase; inactivation; kinetics; formaldehyde

Introduction

Chitin, one of the most abundant organic compounds in nature, is a structural polysaccharide composed of N-acetyl-β-D-glucosamine (NAG) residues. The polysaccharide, sometime referred to as "animal cellulose", is a major component of the crustacean exoskeleton. Crustacean growth and development are achieved by ecdysis, the periodic shedding of the rigid exoskeleton [1]. Three chitinolytic enzymes, exo-chitinase, endo-chitinase and N-acetyl-β-D-glucosaminidase (NAGase, EC 3.2.1.52), are necessary for degradation of chitin to NAG. Chitinases cleave chitin into dimmer and trimer oligomers of NAG, which are further hydrolyzed by NAGase to monomer NAG. In marine species, chitinolytic enzymes, particularly associated with the moulting processes of arthropods and crustaceans, are not only involved in the moulting process but also act as hatching enzymes in brine

Received on Mar. 23, 2006

* Corresponding author. Tel/Fax: +86-592-218 5487, E-mail: chenqx@jingxian.xmu.edu.cn

shrimp [2]. The NAGases from the crustaceans such as Antarctic krill [3, 4], lobster (*Homarus americanus*) [5], fiddler crab (*Uca pugilator*) [6] and Northern shrimp (*Pandalus borealis*) [7] have been reported about their purification, concentrations in different growth stage and distribution in different organs. NAGase from Antarctic krill exists in two isoenzymes which are involved in digestion and molting processes, respectively [3, 4]. Their simultaneous occurrence may indicate a physiological adaptation utilizing a mechanism of altering isoenzyme concentrations. The investigation of enzymatic properties is an essential mission to study physiological adaptations expressed by organisms in response to different environmental conditions. However, the NAGase from prawn (*Penaeus vannamei*) has hardly been known. Recently, we purified a NAGase from prawn and discussed the enzymatic characterization and the effects of metal ions on the enzyme activity [8].

The life environment of prawn is a complex system containing not only lots and lots of necessary organic and inorganic compounds but also all varieties of pollutants such as heavy metal ions or organic solvents and so on. While pollutants are assimilated, the activity and conformation of prawn NAGase can be affected, and growth and survival of the animal is threatened. Formaldehyde is a kind of organic solution widely used in current industry. So formaldehyde is a sort of main organic pollutant. Absorbing superfluous formaldehyde might induce various forms of distant-site toxicity [9]. It is very important to research the influence of formaldehyde solvents on the enzyme activity and the enzyme performance change in formaldehyde solvents. No information is available on the effects of formaldehyde on the NAGase activity. In our investigation, we found that the prawn NAGase activity could be affected by formaldehyde, and the inactivation of the enzyme in formaldehyde solutions was showed to be reversible. The aim of this paper is, therefore, to carry out a kinetics study on the inactivation of NAGase in the formaldehyde solvent. It is of great significance to inspect the pollution of the breeding aquatic environment by applying a high delicacy of enzyme to organic solvents.

1 Materials and methods

1.1 Materials

Preparation of prawn NAGase (EC3.2.1.52) was as described previously [8]. The crude preparation was further chromatographed on a Sephadex G-100 column following on the DEAE-cellulose column. The final preparation was homogeneous on PAGE and SDS-PAGE. *p*-Nitrophenyl-N-acetyl-β-D-glucosaminide (pNP-NAG) was purchased from the Biochemistry Lab of Shanghai Medicine Industry Academy (China). Sephadex G-100 was Pharmacia products. DEAE-cellulose (DE-32) was from Whatman. Formaldehyde and all other reagents were local products of analytical grade. The water used was re-distillated and ion-free.

1.2 Assay methods

Enzyme concentration was measured by the Lowry method [10] (Lowry et al., 1951). Enzyme activity was determined at 37 °C by following the increasing absorbance at 405 nm accompanying the hydrolysis of the substrate (pNP-NAG) [11]. A portion of 10 μl of enzyme solution was added to the

reaction media (2.0 mL) containing 0.5 mmol·L^{-1} pNP-NAG in 0.1 mol·L^{-1} sodium phosphate buffer (pH6.2). Absorption was carried out using a Beckman UV-650 spectrophotometer. The pNP molar absorption coefficient was determined to be of 5.22×10^3 mol^{-1}·L·cm^{-1} at pH 6.2 condition.

1. 3 Microscopic inactivation rate constants of the enzyme

The progress-of-substrate-reaction theory previously described [12, 13] was applied to the current study of the inactivation kinetics of prawn NAGase by formaldehyde. In this method, 10 μl of enzyme (2.13 μmol·L^{-1}) was added to 2.0 ml of assay system containing different concentrations of substrate in 0.1 mol·L^{-1} sodium phosphate buffer (pH 6.2) with different concentrations of formaldehyde. The substrate reaction progress curve was analyzed to obtain the reaction rate constants as detailed below. The reaction was carried out at a constant temperature of 37 °C. The time course of hydrolysis of the substrate in the presence of different formaldehyde concentrations showed that, at each concentration of formaldehyde, the rate decreased with increasing time until a straight line was approached. The results showed that the inactivation reaction was a reversible reaction with fractional residual activity. This can be written as [13, 14]:

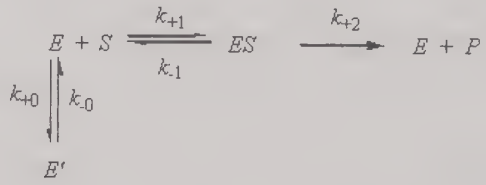

E, *E*′, *S* and *P* denote native enzyme, denatured native, substrate, formaldehyde and product, respectively; *ES* are enzyme-substrate compounds. The product formation can be written as [14]:

$$[P]_t = \frac{Bv}{A+B}\cdot t + \frac{Av}{(A+B)^2}(1-e^{-(A+B)\cdot t}) \quad (1)$$

$$A = \frac{k_{+0}\cdot K_m}{K_m + [S]} \quad (2)$$

$$B = k_{-0} \quad (3)$$

where [*P*]t is the concentration of the product formed at the time *t*, which is the reaction time; *A* and *B* are the apparent rate constants for the forward and reverse reactions of inactivation, respectively; [*S*] are the concentrations of the substrate; *v* is the initial rate of reaction in the absence of formaldehyde, and $v = \frac{V_m\cdot[S]}{K_m+[S]}$. When *t* is sufficiently large, the curves become straight lines and the product concentration is written as [*P*]calc:

$$[P]_{calc} = \frac{Bv}{A+B}\cdot t + \frac{Av}{(A+B)^2} \quad (4)$$

Combining Eqs. (1) and (4) yields

$$[P]_{calc} - [P]_t = \frac{Av}{(A+B)^2} \cdot e^{-(A+B)\cdot t} \quad (5)$$

$$\ln([P]_{calc} - [P]_t) = -(A+B)\cdot t + \text{constant} \quad (6)$$

where $[P]_{calc}$ is the product concentration to be expected from the straight-line portions of the curves as calculated from Eq. (4) and $[P]_t$ is the product concentration actually observed at the time t. Plots of $\ln([P]_{calc}-[P]_t)$ versus reaction time (t) give a series of straight lines at different concentrations of formaldehyde with slopes of -(A+ B). From Eq. (4), a plot of $[P]_{calc}$ against time, t, gives a straight line with a slope of $\frac{Bv}{(A+B)}$. According to the values of $\frac{Bv}{(A+B)}$ and (A + B) gotten from the above plots, and $v = \frac{V_m \cdot [S]}{K_m + [S]}$ obtained from experiment of the substrate reaction in the absence of formaldehyde at different substrate concentrations, A and B can be obtained. The rate constant $k_{-0} = B$ can be easily determined.

Combining Eq. (2) and $v = \frac{V_m \cdot [S]}{K_m + [S]}$, we can get

$$\frac{A}{v} = \frac{K_m \cdot k_{+0}}{V_m} \cdot \frac{1}{[S]} \quad (7)$$

A plot of A/v versus 1/[S] gives a straight line with $\frac{K_m \cdot k_{+0}}{V_m}$ as the slope of the straight line, which passes through the origin. As K_m and V_m are known quantities from measurements of the substrate reaction in the absence of formaldehyde at different substrate concentrations, the rate constant k_{+0} can be easily determined.

2 Results

2.1 Determination of the kinetic parameters of the enzyme

The kinetic behavior of NAGase in catalyzing the hydrolysis of pNP-NAG was studied. Under the condition employed in the present investigation, the hydrolysis of pNP-NAG by NAGase follows Michaelis-Menten kinetics (the inset of Fig. 1). The kinetic parameters for NAGase obtained from a Lineweaver-Burk plot (Fig. 1) showed that K_m was equal to 0.182 mmol·L^{-1} and V_m was equal to 17.12 μmol·L^{-1}·min^{-1}.

2.2 Effect of formaldehyde on the enzyme activity

The effect of formaldehyde on the hydrolysis of pNP-NAG by prawn NAGase was first studied.

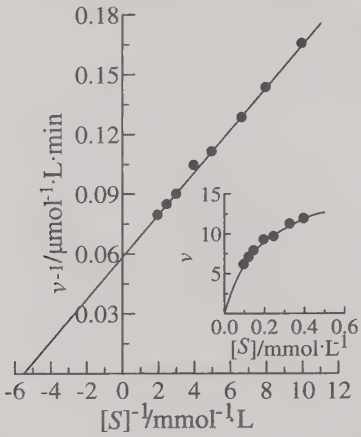

Fig. 1 Lineweaver-Burk plot for the determination of K_m and V_m for NAGase on the hydrolysis of pNP-β-D-GlcNAc. Conditions were 2 mL system containing 0.1 mol • L^{-1} sodium phosphate buffer (pH6.2) at 37 °C. The enzyme final concentration was 0.01 μmol • L^{-1}. The inset showed the relationship between the intial rate and the substrate concentration.

The relationship between the residual enzyme activity and the concentrations of formaldehyde was shown in Fig. 2. The effect of formaldehyde on the enzyme was concentration dependent. The residual enzyme activity rapidly decreased with the increasing concentrations of formaldehyde. The formaldehyde concentration leading to the loss of 50 % activity (IC_{50}) was estimated to be 1.05 mol·L^{-1}. The inactivation mechanism of formaldehyde on the enzyme was studied. Fig. 3 showed the relationship of enzyme activity with its concentration in the presence of different concentrations of formaldehyde. The plots of the remaining enzyme activity *versus* the concentrations of enzyme in the presence of different concentrations of formaldehyde gave a family of straight lines, which all passed through the origin.

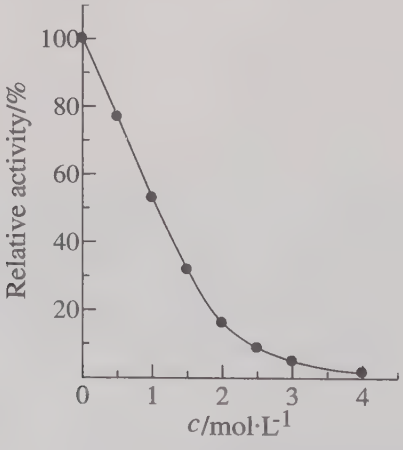

Fig. 2 Inactivation of the enzyme in different concentrations of formaldehyde solutions. Assay conditions were as described for Fig.1 except that the substrate concentration was 0.5 mmol • L^{-1}.

Increasing the formaldehyde concentration resulted in the descending of the line slope, indicating that the inactivation of formaldehyde on the enzyme was reversible. The presence of formaldehyde did not bring down the amount of the efficient enzyme, but just resulted in the inactivation and the descending of the activity of the enzyme.

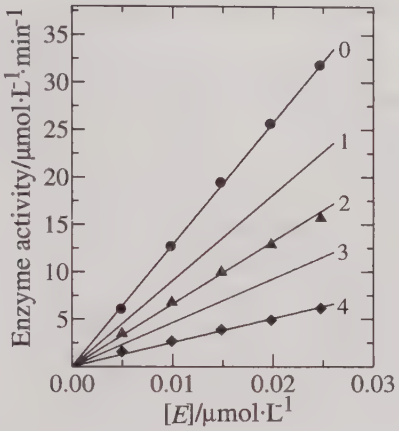

Fig. 3 Effects of the enzyme concentration on its activity at different concentrations of formaldehyde. The concentrations of formaldehyde for curves 0-4 were 0, 0.5, 1.0, 1.5 and 2.0 mol·L^{-1}, respectively. Assay conditions were the same as in Fig.2.

2.3 Determination of the inactivation type of formaldehyde on the enzyme

In the presence of formaldehyde, the inactivation kinetics of the enzyme was showed in Fig. 4 as the plots of Lineweaver-Burk. The results showed that the inactivation of formaldehyde on the enzyme

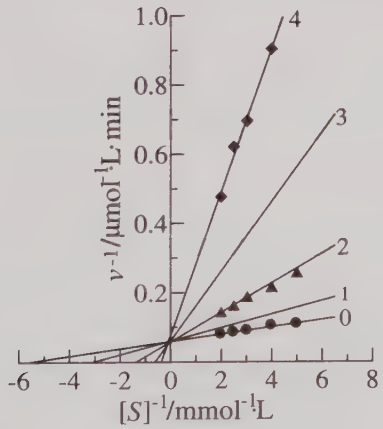

Fig. 4 Lineweaver-Burk plots for the hydrolysis of pNP-β-D-GlcNAc by the enzyme in different concentrations of formaldehyde. The formaldehyde concentration for lines 0-4 was 0, 0.5, 1.0, 1.5 and 2.0 mol • L^{-1}, respectively. The assay conditions were the same as Fig.1.

was a competitive type since increasing the formaldehyde concentration resulted in a family of lines with different slope and same intercept. This behavior observed indicated that only free enzyme inactivated in formaldehyde solution, and the enzyme-substrate complex was not affected by formaldehyde. Substrate had a protective function for enzyme in the formaldehyde solution.

2.4 Kinetics of the substrate reaction in the presence of different concentrations of formaldehyde

The temporal variation of the product concentration during the substrate hydrolysis in the presence of different formaldehyde concentrations is shown in Fig. 5a. At each concentration of formaldehyde, the rate decreases with the increasing time until a straight line is approached, the slope of which decreases with increasing formaldehyde concentration. The results as analyzed by Tsou's method [12], suggest that the denatured NAGase still has partial residual activity (curves 1-4). According to Eq. (6), plots of $\ln([P]_{calc} - [P]_t)$ versus t give a series of straight lines shown in Fig. 5b.

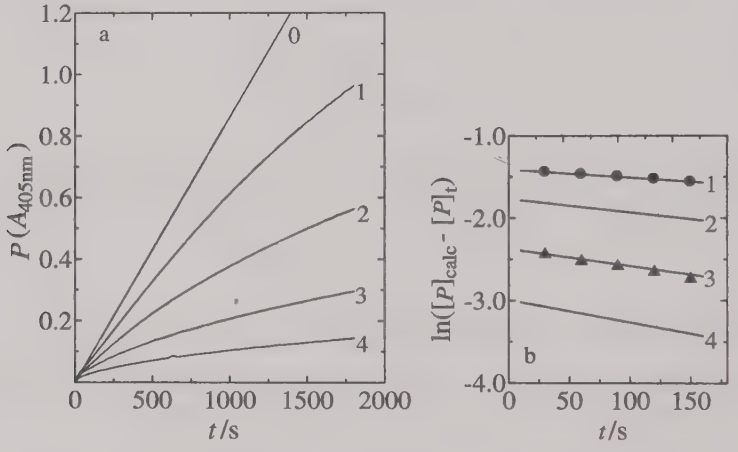

Fig. 5. Course of inactivation of enzyme in different concentrations of formaldehyde. The assay conditions were the same as in Fig. 1 with the exception of 0.4 mmol·L^{-1} pNP-β-D-GlcNAc. (a) Substrate reaction course. The final formaldehyde concentrations for curves 0-4 were 0, 0.5, 1.0, 1.5, and 2.0 mol·L^{-1}, respectively. (b) Semilogarithmic plots of $\ln([P]_{calc}-[P]_t)$ against time. Data were taken from curves 1-4 in (a).

2.5 Kinetics of the reaction at different substrate concentrations in the presence of formaldehyde

Fig. 6a showed the kinetic courses of the reaction at different substrate concentrations in the presence of 1.0 mol·L^{-1} formaldehyde. It can be seen from Fig. 6a that when t is sufficiently large, both the initial rate and the slope of the asymptote increase with the increasing substrate concentration. Similarly, plots of $\ln([P]_{calc} - [P]_t)$ versus t give a family of straight lines at different concentrations of the substrate with slopes of $-(A + B)$ as shown in Fig. 6b.

2.6 Determination of the microscopic rate constants of inactivation of the enzyme by formaldehyde

The kinetic course of the hydrolysis reaction at different substrate concentrations in the presence of

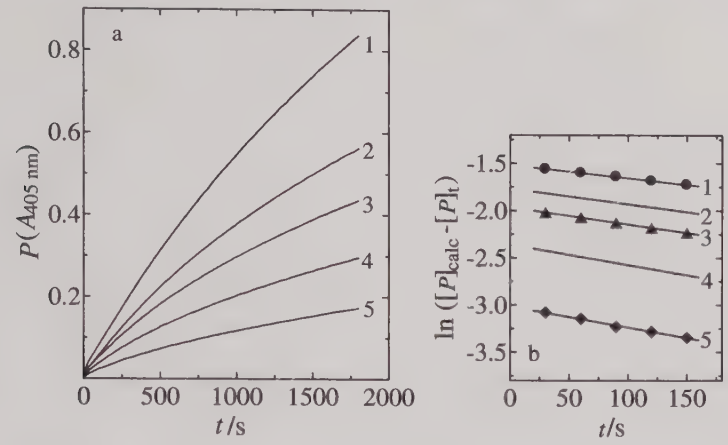

Fig. 6 Determination of the inactivation rate constants for enzyme inactivation in 1.0 mol·L-1 of formaldehyde solution. (a) Substrate reaction courses of the enzyme. Curves 1-5 are progress curves with 0.50, 0.40, 0.33, 0.25 and 0.20 mmol·L-1 of substrate, respectively. The assay conditions were the same as Fig. 1. (b) Semilogrithmic plot of ln ($[P]_{calc} - [P]_t$) against time. Data were taken from curves 1-5 in (a).

formaldehyde was studied. When the time is sufficiently large, a straight line is approached at each concentration of substrate. From Eq. (4), a plot of $[P]_{calc}$ against time t gives a straight line with a slope of $B \cdot v/(A + B)$. Both the initial rate and the slope of the asymptote $(\frac{Bv}{A+B})$ increase with the increasing substrate concentration (Fig. 6a). From Eq. (6), plots of $\ln([P]_{calc} - [P]_t)$ versus t give a series of straight lines at different concentrations of substrate, whose slopes are equal to the apparent rate constant $(A + B)$ (Fig. 6b). According to the values of $\frac{Bv}{(A+B)}$ and $(A + B)$ obtained from the above plots, and v obtained from the experiment on the substrate reaction in the absence of formaldehyde at different substrate concentrations, A and B can be calculated.

According to B values as calculated above, plots of B versus $[S]$ at different formaldehyde concentrations give a series of straight lines shown in Fig. 7. The result showed that all lines paralleled the X-axis, indicating the value of B was not affected by the substrate concentrations. The value of B, equal to the microscopic rate constant, k_{-0}, was determined and the results were given in Tab. 1.

From Eq. (7), a plot of $\frac{A}{v}$ versus $1/[S]$ gives a series of straight lines which passes through the origin, Fig. 8, where the slope gives the value of $\frac{k_{+0} \cdot K_m}{V_m}$, which were used to determine the inactivation rate constants k_{+0}. These rate constants were also shown in Tab. 1.

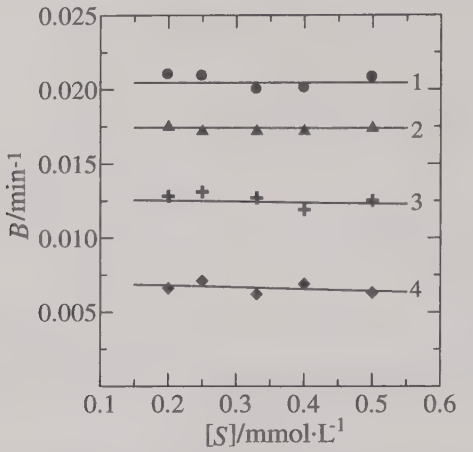

Fig. 7 Plot of *B* versus [*S*]. The final formaldehyde concentration for curves *1-4* are 0.5, 1.0, 1.5 and 2.0 mol·L^{-1}, respectively.

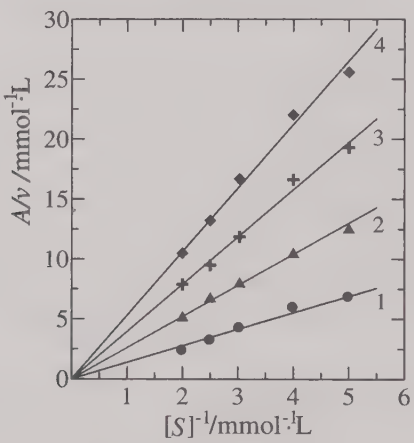

Fig. 8 Plot of *A*/*v* versus 1/[*S*]. The final formaldehyde concentration for curves *1-4* are 0.5, 1.0, 1.5 and 2.0 mol·L^{-1}, respectively.

Tab. 1 Microscopic Rate Constants of the Inactivation of *P. vannamei* NAGase in Formaldehyde Solutions

c(formaldehyde) / mol·L^{-1}	Rate constants / × 10^3 s^{-1}		Residual activity / %
	k_{+0}	k_{-0}	
0	0	0	100.0
0.5	2.16±0.25	0.35±0.05	76.9±0.80
1.0	4.07±0.30	0.29±0.02	52.9±0.45
1.5	6.18±0.45	0.21±0.025	31.8±0.30
2.0	8.31±0.30	0.11±0.02	16.1±0.15

3 Discussion

Enzymes and proteins in organic solvents have received more and more attention in the past decade, and some novel properties have been reported while enzymes work in organic solvents, which benefit both biotechnology and pharmaceutical industry. Formaldehyde can chiefly modify the amino groups in protein in acidic condition [15]. Lin et al reported formaldehyde could modify the amino groups of *T. cornutus* NAGase [16]. The chemical modification of formaldehyde on the enzyme induced enzyme inactivation, which showed the amino group was the enzyme's functional group [16]. When the amino groups of the protein are modified, the protein conformation and its function may change and easily induces disease or endangers the animal's survival. The investigation of the effect of formaldehyde on the prawn NAGase is of important significance for breeding *Penaeus vannamei*.

However, the inactivation of *Penaeus vannamei* NAGase in the formaldehyde solution has not been investigated. In order to further study its inactivation mechanism in detail, the present paper investigates the inactivation kinetics of the enzyme activity by formaldehyde. The results indicate that formaldehyde is a competitive inactivator of the enzyme, which is different from dioxane. The inactivation mechanism of enzyme in the dioxane solution is a mixed type [17]. Formaldehyde can only bind with the native enzyme and can not bind with the enzyme-substrate. High concentration substrate can protect the native enzyme from inactivation in the formaldehyde solution. Formaldehyde is widely used in current industry. The increasing content of formaldehyde in breed seawater from industrial pollution thus could affect the growth and reproduction of prawns, which are an important economic marine animal nowadays. The studies in this field are carried out in our lab and have got some interesting positive evidences, which will be valuable to the seawater aquiculture of other marine economic animals against pollutants.

Acknowledgments

This work was supported by the Scientific and Technological Innovation Fund for the Young Scholars of Fujian Province (No. 2004J054) and Plan Project of the Education Bureau of Fujian Province (No. JA04260).

References

[1] Zou E, Fingerman M. Effects of Estrogenic Agents on Chitobiase Activity in the Epidermis and Hepatopancreas of the Fiddler Crab, *Uca pugilator*. Ecotoxicol. Environ. Safety, 1999, 42B: 185-190.

[2] Funke B, Spindler K D. Characterization of chitinase from the *Brine Shrimp artemia*. Comp. Biochem. Physiol., 1989, 94B: 691-695.

[3] Peters G, Saborowski R, Mentlein R et al. Isoforms of an N-Acetyl-β-D-glucosaminidase from the Antarctic krill, *Euphausia superba*: purification and antibody production. Comp. Biochem. Physiol., 1998, 120B: 743-751.

[4] Peters G, Saborowski R, Buchholz F et al. Two distinct forms of the chitin-degrading enzyme N-Acetyl-β-D-glucosaminidase in the Antarctic krill: specialists in digestion and moult. Mar. Biol., 1999, 134: 697-703.

[5] Lynn K R. Chitinases and chitobiases from the American lobster (*Homarus americanus*). Comp. Biochem. Physiol., 1990, 96B: 761-766.

[6] Zou E, Fingerman M. Chitobiase activity in the epidermis and hepatopancreas of the fiddler crab *Uca pugilator* during the molting cycle. Mar. Biol., 1999, 133: 97-101.

[7] Esaiassen M, Myrnes B, Olsen R L. Isolation and substrate specificities of five chitinases from the Hepatopancreas of Northern shrimp, *Pandalus borealis*. Comp. Biochem. Physiol., 1996, 113B: 717-723.

[8] Xie X L, Chen Q X, Lin J C et al. Purification and some properties of β-N-Acetyl-D-glucosaminidase from prawn (*Penaeus vannamei*). Mar. Biol., 2004, 146: 143-148.

[9] Heck H.d'A, Casanova M. The implausibility of leukemia induction by formaldehyde: a critical review of the biological evidence on distant-site toxicity. Regul. Toxicol. Pharm., 2004, 40: 92–106.

[10] Lowry O H, Rosebrough N J, Farr A L et al. Protein measurement with the Folin phenol reagent. J. Biol. Chem., 1951, 193: 265-269.

[11] Kono M, Matsui T, Shimizu C et al. Purifications and some properties of chitinase from the liver of a prawn, *Penaeus japonicus*. Agric. Biol. Chem., 1990, 54: 2 145-2 147.

[12] Tsou C L. Kinetics of substrate reaction during irreversible modification of enzyme activity. Adv. Enzymol. Related Areas Mol. Biol., 1988, 61: 381-436.

[13] Chen Q X, Zhang W, Zheng W Z et al. Comparison of inactivation and unfolding of green crab (*Scylla serrata*) alkaline phosphatase during denaturation by guanidinium chloride. J. Protein. Chem., 1996, 15: 359-365.

[14] Zhou X W, Zhuang Z L, Chen Q X. Kinetics of inhibition of green crab (*Scylla serrata*) alkaline phosphatase by sodium (2,2"-bipyridine) oxodiperoxovanadate. J. Protein Chem., 1999, 18: 735-740.

Zhang H, Huang X, Fukamizo T et al. Site-directed mutagenesis and functional analysis of an active site tryptophan of insect chitinase. Insect Biochem. Mol. Biol., 2002, 32: 1 477-1 488.

[15] Lin J C, Chen Q X, Shi Y et al. The chemical modification of the essential groups of β-N-acetyl-D-glucosaminidase from *Turbo cornutus* Solander. IUBMB Life, 2003, 55: 547-552.

[16] Xie X L, Chen Q X. Inactivation Kinetics of β-N-Acetyl-D-glucosaminidase from Prawn (*Penaeus vannamei*) in Dioxane Solution. Biochem. (Moscow), 2004, 69: 1 675-1 682.

甲醛对南美白对虾(*Penaeus vannamei*) β-N-乙酰-D-氨基葡萄糖苷酶的失活动力学研究

谢晓兰[1,2]，石 艳[1]，黄乾生[1]，陈清西[1]

(1. 细胞生物学与肿瘤细胞工程教育部重点实验室，厦门大学生命科学学院，福建 厦门 361005；
2. 泉州师范学院化学系，福建 泉州 362000)

摘 要：β-N-乙酰-D-氨基葡萄糖苷酶与南美白对虾的食物消化吸收、蜕壳生长有着密切关系。海水里存在的有机污染物将影响酶生理功能，从而进一步影响虾的正常蜕壳，严重将导致对虾的死亡。甲醛是常用的有机溶剂，故本文应用动力学方法研究了南美白对虾 β-N-乙酰-D-氨基葡萄糖苷酶在甲醛溶液中以 pNP-NAG 为底物时酶活力的变化规律。表明酶在甲醛浓度低于 2.0 mol·L^{-1}，酶的失活过程是可逆的，测得甲醛对酶抑制的 IC_{50} 为 1.05 mol·L^{-1}。用双倒数作图法测定甲醛对酶的抑制类型，结果显示甲醛是酶的竞争性抑制剂，甲醛只能与游离酶(E)结合，底物对酶的失活具有保护作用。用底物反应动力学方法观测在不同底物浓度下酶在 0.0、0.5、1.0、1.5、2.0 mol·L^{-1} 的醋酸酐溶液中的失活过程，分别测定了酶的微观失活速度常数 k_{+0} 及复活速度常数 k。并加以比较，结果表明甲醛对酶的影响是缓慢结合同时导致失活的过程，比较微观失活速度常数 k_{+0} 及复活速度常数 k_{-0}，结果暗示在高浓度的甲醛溶液中，酶将完全失活。

关键词：南美白对虾；β-N-乙酰-D-氨基葡萄糖苷酶；失活；动力学；甲醛

Isolation of Denitrifying Bacteria in Sea Sediment and Simulated Experiment of Removing Nitrate-N from Seawater

QUAN Weimin (全为民)[1*], SHEN Xianqiang (沈新强)[1], GAN Juli (甘居利)[2],
SHEN Xiaosheng (沈晓盛)[1], CHEN Yaqu (陈亚瞿)[1]

1. *Key and Open Laboratory of Marine and Estuarine Fisheries, Ministry of Agriculture, East China Sea Fisheries Research Institute, Chinese Academy of Fisheries Sciences, Shanghai* 200090, *China;*
2. *Key and Open Laboratory of Fisheries Ecological Environment, Ministry of Agriculture, South China Sea Fisheries Research Institute, Chinese Academy of Fisheries Sciences, Guangzhou* 510300, *China*

Abstract: The objective of this research was to isolate denitrifying bacteria from sea sediment and simulate the removal efficiency of nitrate-N by denitrifying bacteria from seawater. The result showed that the isolated denitrifying bacteria could effectively remove nitrate-N from seawater. About 90 % of nitrate-N was removed by denitrifying bacteria from seawater within a week in the simulated experiment I (the initial concentration of nitrate-N was 100 mg/L). The removal efficiency of nitrate-N reached about 70 % within one day in the simulated experiment Ⅱ (initial concentration of nitrate-N was 1 mg/L). The final removal efficiency was about 98 % and 85 % in the simulated experiments I and Ⅱ, respectively. It was found that there was positive correlation between the concentration of nitrate-N and the number of denitrifying bacteria in seawater. Lots of denitrifying bacteria would disappear and the seawater would become transparent once the process of bioremediation was completed.

Keywords: Denitrifying bacteria; Bioremediation; Nitrate-N; Removal

In last decades, with the fast economic development and accelerating urbanization as well as the development of mariculture in the coastal area, the coastal ecosystem became more and more polluted as a result of large input of contaminants, which has become an international environmental problem [1]. In the 1980s, petroleum leaking led to the serious pollution of beach in Alaska, USA. EPA obtained success in reducing the petroleum pollution by use of bioremediation technique. After that, the bioremediation technique provided new chance and hope for the human to reduce and prevent marine pollution [2]. At present, it is mainly used to reduce the following marine contamination: polycyclic aromatic hydrocarbon (PAHs), petroleum, pesticide, organic chemical, red tides et al. However, the study on bioremediation of nitrogen and phosphorus pollution was very few in the estuarine and coastal areas thus far [2-5].

Recent monitoring result showed that the concentration of nitrogen and phosphorus was very rich in the Changjiang River estuary and its adjacent East China Sea, especially high Nitrate-N, which

Received on Oct. 9, 2005

* Corresponding author. E-mail: quanweim@163.com

accounted for about ninety percent of the total inorganic nitrogen and led to serious eutrophication of coastal ecosystem [6, 7]. Therefore, the bioremediation technique for inorganic nitrogen pollution should be one of the most important and preferential research items in the coastal area. It is well known that microbe plays an important role in the biogeochemical process of nitrogen. For example, nitrification-denitrification process is the key mechanism of nitrogen release in the soil and wetland. In the biological denitrification process, denitrifying bacteria convert nitrate into harmless nitrogen gas and small amounts of nitrous and nitric oxides using a cascade of anaerobic respiration processes [8]. Based on the above-mentioned principle, some researchers proposed to remove nitrate-N and purify the polluted water by the immobilized denitrifying bacteria technique. At present, biological denitrification has been used successfully in removing nitrate-N from wastewater and enclosure of freshwater lakes, and the removal efficiency of nitrate-N is also very high [8-10]. The objectives of this study were 1. to isolate the denitrifying bacteria from sea sediment, and 2. to simulate the removal efficiency of nitrate-N by isolated denitrifying bacteria from seawater.

1 Materials and methods

1.1 Isolation of denitrifying bacteria

We made a field survey and obtained a sediment sample in the Changjiang River estuary on May, 2004. The sediment sample was freezed and returned to the laboratory. Three isolated culture devices and the medium of denitrifying bacteria were prepared in advance. The isolated devices included a triangle flask and a ferment pipe. About 1 g fresh sediment was put into two denitrifying devices, respectively. Another denitrifying equipment was the control without addition of any fresh sediment. Then, the medium of denitrifying bacteria was added to the bottle-neck of the triangle flask. About 2 mL 20 % KOH was dropped into the top of the ferment pipe. It was used to absorb the dioxide carbon which was produced in the process of bacteria growth. At once, the triangle flask was airtight with the glum stopper. The flask was cultured in a constant-temperature incubation box at 30 ℃. After seven days, 1 mL incubated liquid was taken out and inoculated in the fresh medium. After three repeats, the incubated liquid was used as denitrifying bacteria solution in the experiment. The method of the denitrifying bacteria isolation was described in detail by Li B D et al (1996) [11].

The medium of denitrifying bacteria contained the following ingredients (g/L): Potassium Nitrate(KNO_3, pour analyses), 2.0; Magnesium Sulfate ($MgSO_4 \cdot 7H_2O$, pour analyses), 0.03; Dibasic Potassium Phosphate (K_2HPO_4, pour analyses), 0.5; Kalium-Natrium-Tartrat ($C_4H_4O_6KNa \cdot 4H_2O$, pour analyses), 20; Sodium Chloride (NaCl, pour analyses), 5. The pH of the medium was adjusted to 7.5. At once, the medium was sterilized in a high voltage autoclave for 2 h.

1.2 Simulated experiment

Experiment I 143mL high-saline seawater (saline: 35; nitrate-N: 0.100 mg/L) was diluted to 1 000 mL by use of distilled water, which makes the salinity of seawater reduce to about 5. 0.7218 g

KNO_3 was dissolved into 1 L seawater. The initial concentration of nitrate-N is 100 mg/L. At once, the solution was split into four triangle flasks (250 mL) equally. 5 mL denitrifying bacterial solution was added into each flask among three flasks. But no denitrifying bacterial solution was added into the control. The flask was incubated in ambient temperature. Each day the concentration of nitrate-N and the growth of denitrifying bacteria were determined.

Experiment Ⅱ The experiment procedure was the same as the experiment I. But the initial concentration of nitrate-N is 1 mg/L in seawater. Each time only 1ml denitrifying bacteria solution was added into the experimental seawater.

Analytical methods Nitrate-N was determined by the Zn-Cd deoxidization method. The growth of denitrifying bacteria was measured with the absorbed light value (λ_{680}) [12].

2 Results

In the experiment I, the removal efficiencies of nitrate-N in three treatments were 89 %, 87 % and 95 % within seven days, respectively. The removal efficiency of treatment-3 evenly reached 92 % within four days, which was three days ahead of other two treatments. During the whole experiment, there were lots of air bubbles (N_2) produced in the triangle flasks of three treatments. But in the control flask there was no air bubble and the concentration of nitrate-N was totally about 100 mg/L. It revealed that the isolated denitrifying bacteria had strong activity and could remove nitrate-N from seawater rapidly (Fig.1A). Except for the transparent seawater in the control flask, the seawater was turbid in all the treatments. At the early stage the growth mode of denitrifying bacteria was similar to the logistic curve. But at the later stage, the number of denitrifying bacteria began to decrease as their growth was limited by the declined concentration of nitrate-N in seawater step by step (Fig.1B). However, the removal efficiency of nitrate-N continued to ascend and reached about 98 % by the end of experiment I (13 d).

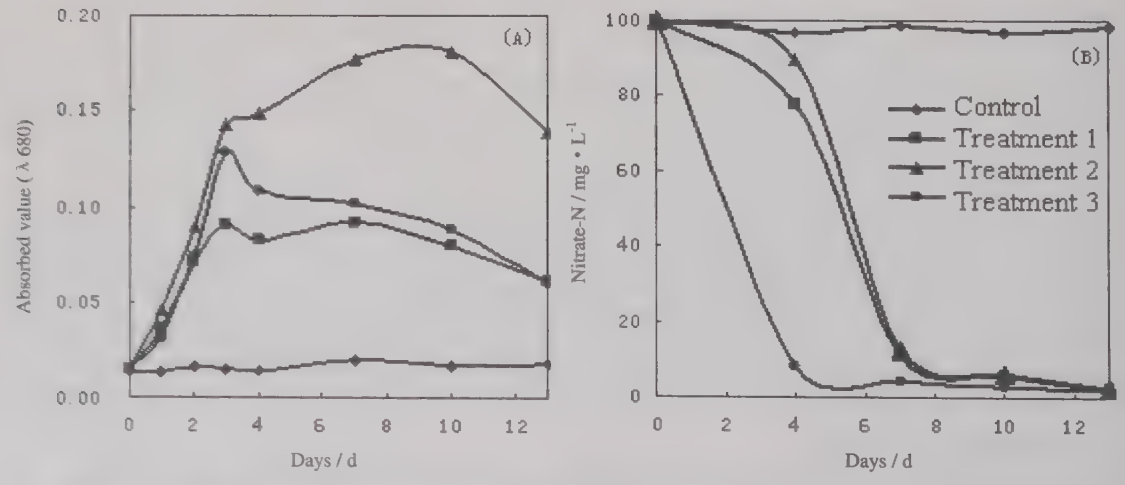

Fig.1 Growth of denitrifying bacteria and removal of nitrate-N in simulated experiment I (initial concentration of nitrate-N: 100 mg/L) (A) growth (B) removal of nitrate-N

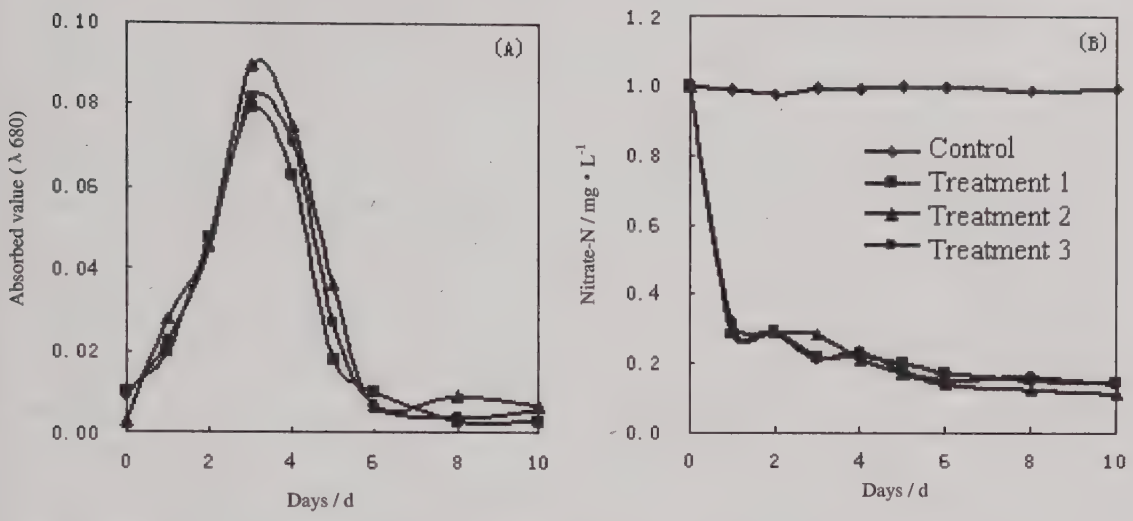

Fig. 2 Growth of denitrifying bacteria and removal of nitrate in simulated experiment II (initial concentration of nitrate-N: 1 mg/L) (A)growth (B)removal of nitrate-N

In the experiment II, removal efficiency of nitrate-N in three treatments reached about 70 % within one day. Within six days it went up to average 85 %. Then, the concentration of nitrate –N kept stable. But in the control the concentration of nitrate-N is totally about 1 mg/L (Fig.2A). During the experiment II, the seawater in the control flask was still clear and transparent. But turbid seawater in three treatments showed growth mode of denitrifying bacteria take on the apex curve. In the third day denitrifying bacteria reached the growth climax. Then the growth rate descended rapidly (Fig.2B). In the sixth day, the seawater in three treatments renewed transparent , which showed that denitrifying bacteria had been disappeared and the concentration of nitrate-N did not continue to decrease after the sixth day.

Compared with experiment I and experiment II, the result showed that growth rate of denitrifying bacteria as well as removal efficiency and final concentration of nitrate-N were positive correlating with initial concentration of nitrate-N in seawater. Namely, higher initial concentration of nitrate-N, higher growth rate of denitrifying bacteria, and higher removal efficiency and final concentration of nitrate-N. For example, removal efficiency of nitrate-N was 98 % in experiment I, while it was 85 % in experiment II.

3 Discussion

Removal of nitrate-N by denitrifying bacteria was a new technique and an international research hotspot. The first step of bioremediation is to isolate the active denitrifying bacteria. Pervious researches isolated and selected denitrifying bacteria from the sewage treatment plant and the sediment of prawn breeding farms. But the present study isolated the denitrifying bacteria from the sea sediment directly.

The result showed that the isolated denitrifying bacteria could effectively remove the nitrate-N from seawater and the removal efficiency was similar to the ones in other studies. But the denitrification rate in the present study was significantly lower than the ones in some studies. For example [13], isolated denitrifying bacteria from the sewage treatment plant could remove 90 % of nitrate-N in 6 h. Denitrification rate may be related with lots of factors, such as site, experiment condition, enrichment and cultivation technique and immobilized technique of denitrifying bacteria[11]. Our result was similar to the conclusion of Li Z C et al [9], namely denitrifying bacteria could effectively remove 90 % of nitrate-N within 7 d.

Whether the bioremediation is successful or not is related with the number and growth rate of degradation microbe in the environment. In general, the growth of bacterial strain is affected by lots of factors, including abiotic factors (pH, temperature, redox potential, dissolved oxygen and saline et al) and biotic factors (competition and predation)[3]. Immobilized technique could improve resistance of bacteria to environment such as pH, concentration of substrate and biotic toxicity. Some studies revealed that low pH had no effect on the denitrification of immobilized bacteria. Although water temperature had a certain effect on the removal efficiency of nitrate-N, at low temperature there was also high denitrification rate, which showed that immobilized denitrifying bacteria had strong capacity to endured low temperature. At present, the immobilized carrier of denitrifying bacteria includes polyethene mellow, active carbon and macromolecule carrier which is manufactured by low temperature radiation[9, 10, 13]. But we did not use the modern technique of immobilized microbe in this study. The simulated experiment of bioremediation was carried out by adding the denitrifying bacteria solution to the seawater directly. As the objective of our research was to resolve the inorganic nitrogen pollution in the coastal marine, we should possibly reduce the ecological risk which would be resulted from the application of immobilized carrier.

Additionally, in simulated experiments seawater was made up of high saline seawater and distilled water. The water body was still clam, clear and transparent, and the salinity was very stable. The experiment condition was totally different from the turbid water and complex hydrology in the Changjiang River estuary and its adjacent East China Sea. Lots of problems need be studied continually before the application of the bioremediation technique.

4 Conclusions

(1) The research obtained a success in isolating the denitrifying bacteria from sea sediment and presented its isolating method.

(2) The results of two simulated experiments showed that the isolated denitrifying bacteria could effectively remove the nitrate-N from seawater. Within a week the average removal efficiency of nitrate-N could reach about 90 %.

(3) The growth rate of denitrifying bacteria was correlated with the concentration of nitrate-N in seawater. Once the bioremediation process was completed, the denitrifying bacteria would disappear

rapidly.

Acknowledgements

This project has been supported by the National Natural Science Fund of China (No.50339040), Special Public Welfare Foundation and Monitoring Items, the Ministry of Science and Technology, China (No.2001DIAI0014-4, No.2001DIBI0082) and an Open Project of Key Laboratory of Fisheries Ecological Environment (No.2003-9), Ministry of Agriculture, China. We would like to thank Han J D and Qian P L for their help in laboratory analysis.

References

[1] Liu H Y, Dai Z J. The analysis and countermeasures on the present pollution in Chinese offing. Environ. Protec. Sci., 2001, 27(4):6-8.

[2] Li Q F, Yuan Y X. Prospect of study on remediation techniques of seawater aquaculture environment. Chin. Fisher. Sci., 2000, 7(2): 90-92.

[3] Zheng T L, Zhuang T C, Cai L Z et al. The role of microbe in remediation of marine polluted environment. J. of Xiamen Univer.(natural science), 2001, 4(2): 524-534.

[4] Tomes A E. The basics of bioremediation. Pollu. Engine., 1994, 26(6): 46-47.

[5] Hicks B N. Bioremediation: A natural solution. Pollu. Engine., 1993, 25(2): 30-33.

[6] Quan W M, Shen X Q. Monitoring and Research on Fisheries Environment Quality of Changjiang River Estuary and Adjacent East China Sea. Marine Fisheries, 2004, 26(2): 93-98.

[7] Quan W M, Shen X Q, Han J D et al. Analysis and assessment on eutrophication status and developing trend in Changjiang River estuary and its adjacent East China sea. Marine Environ. Sci., 2005, 24(3): 13-16.

[8] Wang C C, Lee C M. Denitrification with acrylamide by pure culture of bacteria isolated from acrylonitrile-butadiene-styrene resin manufactured wastewater treatment system. Chemosphere, 2001, 44: 1 047-1 053.

[9] Li Z K, Pu P M, Hu C H et al. Techniques of immobilized bacteria and its application in physico-ecological engineering-aquatic ecosystem remediation with immobilized nitrogen cycling bacteria. Jiangsu J. of Agr. Sci., 2001, 17(4): 248-252.

[10] Wang G X, Pu P M, Huang Y K et al. Distribution and role of denitrifying, nitrifying, nitrosation in the Taihu lake. Chin.Appl. Environ. Biol., 1998, 5(2): 190-194.

[11] Li B D, Yu Z N, He Z J. Experimental techniques of agricultural microbe. Beijing: China Agricultural Press, 1996.

[12] Yan H, Lin Y X, Sun J X. Removal of ammonium and nitrite by bacterial population in seawater. Techni. and Equip. of Environ. Pollu. Control, 2003, 11(4): 44-47.

[13] Tan Y M, Luo Q F. Study on removal of nitrate from drinking water by immobilized denitrifying bacteria. J Environ. Health, 2001, 18(6): 371-373.

海洋沉积物中反硝化细菌的分离及去除硝酸盐氮的模拟试验

全为民[1]，沈新强[1]，甘居利[2]，沈晓盛[1]，陈亚瞿[1]

（1. 中国水产科学研究院东海水产研究所，农业部海洋与河口渔业重点开放实验室，上海 200090；
2. 中国水产科学研究院南海水产研究所，农业部渔业生态环境重点开放实验室，广东 广州 510300）

摘　要：从长江口沉积物中筛选分离出了海洋反硝化细菌，模拟了该细菌对不同浓度水平硝酸盐氮的去除效率。研究结果表明，分离出的海洋反硝化细菌能有效去除海水中硝酸盐氮，在硝酸盐氮的初始浓度为 1 mg/L，1 d 内硝酸盐氮去除率就达到了 70 %；在 100 mg/L 硝酸盐氮模拟试验中，约在一周内能将 90 % 硝酸盐氮去除。试验证明反硝化细菌的生长与水体中硝酸盐氮浓度有一定的相关关系，一旦生物修复过程完成，反硝化细菌就会大量死亡，水体重新恢复到清澈透明状况。

关键词：反硝化细菌；生物修复；硝酸盐氮；去除

Optimization of Fermentation and Product Collection Process of the Functional Bacteria for Bioremediation of Shrimp Culture Environment

LI Qiufen (李秋芬)*, ZOU Yuxia (邹玉霞), XIN Fuyan (辛福言), QU Keming (曲克明), CHEN Minshan (陈民山), MA Shaosai (马绍赛)

Yellow Sea Fisheries Research Institute, CAFS, Qingdao 266071, *Shandong, China*

Abstract: In order to implement industrial production of selected functional bacteria for bioremediation of shrimp culture environment, the fermentation conditions of the three functional bacteria, which have high ability in degrading organic pollutants at the bottom of shrimp ponds, were studied. The results showed that the favorable fermentation medium (per L) was 25 g of peptone, 5 g of yeast extract, and 0.2 g of ferric phosphate, and the initial pH value of the medium was 8.0. The optimum fermentation time was 20 h. The optimum stirring way was stirring one hour after one hour. Iso-electric point sedimentation collecting method was the most efficient and economic method to collect the bacteria cells after fermentation, with the optimum sediment pH of 3.67, 4.02, and 3.40 for the strains Lt7222, Gy7018 and Lt7511, respectively. It was also indicated that the survival and reproducing ability of the bacterial cells were not affected by the sedimentation process.

Keywords: Aquaculture environment; Bioremediation; Functional bacteria; Fermentation

With the fast development of industries and the rapid growth of population in coastal areas, environment pollution has become very serious. In only 50 % of the aquacultural area, the water quality can meet the standard for fisheries. Especially in the mariculture area which needs feeding, large amounts of feed residue, faeces and corpses of plants or animals are accumulated at the bottom, thus leading to serious organic pollution. This problem has limited the normal development of production potential of the aquaculture systems, furthermore, some areas have lost their function due to pollution [1]. So, it is very critical to do something to remedy the polluted mariculture environment. Our laboratory is to utilize microorganisms with special ability as functional organisms to improve the environment of shrimp culture. Several functional bacteria strains with high ability of degrading organic pollutant at the bottom of shrimp ponds were isolated[2], and their function of decreasing the accumulation of organic matter and significantly improving the environment of shrimp pond has been approved through simulative application[3]. For the extensive application of the bacteria products in shrimp ponds, it is necessary to solve the problem of mass production. Industrial fermentation is the most popular method to obtain larges amount of microorganism cells [4]. This paper reported the optimization of fermentation

Received on October 9, 2005

* Corresponding author. E-mail: liqf@ysfri.ac.cn

and product collection process of the functional bacteria.

1 Material and methods

1.1 Materials

Bacteria strains: Lt7222(*Bacillus firmus*), Gy7018(*B.subtilis*)and Lt7511(*B. circulans*), organic pollutant-degrading bacteria, were selected by our research group [2].

Media: Based on the Zobell's 2216E (peptone 0.5 %, yeast extract 0.1 %, ferric phosphate 0.2 %), the amount of each component was adjusted, some materials were replaced with industrial product, and the solvent was the sand-filtrated sea water.

1.2 Methods

1.2.1 Selection of the optimum concentration of the fermentation medium.

The amount of the media components was increased to 2, 4, 6, 9 and 12 times those of 2216E medium, and the original 2216E medium was used as control group. The Lt7222 was incubated and cultivated in 1000ml Erlenmeyer flasks. Thirty ml of culture was sampled every 6 h after 12 h. The wet bacteria cells were weighted after centrifugation.

12.2 Selection of the pH of the medium before autoclaving

The experiments were undertaken in four 50 L fermentation tanks, in each tank, there were 500 g of peptone, 100 g of yeast extract and 4 g of ferric phosphate, dissolved with hot water and filtrated, 16 L of sea water, and 3 L of fresh water, the pH was adjusted to 7.0, 7.5, 8.0, 8.5, respectively, and then they were autoclaved with filtrated steam at 121 ℃ for 30min. After being cooled to room temperature, they were inoculated with 2.5 % (V/V) of strain Lt7222 culture, and then fermented at 28 ℃ ± 0.5 ℃. The OD_{600nm} of the culture in each tank was determined 20 h later and the pH values of the media were also determined after autoclaving and fermenting.

1.2.3 Selection of optimum stirring way

Four tanks of media were prepared and their pH values were adjusted to 8.0 according to the result of the second experiment, then autoclaved and inoculated as in the second experiment, but they were stirred in four ways during fermenting, totally static, stirring 1h after 2 h (intermittent stirring type Ⅰ), stirring 1h after 1h (intermittent stirring type Ⅱ) and continuously stirring, respectively. The OD_{600nm} of the culture in each tank was determined 20h after inoculating.

1.2.4 Selection of optimum fermentation time

According to the results of the former experiments, 4 tanks of media were prepared in 50 L tanks, and the pH was adjusted to 8.0. They were autoclaved and inoculated as in the former experiment, fermented at 28 ℃ ± 0.5 ℃, and stirred with the intermittent stirring type Ⅱ. Samples were taken every 3 h 12 h after inoculation, the values of OD_{600nm} were determined and the activity of the bacteria was observed with microscopy.

1.2.5 Determination of the iso-electric points of the fermented broth.

The fermented broth was delivered into 50 mL color comparison tubes, adjusted to different pH with 1 mol/LHCl, kept static for 48 h to make the bacteria cells settle, and then the OD_{600nm} of supernatants was determined. The pH corresponding to the lowest OD value was considered as the iso-electric point of each functional bacteria strain.

1.2.6 Testing of the survival and reproducing ability of the bacteria after collection

The pH of each fermented broth was adjusted to its iso-electric point and kept static for 48h, then the sediments were collected, and were inoculated in solid and liquid 2216E media, respectively, after being diluted with sterile sea water. The original fermented broths were also inoculated as control. Their survival and reproduction ability were determined through enumerating.

2 Results

2.1 The relationship between the product and the concentration of the media

It can be seen from Fig. 1 that to some extent, the yield of the bacteria increased with the rising of the concentrations of the media components, and got to the highest in the medium with the concentration 4 times that of the 2216E medium. However, the product began to decrease when the concentration continued to rise for 6 times. So, the concentration of the fermentation medium can choose 5 times that of the 2216E medium, but it is enough for the concentration of $FePO_4$ to be raised to 2 times for its low solubility.

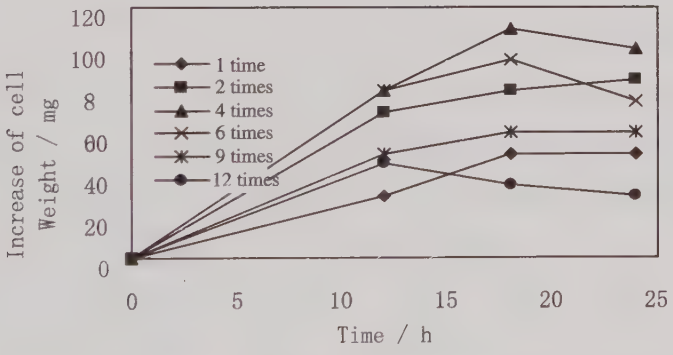

Fig. 1 Relationship between media concentration and the product of functional bacteria

2.2 Selection of the pH value of fermentation media before autoclaving

Because the pH of the condensed water produced in autoclaving may influence the pH of the media, its pH value before autoclaving should be determined through experiments. As shown in Table 1, the process of autoclaving and fermentation both led to the decrease of the pH value, and the bacteria grew

best in the tank in which the pH was adjusted to 8.0 before autoclaving, and in the tank with pH 8.5, the growth ranked second, but in other two tanks, the bacteria seldom grew because of the too low pH value (as shown in Fig.2). Therefore, it is suitable to adjust the pH value of the media to 8.0 before autoclaving.

Tab. 1 The change of pH of the media at different time

Time	pH of the media			
Before autoclaving	7.0	7.5	8.0	8.5
After autoclaving	6.4	7.0	7.7	8.1
End of fermentation	6.5	6.8	7.6	7.9

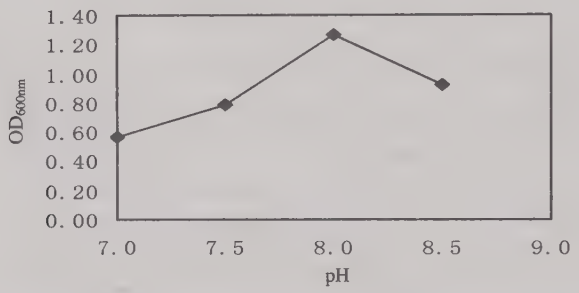

Fig. 2 Relationship between pH of medium and the product of functional bacteria

2.3 Selection of the optimum stirring way

Since the selected functional bacteria strains are aerophilic bacteria, the level of the dissolved oxygen in the media significantly influences the growth of the bacteria. The fermentation result showed that (Table 2), the bacteria grew significantly better with stirring than being kept static. However, the process of stirring can expedite evaporation, only 8.4 L fermented broth was left after 20 h if continuously stirred. The total yield was only 98.5 g even though the concentration of the bacteria body is high. The highest yield was got in the tank with stirring 1h after 1h, therefore, this stirring can be considered as the optimum stirring way.

Tab. 2 The fermentation results in different stirring ways

Results of fermentation	Totally static	Intermittent stirring type I	Intermittent stirring type II	Continuously stirring
OD_{600nm}	0.789	1.39	1.96	2.30
Volume of the fermented broth / L	22	19.6	18.7	8.4
Weight of the wet bacteria bodies / g	80.6	145.9	183.2	98.5

2.4 The influence of the fermentation time on the product

It can be seen from Fig. 3 that the concentration of the bacteria continuously increased as time went on, and the value of OD_{600nm} got to the peak 24 h after inoculating, however the continued increase of OD_{600nm} was due to evaporation. Under microscopy, the bacteria cells were observed to be thin and inactive in the first 16 h, fat and active with even size from 18h to 22 h, but after 24 h, the size was uneven, the activity decreased significantly, and some cells had been broken. Because the fermentation products will be used as seed, it is suitable to stop fermenting 18 - 20 h after inoculating in seed fermentation in order to keep their strong living ability.

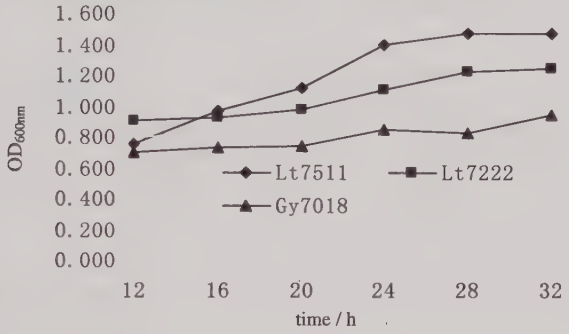

Fig. 3 The relationship between the bacteria growth rate and the fermentation time

2.5 Collection of bacteria cells

It was shown in Fig. 4 that the OD_{600nm} of the supernatants of the fermented broth of strain Lt7222 was the lowest when the pH was 3.67, which means this pH point is the closest to the iso-electric point of this strain. In the same way, as Fig. 5 and Fig. 6 showed, pH 3.4 and 4.02 are close to the iso-electric points of strain Lt7451 and Gy7018, respectively. So, the pH of the fermented broths can be adjusted to the iso-electric point of each bacteria strain to make most the bacteria cells settle after 48 h.

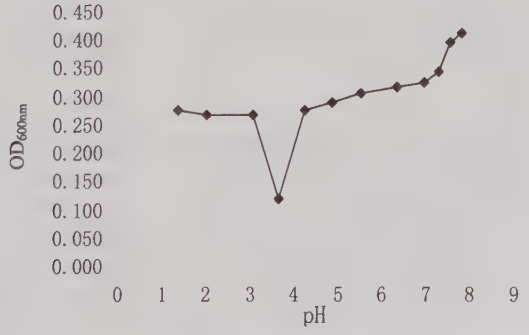

Fig. 4 Sedimentation of strain Lt7222 at different pH

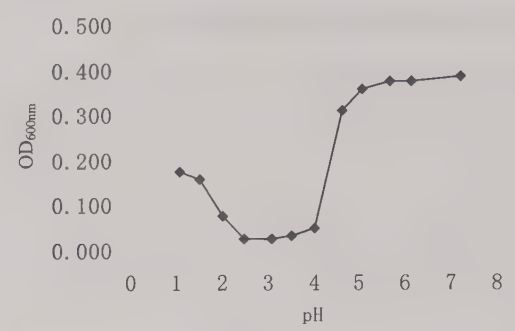

Fig. 5 Sedimentation of strain Lt7511 at different pH

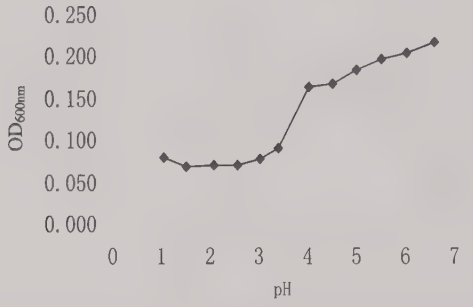

Fig. 6 Sedimentation of strain Gy7018 at different pH

2.6 The survival and reproduction ability of the bacteria after being collected by the iso-electric point sediment

As shown in Table 3, through enumeration with the spreading plant method, the reclamation rate of this collection method was up to 90 %. Almost the same concentration of the culture was obtained after inoculating the same amount of original fermented broth and the re-suspended bacteria cells into the liquid 2216E medium, which indicated that this collection method has no impact on the survival and reproduction ability of the bacteria.

Tab. 3 The survival and reproduction ability of the precipitated bacteria

Bacteria strains	Bacteria concentration of the fermentation broth / CFU • mL^{-1}	Bacteria concentrations of the culture / CFU • mL^{-1}
Lt7222	1.26×10^9	1.20×10^9
Lt7451	1.45×10^9	1.41×10^9
Gy7018	0.79×10^9	0.79×10^9

3 Discussion

The production ability of microbial-fermentation depends not only on the property of the bacteria strains but also on the fermenting condition [5], for example, in the antibiotic and enzyme production, the condition suitable for growth may not meet the requirement for the accumulation of metabolic products, both of them should be met in exterminating the parameters of fermenting process [6]. But in the fermentation to produce bacteria cells, the growth of bacteria is parallel with the accumulation of the product, the stage with highest growth rate is also the stage when the product compose fastest [4]. So, the fermentation parameters were determined according to the concentration of cells and the yield in this paper.

The curve of the production and fermenting time indicated that the product got to the peak 24 h after inoculating, but the activity of the cells was observed to decrease, some cells were dead and broken. So, it is not a good time to collect product since the product is to be used as seed in shrimp ponds. Therefore, 18 - 20 h after inoculation was chosen as the time to stop fermenting and collecting the product.

Usually, there are not only bacteria cells but also nutrient residue in the ferment broth, which may lead to pollution if it is applied directly to the shrimp culture environment. So, the bacteria cells should be extracted from the fermented broth before utilization. In fungi fermentation industries, the fungi cells are usually collected through filtration, but it is difficult for bacteria cells to use this method because of their too small size. Centrifugal separation has the advantage of high reclamation rate and not being liable to be contaminated, but it has the disadvantages of high cost and low efficiency, and obviously, it can not meet the requirement of industrial production because tons of fermented broth is produced in one fermentation cycle. Spontaneous sedimentation needs too long a time, which may lead to death or contamination. Iso-electric point sedimentation is based on the mechanism that the bacteria cells will settle if its surface negative charge is equal to the positive charge of the solution. Through adjusting the pH value of the solution to the bacteria' iso-electric point, we can make the bacteria cells settle and collect them after a relatively short time, and our experiment indicated that the survival and reproduction ability of the collected bacteria are not influenced. So, iso-electric point sedimentation is an easy-to-operate, time-effective and cost-effective bacteria cells collecting method for mass fermentation product, a good method worth widely popularizing.

Acknowledgments

The paper is supported by the national high-technology development project (819-2-07) and the project of NSFC(30200209).

References

[1] Li Q F, Yuan Y X. Outlook for bioremediation researches on marine aquacultural environment. J. of Fishery Sciences of China, 2000, 7(2): 90-92.

[2] Li Q F, Qu K M, Xin F Y et al. Isolation and selection of functional bacteria for bioremediation of shrimp culture environment. Chin. J. Appl. Envirion. Biol. 2001, 7(3): 281-285.

[3] Xin F Y, Li Q F, Zou Y X et al. Stimulated application of functional bacteria in bioremediation of shrimp culture environment. Chin. J. Appl. Envirion. Biol. 2002, 8(1): 75-77.

[4] Yin G L, Zhan L K et al. chief edited. Manual for fermentation industry. Beijing: Chinese Medical Science & Technology Press, 1996.

[5] Yu J T, Tang X X. Chief edited. Biotechnology，Shanghai：East China University of Science and Technology Press, 1991.

[6] Zhong W H, Wang Q J, Cen P L. Study on alkaline pectinase producing conditions by Spirillospora. Chin. J. Appl. Envirion. Biol. 2000, 6(5): 468-472.

虾池环境生物修复作用菌的生产发酵与菌体收集工艺优化

李秋芬，邹玉霞，辛福言，曲克明，陈民山，马绍赛

（中国水产科学研究院海洋食品安全与环境控制重点开放实验室，黄海水产研究所，中国水产科学研究院，青岛 266071）

摘　要：为了实现所筛选的对虾养殖环境生物修复作用菌的产业化生产，本文选择三株具有高效降解有机污染物能力的菌株为代表，对作用菌的发酵生产和菌体收集工艺进行了优化。结果表明，作用菌的最适发酵培养基配方（g/L）为蛋白胨 25，酵母粉 5，磷酸铁 0.2，灭菌前培养基的 pH 可先调为 8.0，搅拌方式为搅拌 1h 间隔 1h，出罐时间以 20h 为宜。菌体收集以等电点沉降法效率最高、成本最低，其中菌株 Lt7222 的最适沉降 pH 为 3.67、Gy7018 为 4.02、Lt7511 为 3.40。菌体回收率可达 90％，回收后菌体的存活能力几乎不受影响。

关键词：养殖环境；生物修复；作用菌；发酵工艺；菌体收集

Sea Surface Roughness Derivation from Wind Speed Estimated by Satellite Altimeter

ZHOU Liangming (周良明)*, GUO Peifang (郭佩芳), WANG Aifang (王爱方)
Department of Oceanography, College of Physical and Environmental Oceanography, Ocean University of China, Qingdao 266003, *China*

Abstract: For open sea conditions the sea surface roughness is described as a function of surface stress and wind speed over sea surface by Charnock relation. The sea surface roughness in the North-west Pacific Ocean is derived successfully using wind speed data estimated by the TOPEX satellite altimeter. From the results we find that: (1) the mean sea surface roughness in winter is greater than in summer; (2) compared with other sea areas, the sea surface roughness in the sea area east of Japan (N30° — 40° , E135° — 150°) is larger than in other sea areas; (3) sea surface roughness in the South China Sea changes more greatly than that in the Bohai Sea, Yellow Sea and East China Sea.

Keywords: Sea surface roughness; satellite altimeter; sea surface wind speed; normalized radar cross section; wind stress coefficient; friction velocity

Introduction

The sea surface roughness plays a key role in the momentum exchange process between wind and waves and thus in the air-sea interaction in general.

The sea surface roughness is low compared with land surface. However, the roughness is not constant with the wind speed like for land surfaces, but depends on the wave field present, which in turn depends on wind speed, upstream fetch (distance to coastal), water depth, etc. Different models have been proposed to describe these dependencies, and numerous attempts have been made to improve this description by including more information about the wave field, by including wave age c_p / u_* (c_p is the peak wave velocity and u_* is the friction velocity) or wave steepness H_s / L_p (where H_s is the significant wave height, and L_p is the peak wave length) as additional parameters.

For open sea conditions the Charnock relation has been applied successfully, which describes the sea surface roughness as a function of surface stress (Blackadar, 1968) [1]

$$z_0 = \alpha \frac{u_*^2}{g} \qquad (1)$$

where u_* is the friction velocity, g is the gravitational acceleration, and α is a constant with different values depending on water depth and coastal proximity.

Received on Dec. 15, 2005

* Corresponding author. E-mail: zhou5299@ouc.edu.cn

In this paper we'll first introduce the Geophysical Model Function (wind speed algorithm from the normalized radar cross section), and then derive the sea surface roughness in the North-west Pacific Ocean using wind speed data estimated by the TOPEX satellite altimeter.

1 Wind speed derivation from satellite altimeter

The scheduled February 1985 launch of a radar altimeter aboard the U. S. Navy satellite Geosat has motivated an in-depth investigation of wind speed retrieval from satellite altimeters. The accuracy of sea surface wind speed estimated by the Seasat altimeter is examined by comparison with the wind speed estimated by the Seasat scattermeter. There are systematic differences between altimeter and scattermeter wind speed estimates. These differences are traced to errors in the Seasat altimeter geophysical data record wind speed algorithm. Chelton and Mccabe (1985) [2] proposed a new model function for wind speed estimation from corrected values of the normalized radar cross section σ_0. The new model function estimates the wind speed at 19.5 m by

$$U_{19.5} = 10^{(\sigma_0/10+A)/B} \qquad (2)$$

where $A = -1.502, B = -0.468$. Using the new algorithm, the rms difference between spatial and temporal averages of the two wind speed estimates is less than 1 m/s, and their correlation is greater than 0.9. But in this model the wind speed is limited to about 4 - 14 m/s.

Chelton and Wentz (1986) [3] used a new approach which gives a wind speed model function applicable over the range 0 to 21 m/s. The method is based on comparing 50 km along-track averages of the altimeter normalized radar cross section σ_0 measurements with neighboring off-nadir scatterometer wind speed measurements. The scatterometer winds are constructed from 100 km binned measurements of radar cross section and are located approximately 200 km from the satellite subtrack. The new model function agrees very well with earlier versions up to the wind speed of 14 m/s but differs significantly at higher wind speeds.

Estimation of the near-surface wind speed to an rms accuracy of 2 m/s from altimeter measurements of σ_0 has been convincingly demonstrated by numerous past studies. However, developing a new model function relating σ_0 to the wind speed for each altimeter can be difficult. It is argued that the σ_0 distribution measured by an altimeter is relatively stable over a sufficiently large geographical region and a long enough time period. Systematic differences between σ_0 estimated from two altimeters can therefore be identified based on comparisons of their σ_0 histograms. Any such systematic differences can then be corrected using independent σ_0 estimates. Witter and Chelton(1991)[4] applied this method to the Geosat and Seasat altimeters and gave a modified wind speed model function relating σ_0 to wind speed at 19.5 m and 10 m above the sea surface. They got the conclusions that (1) the σ_0 distribution is stable, and (2) the Seasat altimeter estimates of σ_0 were miscalibrated. After modifying the existing Seasat altimeter wind speed algorithm to account for this apparent σ_0 error, the resulting Geosat estimates of wind speed agree with high-quality buoy observations to within an rms difference of less

than 2 m/s.

The WC model is also applied to those satellite altimeters of ERS-1, ERS-2 and TOPEX/Poseidon.

2 Sea surface roughness

Under conditions of neutral thermal stability, the wind speed profile in the atmospheric surface layer is commonly described by Monin-Obukhov theory as (Tennekes) [5]

$$U = \frac{U_*}{k}\ln(\frac{z}{z_0}) \tag{3}$$

Here, U means the wind velocity at the elevation z above the sea surface; k denotes the von Karman constant (normally taken as 0.4) (Amorocho, 1980) [6]; u_* friction velocity; z_0 aerodynamic roughness length (sea surface roughness); u_* in the form (1) is equal to $(\tau_w / \rho_a)^{1/2}$, where τ_w is the wind shear stress at the water surface, and ρ_a is the air density.

Because it is not always practical to perform velocity profile measurements in field situations, it has become customary to express the relationship between the wind shear stress and the velocity measured at a single location z above the mean water level by the expression

$$C_z = \frac{\tau_w}{\rho_a U_z^{\ 2}} \tag{4}$$

where C_z is the wind stress coefficient.

From (4) and the expression of u_*, it follows that

$$C_z = (\frac{u_*}{U_z})^2 \tag{5}$$

One of the most complete summaries of published values of C_z was assembled by WuJing (1969) and comprises data from 42 different investigations.

$$C_{10} = 0.5U_{10}^{\ 1/2} \times 10^{-3} \tag{6}$$

where U_{10} and C_{10} represent the wind velocity at 10 m above sea surface and the wind stress coefficient versus U_{10} respectively (we customarily take z = 10 m as a reference height).

Then, from (3), (5) and (6) we get the relationship between z_0 and U_{10} as follows

$$z_0 = 10e^{-aU_{10}^{-1/4}} \tag{7}$$

where $a = 17.89$。

3 Sea surface roughness in North-west Pacific Ocean

We use wind speed data of 1993 and 1998 estimated by the TOPEX satellite altimeter and studied the sea surface roughness of North-west Pacific Ocean (E105° — 150° , N 5° — 45°). Fig. 1 shows the distribution of sea surface roughness of North-west Pacific Ocean in July 1998.

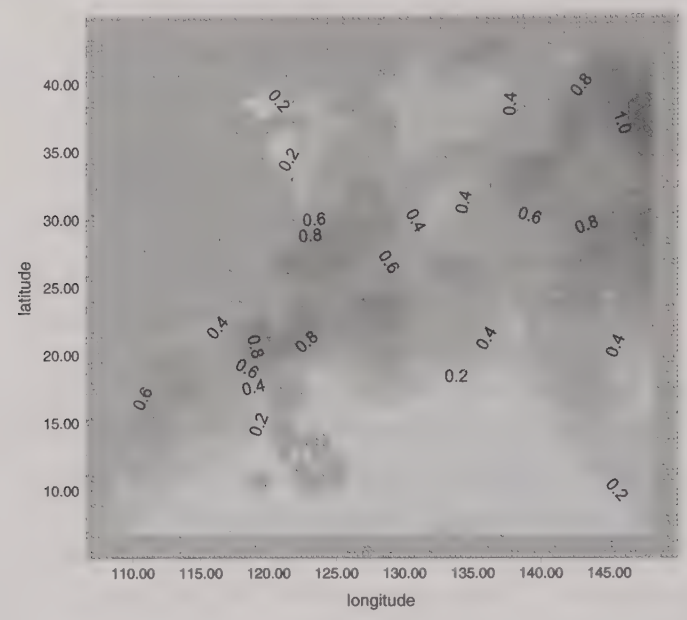

Fig. 1 The distribution of sea surface roughness derived from wind speed data in the North-west Pacific Ocean, July 1998

From the results we find some characteristics as follows:

1) The sea surface roughness in the sea area east of Japan (N30° — 40°, E135° — 150°) is larger than in other sea areas. Fig. 2 shows the changes of sea surface roughness from January to December, where the triangular line represents the sea area east of Japan, and the rectangular line represents the North-west Pacific Ocean. From this figure we find that the sea surface roughness in the sea area east of Japan is always larger than that in the North-west Pacific Ocean.

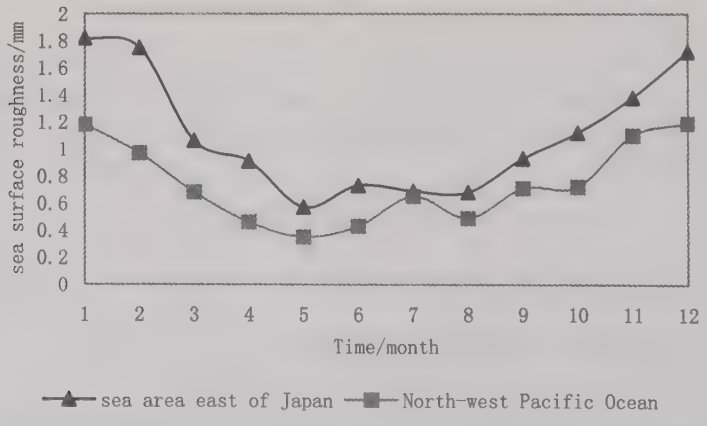

Fig. 2 Changes of sea surface roughness from January to December (where the triangular line represents the sea area east of Japan, and the rectangular line represents the North-west Pacific Ocean)

2) The mean sea surface roughness of the whole sea area we studied changes regularly according to months. From January to June it reduces gradually, and from July to December it increases gradually. In general, the mean sea surface roughness in winter is greater than in summer.

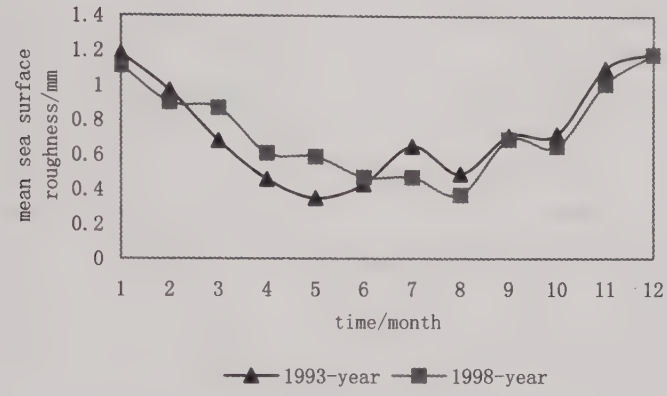

Fig. 3 The mean sea surface roughness of North-west Pacific Ocean from January to December (the data of 1993 are denoted by triangular, and the data of 1998 by rectangular.)

3) In order to study the sea surface roughness of China Seas, we choose four points in the Bohai Sea, Yellow Sea, East China Sea and South China Sea respectively, which are marked as A, B, C and D (see Fig. 4). Table 1 lists the mean sea surface roughness of A, B, C and D (from January to December). The common characteristic of four points is that the sea surface roughness of winter is

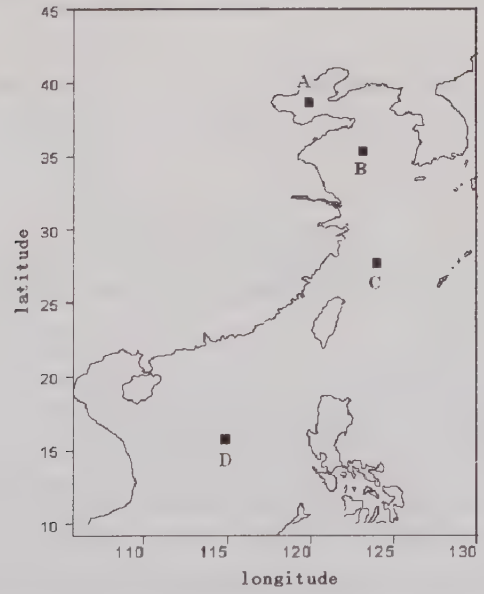

Fig. 4 Four points of China Sea in order to study the sea surface roughness of China Sea

greater than that of summer. Compared with other three points, the sea surface roughness of point D changes more greatly than A, B and C.

Tab. 1 Mean sea surface roughness of A, B, C and D from January to December

Sea area	Point	Latitude	Longitude	Mean sea surface roughness / mm											
				1	2	3	4	5	6	7	8	9	10	11	12
Bohai Sea	A	39.00°	120.00°	1.03	1.24	0.52	0.39	0.17	0.17	0.15	0.53	0.51	1.43	1.78	1.29
Yellow Sea	B	35.00°	123.00°	1.02	0.89	0.52	0.25	0.56	0.21	0.55	0.13	0.77	0.55	0.87	0.87
East China Sea	C	27.00°	125.00°	1.10	1.01	1.27	0.61	0.42	0.59	0.95	0.50	0.96	0.66	1.57	1.28
South China Sea	D	15.00°	115.00°	0.91	0.19	0.20	0.10	0.37	0.27	0.69	0.16	0.74	1.03	1.22	1.92

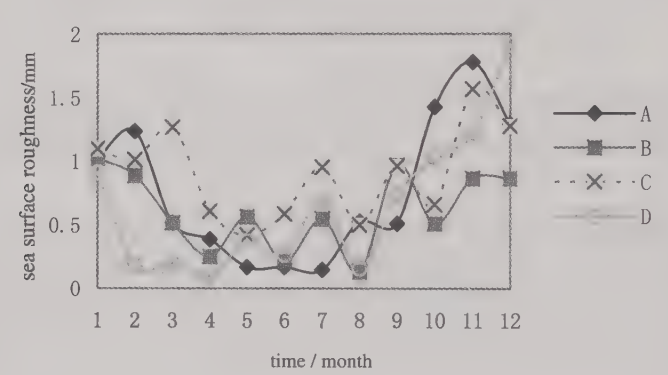

Fig. 5 The mean sea surface roughness of A, B, C and D change according to months

4 Discussion

Sea surface roughness is derived using TOPEX satellite altimeter wind speed data. The key of sea surface roughness derivation is the precision of wind speed. The CW wind speed model function gives wind speed over the range 0 to 21 m/s, so we can't get sea surface roughness versus high wind speed over 21 m/s.

Another key of sea surface derivation is the relation of the wind stress coefficient with the wind speed over sea surface. The relation we used in this paper is given by WuJing (1969) [7]. Numerous investigatiors (Smith, 1980; Carrant, 1977; Sheppard, 1950; Amorocho, 1980) [6, 8-10] have carried out measurements of wind stress over sea surface, both in the laboratory and at sea. A large volume of data have been collected, but no concensus has been reached yet on their interpretation, the values of C_z have been disputed, and the appropriate expressions are needed to represent them.

Aside from the satellite altimeter, scattermeter and SAR also estimate the wind speed. The author will derive the sea surface roughness from the wind speed estimated by satellite scattermeter and SAR next.

References

[1] Blackadar A K amd Tennekes H. Asymptotic similarity in neutral barotropic planetary boundary layers. J. Atmos. Sci., 1968, 25: 1 015-1 020.

[2] Chelton D B, McCabe P J. A review of satellite altimeter measurement of sea surface wind speed: with a proposed new algorithm. J. G. R., 1985, 90(C3): 4 707-4 720.

[3] Chelton D B and Wentz F J. Further development of an improved altimeter wind speed algorithm. J. G. R., 1986, 91: 14 250-14 260.

[4] Witter D L and Chelton D B. A Geosat altimeter wind speed algorithm and a method for altimeter wind speed algorithm development. J. G. R., 1991, 96: 8 853-8 860.

[5] Tennekes H. Free convection in the turbulent Ekman layer of the atmosphere. J. Atmos. Sci., 1970, 27: 1 027-1 034.

[6] Amorocho J and Devries J J. A new evaluation of the wind stress coefficient over water surfaces. J. G. R., 1980, 85(c): 433-442.

[7] Wu J. Wind stress and surface roughness at air-sea interface. Geophys, res., 1969, 21(5): 707-714.

[8] Smith S D. Wind stress and heat flux over the ocean in gale force winds, J. P. O, 1980, 10: 709-726.

[9] Carratt J R. Review of coefficients over oceans and continents. Monthly weather review, 1977, 105: 915-929.

[10] Seppard F P and inman D L. Nearshore water circulation related to bottorm topography and wave refractcon, trans. Am.geophys. Un, 1950, 31(2): 196-211.

利用卫星高度计风速资料研究海面粗糙度

周良明，郭佩芳，王爱方

（中国海洋大学海洋环境学院 青岛 266003）

摘 要：海面粗糙度对于海洋工程和海洋军事都非常重要，但对海面粗糙度的现场观测资料非常少， 这大大制约了对海面粗糙度的认识。利用 TOPEX 高度计风速资料实现了对海面粗糙度的反演，并利用 1993 年和 1998 年两年的资料对西北太平洋海域的海面粗糙度进行了研究。

关键词：海面粗糙度；卫星高度计；海面风速；后向散射系数；阻力系数；摩擦风速

Distribution Characteristics of COD in the Waters of Pearl River Estuary

YANG Meilan (杨美兰)*, LIN Qin (林 钦), HUANG Honghui (黄洪辉), GAN Juli (甘居利), CAI Wengui (蔡文贵), Lü Xiaoyu (吕晓瑜), WANG Zenghuan (王增焕), LI Chunhou (李纯厚), DU Feiyan (杜飞雁), HU Derong (胡德蓉)

Key Laboratory of Fishery Ecology Environment, Ministry of Agriculture, Key Laboratory of Fishery Ecology Environment, Guangdong Province, South China Sea Fisheries Research Institute, Chinese Academy of Fishery Sciences, Guangzhou 510300, *Guangdong, China*

Abstract: The surveys on the COD in the Lingdingyang waters of Pearl River estuary were carried out in May and August of 2002. The results showed that the concentrations of COD in the waters ranged from 0.41 to 2.72mg • L^{-1} with an average of 1.21 mg • L^{-1}.The spatial distributions showed that COD concentration decreased gradually from the north to south of Pearl River estuary, and the concentration near coastal waters was higher than that in offshore waters. The concentration of COD in summer was higher than in spring. Evaluated by the first class (COD ≤ 2 mg • L^{-1}) of sea water quality standard (Chinese standard), there were about 15 % of COD concentrations over the standard. The concentration of COD showed a positive correlation with the concentration of suspend substances in spring and summer, but in summer it showed a negative correlation with the concentrations of inorganic nitrate and phosphate.

Keywords: COD; Pearl River estuary; Distribution characteristics

Introduction

Lingdingyang waters of Pearl River estuary is located in the Pearl River delta. The rivers directly flowing into this area are Pearl River, Shenzhen River and Qianshan River. In recent years, along with the intensive exploitation and rapid increase in the population of the Pear River delta, the environment has been deteriorating [1, 2], therefore it has become the focus waters which attracts people's attention and study. In order to understand the water quality condition of Pearl River estuary, this paper elaborates on the distribution characters of COD in the waters.

1 Materials and methods

Twenty sampling stations were set up in the Pearl River estuary waters (Fig. 1). Sampling time was arranged in May (spring) and August (summer) of 2002. The measurement of chemical oxygen demand

Received on Sept. 1, 2005

* Corresponding author. E-mail: scsyml@tom.com

is based on the National Standard of PRC (GB17378.4-1998), the specification for marine monitoring Part 4: Seawater analysis[3], which was issued by the State Quality and Technical Supervision Administration.

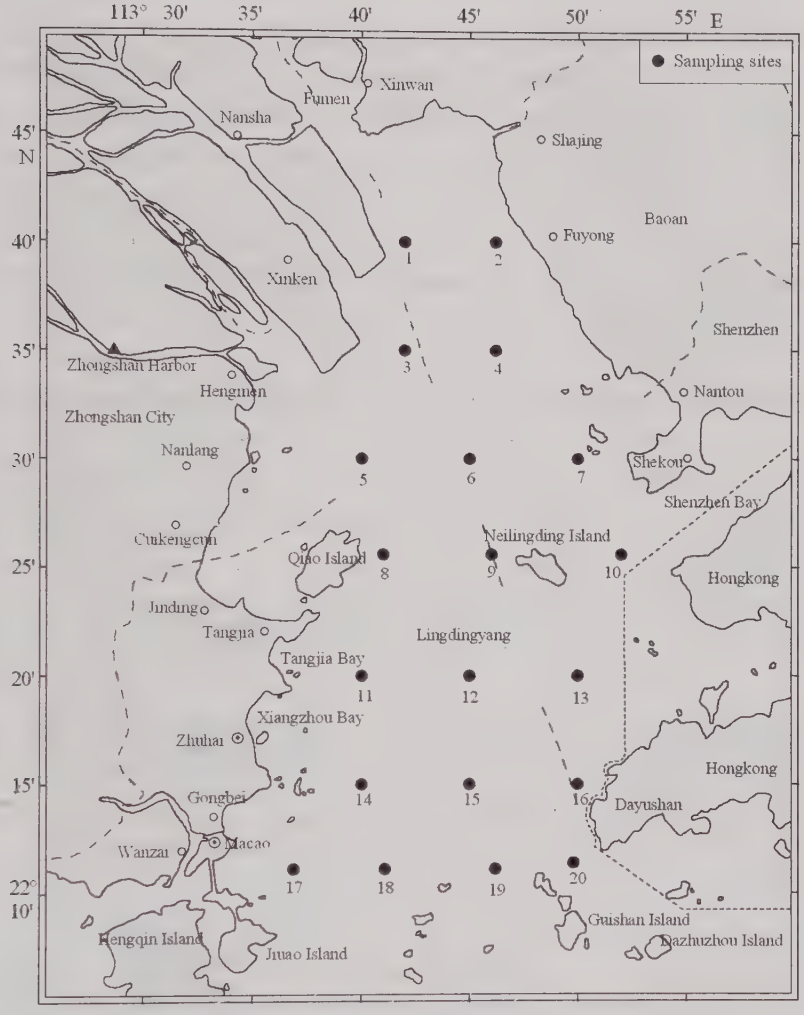

Fig. 1 Sampling stations in the Lingdingyang waters of Pearl River estuary

2 Results and discussion

2.1 The concentration of COD and spatial distributions

During the survey, the concentration of COD in the Lingdingyang waters ranged from 0.41 to 2.72 mg • L^{-1} with an average of 1.21 mg • L^{-1} (Table 1). The concentration of COD was maximum near the northwest of Humen and a belt of Jiaomen outlet (Stations 1and 3), the average was between 1.9 and 2 mg • L^{-1}. In the waters around Qi'ao Island and Nei Lingding Island in the middle Pearl River estuary

(Stations 5 to 9), the waters of Zhuhai (Station 11) and nearby Macao (Station 17), the average concentration fluctuated around 1.5 mg • L^{-1}, the waters with the minimum concentration was located in the areas west to Lantao Island in Hongkong and north to Guishan Island which lies in the estuary (Stations 13, 15, 16, 18, 19, 20), with the average under 0.8 mg • L^{-1} (Fig. 2). Thus, the concentration distribution of COD has two characteristics in the Lingdingyang water area. (1) The concentration of COD gradually decreased from northwest to southeast. (2) The concentration of COD in the coastal waters was higher than that in the offshore waters. The main reason is that the northwest waters of Pearl River estuary was affected by the runoff of Humen, Jiaomen, and Hongqili and the discharges of domestic sewerage and industrial effluent from the coast. The effect was relatively conspicuous in the waters of Zhuhai and nearby Macao. The concentration of COD was lower in the southeast waters of the estuary, owing to the fact that it is far from the coast and communicates with the South China Sea, and is propitious to the exchange of waters.

Tab. 1 The concentration of COD (mg • L^{-1}) in the Lingdingyang waters of Pearl River estuary

Station	1	2	3	4	5	6	7	8	9	10	11	12	13	14	15	16	17	18	19	20
May	1.11	0.99	1.40	1.10	1.37	0.74	1.11	1.24	1.40	0.95	0.58	0.41	0.58	0.66	0.54	0.62	1.03	0.82	0.68	0.43
August	2.72	1.73	2.60	1.37	1.62	1.57	1.72	1.68	1.50	1.10	2.29	1.15	1.07	1.25	1.07	0.99	1.65	1.32	1.24	0.78
Average	1.91	1.36	2.00	1.28	1.60	1.16	1.48	1.46	1.45	1..02	1.44	0.78	0.82	0.96	0.80	0.80	1.34	1.07	0.96	0.60

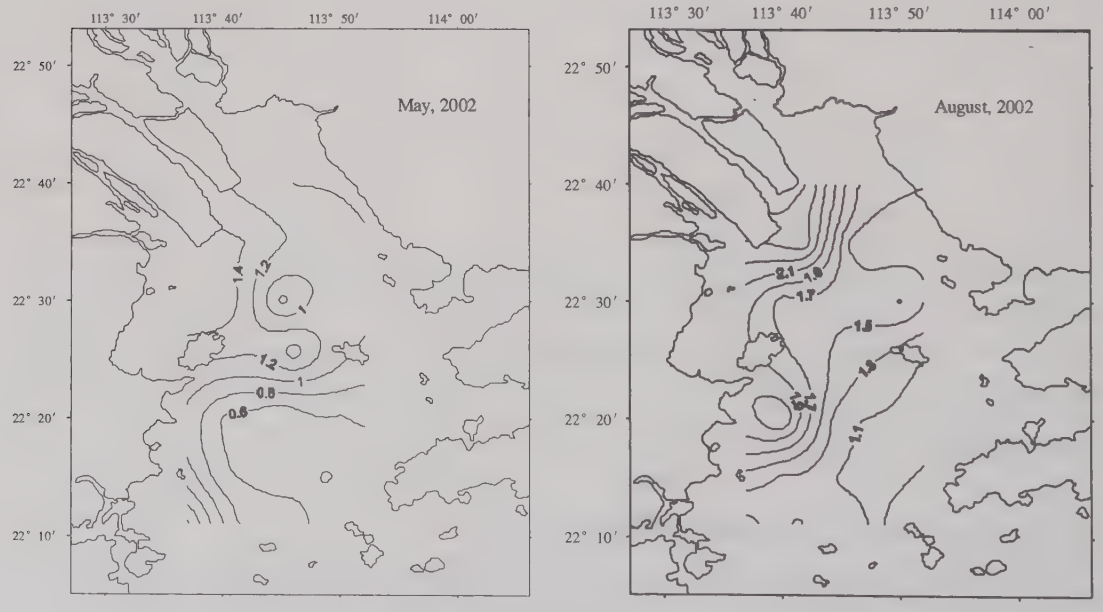

Fig. 2 Concentration distribution of COD (mg • L^{-1}) in the Lingdingyang waters of Pearl River estuary

2.2 The seasonal differences of COD

The concentration of COD in the waters of Pearl River estuary was 0.41 - 1.65 mg • L^{-1} in spring (the average was 0.94 mg • L^{-1}) and 0.78 - 2.72 mg • L^{-1} in summer (the average was 1.49 mg • L^{-1}). The range and average of COD concentration in summer were higher than that in spring and the difference of the average was 0.5 mg • L^{-1}. Obviously, the concentration of COD showed seasonal differences. The main reason was that summer was a flood period of rainy season with larger runoff, and brought on larger sewerage and suspended substances from coast. This is very evident in the northwest waters of the Pearl River estuary, or nearby Humen and Jiaomen, and the waters around Zhuhai City.

2.3 The assessment of COD

The concentration of COD is one of the important indicators that reflect the extent of pollution of organic substance in waters. The survey results are evaluated by the first class (COD< 2 mg • L^{-1}) of sea water quality standard (Chinese standard)[4], and the contamination index of >1 is deemed exceeding the standard. The contamination indexes of COD from this study were between 0.20 and 1.36 with an average of 0.52 (Fig. 3). Among them, the contamination indexes of COD in spring were between 0.20 and 0.82 with an average of 0.47, and didn't exceed the set standard; while in summer the contamination index was relatively higher, and were between 0.50 and 1.36 with an average of 0.74, and the rate of exceeding the set standard was 15 %. The waters where the set standard was exceeded main appeared in the waters around Humen at the northwest tip of the Pearl River estuary, the outlet of Jiaomen and Zhuhai, the contamination index of COD north of Guishan Island was the minimum which never exceeded the set standard.

During the survey, most contamination indexes of COD in the Lingdingyang waters of Pearl River estuary were < 1 except for individual local waters where it was > 1.

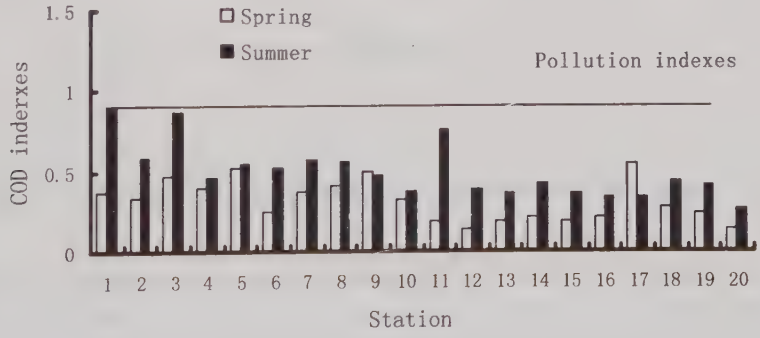

Fig. 3 Pollution indexes of COD in the waters of Pearl River estuary

2.4 The relationship between COD and other environmental factors

One-dimensional regression was made of the concentrations of COD, suspended substances, inorganic nitrate and phosphate in spring and summer, and the results of correlation analysis indicated:

In spring and summer, the concentration of COD was positively correlated with the concentration of the suspended substances (Figs. 4-5), and the correlation coefficient (r) was 0.45 in spring ($p < 0.05$, $n = 20$), and 0.62 in summer ($p < 0.05$, $n = 20$), which showed that the concentration of COD was correlative with the concentration of suspended substances in the waters. COD, as one of the main pollutants, comes from domestic sewerage and industrial and agricultural effluent with a large amount of discharge and a low rate of treatment, which are commonly characterized by great turbidity and contain a large number of colloid, celluloses, suspending substances, deposits and soluble organic matters. The effect is especially obvious when the discharge amount is large.

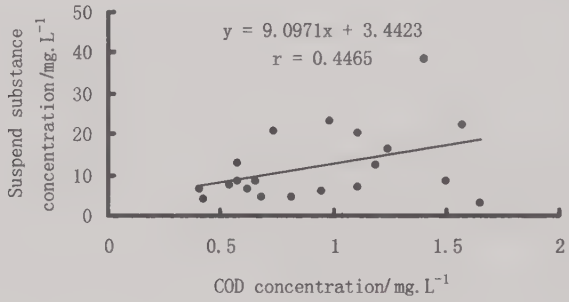

Fig. 4 The correlation of COD concentration with suspended substance in spring

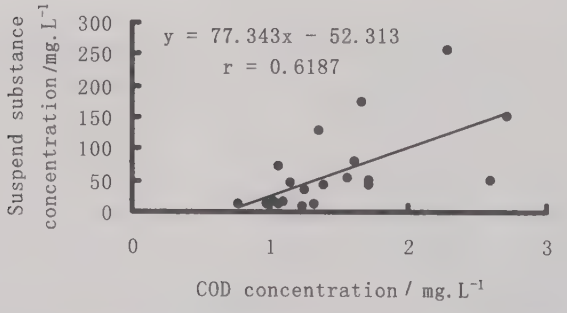

Fig. 5 The correlation of COD concentration with suspended substance in summer

COD showed a negative correlation with the concentrations of inorganic nitrate and phosphate in summer (Fig 6-7), $r = -0.63$ ($p < 0.10$, n = 20) and $r = -0.31$ ($p < 0.10$, $n = 20$). The correlation was complex between the concentrations of COD and the inorganic nitrate, and whether it was positive or negative depends on the environmental condition of the waters [5]. The deoxidized water contains a mass of organic matter, which was decomposed by anaerobic bacteria, and the removal of nitrogen oxidation would take place, and the concentration of nitric acid nitrogen, nitrous acid nitrogen, and ammonium nitrogen is low. COD showed a negative correlation with the three forms of nitrogen. In the oxidative waters, the nitride which comes from organic matter oxidation will continue to be nitrified, and COD

showed a positive correlation with the three forms of nitrogen.

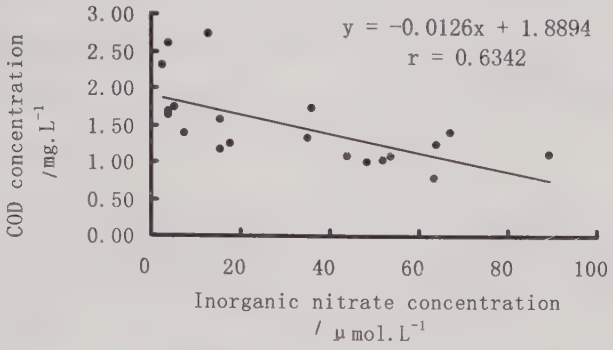

Fig. 6 The correlation of COD concentration with inorganic nitrate in summer

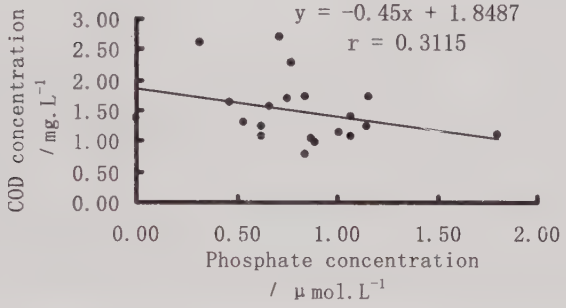

Fig. 7 The correlation of COD concentration with phosphate in summer

3 Summary

The results on the COD in the Lingdingyang waters of Pearl River estuary surveyed in 2002 could be summarized as follows:

(1) During the survey period, the concentrations of COD in sea water ranged from 0.41 to 2.72mg.L^{-1} with an average of 1.21mg.L^{-1} and the concentration in summer was higher than that in spring.

(2) The spatial distribution showed that it gradually decreased from north to southeast, and the concentration in the coastal waters was higher than that in the offshore waters. The concentration of COD was relatively high in the waters of Humen, Jiaomen, Hongqili, around Zhuhai City and Macao. The results were in accordance with the effects of runoff, discharges of domestic sewerage and industrial effluent along the coast.

(3) The contamination indexes of COD were between 0.20 and 1.36 with an average of 0.53. The waters with the contamination index exceeding the standard were the part of the northwest waters and the waters around Zhuhai City. It was lower in the waters north to Guishan Island. Evaluated by the first

class (COD < 2mg • L^{-1}) of sea water quality standard (Chinese standard), the percentage of the COD exceeding the fist class standard was 15 % during the survey.

(4) The concentration of COD had a positive correlation with the concentration of the suspended substances in spring and summer, but in summer it showed a negative correlation with the concentration of inorganic nitrate and active phosphate.

Acknowledgements

The study was supported by the National Special Social Public Welfare Fund (No. 2001DIA10014-2).

References

[1] National Standard of PRC (GB17378.4-1998), the specification for marine monitoring Part 4: Seawater analysis [S].

[2] National Standard of PRC (GB3097-1997), sea water quality standard [S].

[3] Wang W L, Li D S, Dong S L. Inorganic Nitrogen with Stocking Densities of Cultured Animals and Environmental Factors in the Shrimp Culturing Enclosures. Marine Science, 2002, 4(10): 44-47.

[4] Jia X. P, Lin Q. The Effects of Major Pollutions on Marine Culture and Fishery Resource Enhancement along the Coastal Waters of China, Fishery Science of China, 1997, 4 (4): 78-82

[5] Jiang Y J. Marine Polluted Prevention of Coast and General Management Strategic Planning lin Pearl River Estuary, Symposium on Resources and Environment in South China Sea, 1999, 49-56.

珠江口水域化学耗氧量(COD)的分布特征

杨美兰，林 钦，黄洪辉，甘居利，蔡文贵，吕晓瑜，
王增焕，李纯厚，杜飞雁，胡德蓉

（农业部渔业生态环境重点开放实验室，广东省渔业生态环境重点实验室，中国水产科学研究院南海水产研究所，
广东，广州 510300）

摘要：2002 年 5 月和 8 月对珠江口伶仃洋水域水质化学耗氧量（COD）进行了调查研究，结果表明：该水域近期 COD 含量变幅在 0.41 ～ 2.72 mg • L^{-1} 之间，平均值为 1.21 mg • L^{-1}；区域分布呈北部向南部水域逐渐递减以及近岸水域含量大于远岸的变化趋势；夏季 COD 的含量高于春季；以我国 I 类海水水质 COD 含量≤2 mg • L^{-1} 标准评价，超标率为 15 %；COD 含量与同期（春、夏季）的悬浮物含量呈正相关性，与无机氮和活性磷酸盐含量在夏季呈负相关性。

关键词：化学耗氧量　珠江口水域　分布特征

Fluorescence-assisted Image Analysis of Harmful Microalgae

WANG Xuemin (王学民)*, SUN Yong (孙 勇), CAO Hongbao (曹红宝)

School of Precision Instrument and Opto-Electronics Engineering, Tianjin University, Tianjin 300072, China

Abstract: In order to realize the detection and analysis of microalgae in sediment samples with complex scenes, the project takes advantage of the character of microalgae that they can auto-fluoresce when exposed to the illumination of certain exciation waves. The project takes grey-scale and fluorescent pictures of microalgae in the same field of view and uses the image processing technique to deal with the images, such as threshold segmentation, contour and texture analysis and pattern recognition. The results show that the fluorescent image can effectively elimate the yawp in the complex background and make the consequent image processing more effective and easy. Then the project comes to the conclusion that fluorescence-assisted image processing can realize the detection and analysis of microalgae in sediment samples containing complex scenes.

Keywords: harmful microalgae; image segmentation; fluorescence

Introduction

Along with the intensification of marine environment pollution and seawater eutrophication, the harmful microalgae disaster occurs more and more frequently. At present, in the process of microalgae recognition, whether manual observation and analysis of the seawater sample in laboratory or using computer to analyze and recognize automatically, the complex background that microalgae contain is the main factor to restrict the efficiency and speed of pattern recognition, and so far there is no effective way to solve the problem. On the basis of introduction of the fluorescence-assisted method and hardware system, the paper puts emphasis on the discussion of the application of the fluorescence-assisted method in elimating the background yawp and assisting the analysis and recognition of the image of the harmful microalgae. In addition, we have also solved the problem of the detection and analysis of microalgae in sediment samples containing complex scenes.

1 The theory of fluorescence-assisted method and experiments

When a kind of substance is exposed to the illumination of certain light (such as ultraviolet radiation) with certain wavelength, it will eradiate another kind of light (such as visible light) with

Received on Sept. 16, 2005

* Corresponding author. E-mail: xueminw@mail.tju.edu.cn

larger wavelength in extremely short time (10^{-8} s), which is called fluorescence. Because of different molecular structures and energy distributions, different fluorescence substances display different absorption spectra and fluorescence spectra. For a certain fluorescence substance to measure, so long as an appropriate excitation/emission filter is chosen, we can detect the fluorescence [1]. Most harmful microalgae contain chlorophyll A, so when exposed to the exciting light with a given wavelength, the harmful microalgae will eradiate fluorescence, and the wavelength in the center of the fluorescence is 685nm, half-band width is about 20nm. The fluorescence is brighter when excited by waves with a wavelength of about 420 nm. These parameters may vary with the chlorophyll content of different microalgae, different shapes of microalgae and different proportions of other pigments. So the project uses the machine of F－4500FL Spectrophotometer to do experiments to mensurate the parameters of many kinds of microalgae. Fig 1 shows the fluorescence of *chlorella pynenoidosa* under different exciting lights. Fig 1(a) shows the curve of using the exciting light with a wavelength of about 350 nm, Fig 1(b) shows the curve of using the exciting light with a wavelength of about 450 nm, and Fig 1(c) shows the curve of using the exciting light with a wavelength of about 550 nm. There is a wave crest at the wavelength of the exciting light due to Rayleigh scattering in every figure, and the wave crest should not in the fluorescence spectrum. It is shown in the figure that the main wave crest is highest at the wavelengths of 350 nm and 450 nm (because the density is very high, the peak of fluorescence is cut-off at the 1000, and the peak is much higher when the cut-off width is much wider), but there is main wave crest at about the wavelength of 685/20 nm no matter which kind of exciting light is used, hence, the project chooses 685nm as the center wavelength and 20nm as the half-band width in the following experiments.

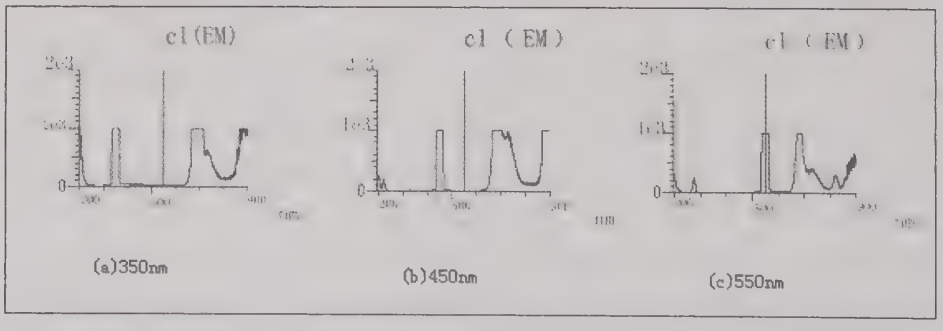

Fig. 1 The fluorescence of *chlorella pynenoidosa* under different exciting lights

Fig. 2 shows the fluorescence spectrum of *chlorella pynenoidosa*, *gymnodinium* sp. and *heterosigma* akashiwo hada, and the center wavelength of the fluorescence is 685 nm. The figure shows that every kind of microalgae has an obvious fluorescence response at the wavelength of 350 nm. So the

project uses the wave length of 350 nm as exciting light to do experiments (In the actual operation, because the wavelength of main fluorescence wave crest is about 685 nm,we can choose the light which wavelength is under 500 nm as exciting light).

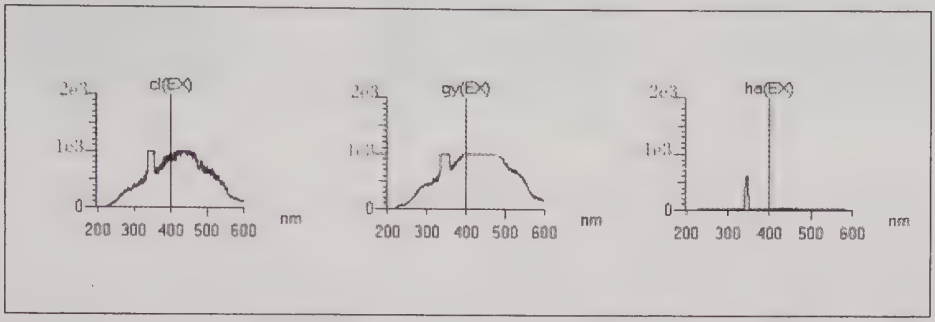

(a) *chlorella pynenoidosa* (b) *gymnodinium* sp. (c) *heterosigma* akashiwo hada

Fig. 2 The intensity curve of 685 nm fluorescence under different exciting light

2 Construction of hardware system

The key to the fluorescence experiments lies in the fluorescence microscope. In the project, to get better effect, in the first stage we used a special fluorescence microscope to do experiments, and in the second stage, to reduce the cost and operate easily, we transform the common microscope to take fluorescent pictures. Fig. 3 shows the whole system of hardware. To transform the common microscope, at the incident photosource we choose the color filter whose center wavelength is 350nm and half-band width is 10 nm and transmittance is 50 %, at the interface to the CCD digital camera we choose the high-pass filter whose center wavelength is 580nm and band width is 20nm. The incident photosource is a cold lamp of 30 – 50 W.

Fig . 3 Construction of hardware system

3 Fluorescence image

In the darkroom, we used the fluorescence microscope to take fluorescent pictures of the microalgae in sediment samples containing complex scenes, and contrasted them to the grey-scale pictures in the same field of view. Fig. 4 shows the fluorescent images taken by a special fluorescence microscope. All fluorescent pictures were taken under the condition that the wavelength of exciting light is 350 nm

(half-band width is 10 nm) and the enlargement factor is 40 times.

(a) *gymnodinium* sp.

(b) crescented-nitzschia pungens

(c) *heterosigma* akashiwo hada

Fig. 4 Fluorescent images

It is shown in Fig. 4 that in the fluorescent pictures, the background is clear, but the contour and the texture are blurry, mainly because the resolving power of fluorescence is lower and pigments in the microalgae are not symmetrical, but this is not a problem for eliminating the background yawp. Fig. 5 shows the contrast of fluorescent and grey-scale images in the same field of view. It is shown in Fig. 5 that the fluorescent images have eliminated the complex background yawp and kept the position of microalgae, and this is just the great significance of fluorescence-assisted method.

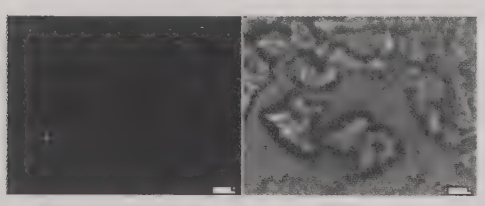

(a) *heterosigma* akashiwo hada

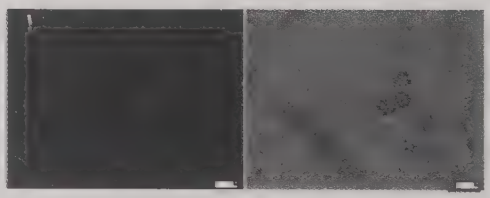

(b) *gymnodinium* sp.

Fig. 5 Contrast of fluorescent and grey-scale images in the same field of view (florescent images are on the left)

4 Processing of fluorescent images

On the basis of fluorescent experiments, we did image segmentation, contour and texture analysis, parttern recognition and counting and so on to the fluorescent images, and contrasted them to the processing result of grey-scale images, from which we have found that the fluorescence-assisted method can make the processing more effective and much easier.

4.1 Threshold segmentation

Image segmentation is a key stage in the image processing, and the final result of image processing mainly depends on the result of images segmentation. Fluorescent images can extract object information from the complex background yawp, which makes great promotion to images segmentation.

Fig. 6(a) shows the segmentation result by the threshold value of the grey-scale image of *gymnodinium* sp. in Fig. 5(b), Fig. 6(b) shows the segmentation result by the threshold value of fluorescent image of *gymnodinium* sp. in Fig. 5(b), and the segmentation algorithm of the self-adaptive threshold(this algorithm is appropriate to the segmentation of the grey-scale image of *gymnodinium* sp.) is used in both pictures. It is shown in the figure that the contour and the texture in Fig. 6(a) are more complete than those in Fig. 6(b), but there is much more background yawp in Fig. 6(a). There is nearly no background yawp in Fig. 6(b), but the contour is not complete, and the texture information is partially lost.

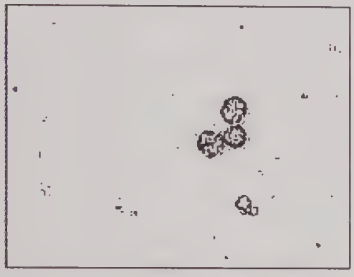

(a) Segmentation of grey-scale images

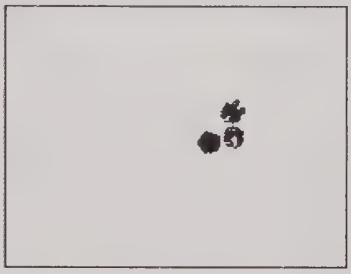

(b) Segmentation of fluorescent images

Fig. 6 Segmentation contrast of grey-scale image and fluorescent image of *gymnodinium* sp.

Fig. 7(a) shows the segmentation result by the threshold value of the grey-scale image of *heterosigma* akashiwo hada in Fig. 5(a), Fig. 7(b) shows the segmentation result by threshold value of fluorescent image of *heterosigma* akashiwo hada in Fig. 5(a), and the segmentation algorithm of the two-dimensional max entropy threshold (this algorithm is appropriate to the segmentation of the grey-scale image of *heterosigma* akashiwo hada) is used in both pictures. It is shown in the figure that in

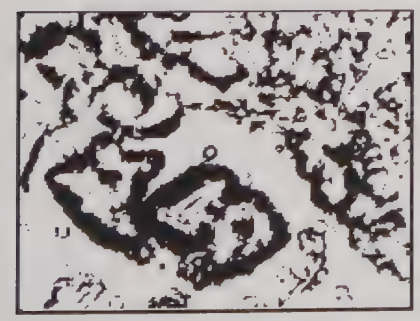

(a) Segmentation of grey-scale images

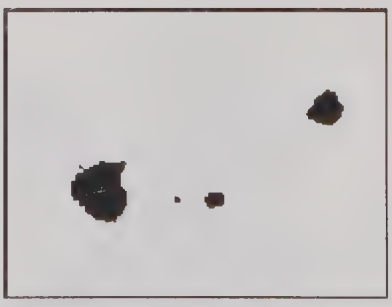

(b) Segmentation of fluorescent images

Fig. 7 Segmentation contrast of the grey-scale image and fluorescent image of *heterosigma* akashiwo hada

the segmentation result of grey-scale image, the microalgae information is nearly completely lost in the background yawp, and there is nearly no background yawp in the fluorescent image, and though part information of contour and texture is lost, the position information of microalgae is kept well, which makes it possible to recognise and count microalgae under the condition of complex background yawp.

4.2 Image contour, texture analysis , pattern recognition and counting

The quality of image has great effect on the image features, and the precision and validity of the image feaatures are the precondition and foundation for the image recognition. The fluorescence-assisted method eliminates the background yawp effectively and improves the image quality, which is of great importance to the image character analysis and pattern recognition.

Combining the position information of fluorescent image with the contour and texture information of grey-scale image, we can use the computer to recognise and count microalgae automatically [3, 4]. The paper selects 15 features including 4 contour featurers (perimeter, area, circle degree, rectangle degree), 7grey featurers (M_0-M_6)[5], and 4 texture featurers (inertia, power, relation, entropy) [6]. With these features, we used the artificial neural network to recognize microalgae. Fig. 8 shows the result of recognition and counting, Fig. 8(a) is the recognition result of Fig. 4(a), the recognition percentage is 95 % in the high density image, which can't be achieved if only basing on the grey-scale image, Fig. 8(b) is the recognition result of Fig. 7(b) combining texture featurers, the recognition can't be achieved only by basing on the grey-scale image if there is no fluorescent image.

If the object is known, we can get the contour and texture characters from the grey-scale image, and set up the database of image characters, then we can use the fluorescent image combining these information to do image recognition. In Fig.8 (b), the impurity between the object 1 and the object 2 is eliminated in the light of the perimeter character (contour character) of *heterosigma* akashiwo hada. Furthermore, some kinds of microalgae have other pigments and fluorescence substance except chlorophyll A, so they can eradiate fluorescence of other wavelengths, which can be used to distinguish the microalgae.

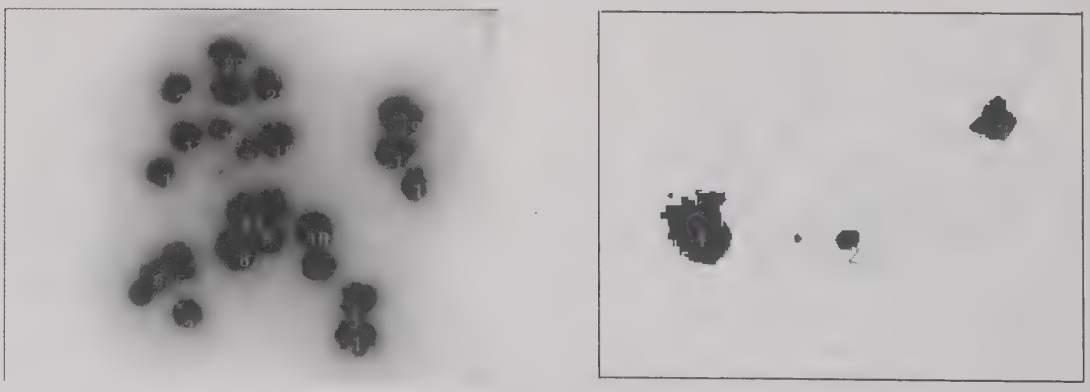

(a) Recognition of *gymnodinium* sp. (b)Recognition of *heterosigma* akashiwo hada

Fig. 8 Recognition results using the combined fluorescent and grey-scale images

5 Discussion: the disadvantages of fluorescence-assisted method

Though the fluorescence-assisted method is of great importance to the image analysis of microalgas, it has the following disadvantages:

(1) The fluorescent images always contain little useable analytical information for species identification, grey-scale images must be used to get accurate recognition result, and the function of fluorescent image is just assistant.

(2) The fluorescent images tend to have low photometric resolution and low contrast as well as low spatial resolution caused by limitations of fluorescence camera.

(3) There is another problem that a fluorescing object acts as a mass of omnidirectional point sources of light, resulting in a blurring effect when imaged by a microscope, which generally requires parallel light for optimal image resolution. To overcome this limitation, a grey-scale image of the same scene is necessary if accurate object classification is required. The fluorescent image is used to locate only fluorescing objects in the grey-scale image, by segmenting those areas of grey-scale that have corresponding parts.

(4) The fluorescent image and the grey-scale image in the same field of view can't be taken at the same time. There are two difficulties, first, there must have an interval of several seconds between the fluorescent image and the grey-scale image, and in the several seconds, due to the movement of the micrealgaes in the sample, there must be position mismatching between two images. It is difficult to solve the mismatching problem. Secondly, the fluorescent image and the grey-scale image should be taken at the same position, otherwise, there occurs the position mismatching problem. The problem of position mismatching can be solved by adding the corresponding process in the hardware and software.[7]

(5) It is inevitable that there must be other impurities not microalgas in the sample that can fluoresce, which also makes it more difficult to apply the fluorescent image to the image recognition.

Due to these disadvantages, it is impossible to recognize microalgae only by fluorescent images, and they must be used along with grey-scale images, and the function of fluorescent image is just assistant.

6 Conclusion

Fluorescent images can eliminate background yawp effectively, provide precise position information for the consequent processing, then combining the contour and texture information of grey-scale image, this is very effective for the pattern recognition and counting of microalgae in the complex background yawp, which is an important application of the fluorescence-assisted method.

Acknowledgments

The project is subsidized by the National High-tech Research Development Plan(863 plan) Project No. 2002AA639260.

References

[1] Xia Yingda et al. Application of Fluorescence Technique In Ocean Environment. Ocean Transaction, 1995, 21(3): 66-72.

[2] Kaitala S et al. Fluorescent analysis of pigment composition of natural phytoplankton. ceanographic Literature Review, 1995, 42(9):47-53.

[3] Wang Xincheng. High Level Image Processing. Beijing: Science and Technology Publishers of China. 2000, 176-182.

[4] Zheng Nanning. Computational Visual Sense and Pattern Recognition. Beijin: National Defence and Industrial Publishers.1998, 80-84.

[5] Sun Jixiang et al. Character Selection and Computational Invariant in Pattern Recognition. Beijin: National Defence and Industrial Publishers. 2001, 248-270.

[6] Furht B et al. Video and image processing in multimedia systems. Kluwer Academic Publishers. 1995, 226-270.

[7] Uchidehama Otsu. Fluorescence-assisted image analysis of freshwater microalgae.Journal of Microbiological Methods .2002, 149-162.

荧光法在赤潮图像分析中的应用

王学民，孙 勇，曹红宝

（天津大学精密仪器与光电子工程学院，天津 300072）

摘 要：赤潮藻样品中往往包含着各种复杂的非藻沉淀物，为解决这些微藻的探测和分析的问题，可以利用微藻类在一定波长的光照射下会产生荧光的特性，对裸甲藻等多种赤潮藻类进行荧光实验处理，并在此基础上对藻类的荧光图像和灰度图象进行图像分割，轮廓和纹理分析及图象识别等后继图象处理。实验证明，荧光法可以有效的去除背景噪声，保留藻类信息，使得后继的图象处理工作更加容易和有效，从而解决了探测和分析包含复杂背景的沉淀物样品中微藻的问题。

关键词：赤潮藻；图象分割；荧光

Research on Prediction of Red Tide Based on Fuzzy Neural Network

ZHANG Rong (张 容), YAN Hong (阎 红), DU Liping (杜丽萍)
Mechanical College, Tianjin Professional University, Tianjin 300402, *China*

Abstract: In this paper, a four-layer fuzzy neural network using the Back Propagation (BP) Algorithm and the fuzzy logic was built to study the nonlinear relationships between different physical -chemical factors and the denseness of red tide algae, and to anticipate the denseness of the red tide algae. For the first time, the fuzzy neural network technology was applied to research the prediction of red tide. Compared with BP network and RBF network, the outcome of this method is better.

Keywords: red tide prediction; fuzzy neural network (FNN); Back Propagation Algorithm

Introduction

Research on the prediction of red tide is quite important in the red tide research, which plays an important role in preventing the harm of red tide, decreasing the economic loss caused by red tide, and protecting the health and safety of people. In recent years, neural network has been widely used in researching the prediction of red tide, such as the Back Propagation Algorithm, the RBF network, and so on. This is because Neural Network has a better nonlinear approaching ability, which can educe the function relationships between the input and output variables based on sample data training. That is to say the neural network can ascertain the coupling value among different nerve cells by its self-learning function, so that the whole network can possess the functions close to that of functions. Thus we can forecast the red tides avoiding the complicated ecological dynamical mechanisms on which the red tides form. However, there are still some problems about the neural network; for example, it does not possess a good model interpreting ability.

Fuzzy neural network is a new technology, which combines fuzzy technology with neural network. It overcomes their disadvantages and integrates their advantages. On the one hand, it enhances the model interpreting ability of the neural network by making use of the interpreting ratiocination ability of the fuzzy system, on the other hand, it overcomes the dependences of the fuzzy technology on the advice of experts and the non-self-adaptability [1] of the fuzzy concourse by making use of the self-learning functions of the neural network. In this paper, we will discuss the structure of the fuzzy neural network used to predict the red tide, as well as the predicting methods.

Received on Dec. 20, 2005

1 The structure of fuzzy neural network

1.1 The model of structure

As is shown in Fig. 1, the model has four layers:

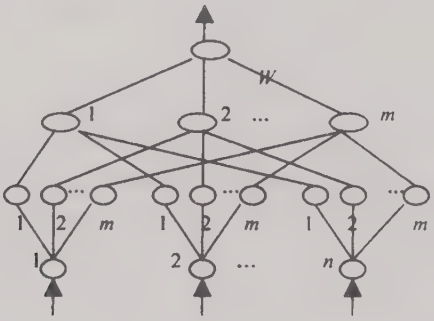

Fig. 1 The Model of Fuzzy Neural Network Structure

The first layer: variable input layer. x_j, j are from 1 to n, and n refers to the number of input variables.

The second layer: fuzzy layer. Each node in this layer represents the precondition of the fuzzy rule, whose input is the output of the first layer. And its output represents the subjection degree of each input variable to the precondition of the rule. The function of subjection degree adopting the standard gauss function is:

$$C_{ij} = \exp[\frac{-(x_j - v_{ij})^2}{\delta_{ij}}], i = 1, 2, \ldots, m, j = 1, 2, \ldots, n$$

Here m refers to the fuzzy rule number, and n refers to the number of input nodes. v_{ij}, δ_{ij} refer separately to the center and width of the gauss function of subjection degree.

The third layer: fuzzy ratiocination layer. The fuzzy complex product in this layer adopting the sup product is: the function of the output nodes of the fuzzy rule of i is:

$$u_i = \prod_{j=1}^{n} C_{ij}(x_j)$$

The fourth layer: relief of fuzzy — output layer. The barycentre method is adopted in this layer to relieve fuzzy. The output of the network is:

$$y = \frac{\sum_{i=1}^{m} u_i w_i}{\sum_{i=1}^{m} u_i}$$

w_i refers to the coupling value of the node of i to the output node in the third layer.

1.2 The learning arithmetic of fuzzy neural network

The learning arithmetic of the network value (v_{ij}、δ_{ij}、w_i) uses the arithmetic of BP (Back Propagation algorithm)

The target function is $E=\frac{1}{2}(y-Y)^2$,

where, y is the output, and Y is the target vector. Regulate the value of v_{ij},δ_{ij},w_j according to the following formula:

$$v_{ij}(t+1)=v_{ij}(t)-\eta\frac{\partial E}{\partial v_{ij}}+\beta\Delta v_{ij}(t)$$

$$\delta_{ij}(t+1)=\delta_{ij}(t)-\eta\frac{\partial F}{\partial \delta_{ij}}+\beta\Delta\delta_{ij}(t)$$

$$w_i(t+1)=w_i(t)-\eta\frac{\partial E}{\partial w_i}+\beta\Delta w_i(t)$$

η, β, Δ separately refer to the learning rate, the coefficient of the momentum item and the error item.

2 The parameter confirmation of the network

2.1 Confirm the number of the input variable n

According to the reference [2], five genes have greater effects on the denseness of red tide algae. So the number of input variables is 5. That is to say $n=5$.

2.2 Confirm the number of the best rules m

The fuzzy clustering arithmetic is adopted in this paper to confirm the number of the best rules of the fuzzy system. The number of the best rules is used as the number of the concealed layer nodes of the network. The greatest advantage of this method is to be able to find out the data structure of the network quickly, but it does not have a good precision. However, the learning ability of neural network can make up for the disadvantage.

2.3 Confirm the Elementary value w_i

Generally speaking, the values constringe along with iterating. But if the elementary values are too big, the network will soon become saturated. In addition, the elementary values have effects on the speed of constringency. Reference [3] shows: If the elementary values are not excessively big, they will not have obvious effects on the integrative capability of the network. The elementary w_i in this paper is 0.05.

2.4 Select the appropriate learning rate η and the coefficient of momentum item β

If the selected learning rate η is too small, the degree of the amendment of the network variables will be too little and the constringency will be too slow; if it is too big, it may cause a durative surge

near the stabilization point and it will be difficult to constringe, although it can quicken the learning speed. The introduction of β can eliminate the high frequent surge during the learning process, so that bigger learning rates can be selected, and the learning speed of the network can be quickened. At present, there is no definite method to confirm the learning rate in theory. For certain problems, we should do some experiments to compare the results of different η, β combinations. By doing some contrastive experiment, we find it is appropriate to choose $\eta = 0.015$, $\beta = 0.8$.

3 Forecast the denseness of red tide algae using various neural networks and compare the results

3.1 Source of the sample data

According to the investigated data in the reference [4] in 1997, there are all together 17 samples. The physical -chemical factors are: the temperature of water T; the dissolve oxygen DO; the salinity S; the amount of nitrogen; the denseness of algae, and so on. As is shown in Table 1, choose 14 samples as the learning samples(1 - 5, 7 - 13, 16 - 17), 3 as the target sample (samples 6, 14 - 15). Calculate separately using the BP neural network, the RBF network and the fuzzy neural network and compare the results.

Tab. 1 Denseness of luminous algae and the data of different physical -chemical factors

Samples	Water temperature	Dissolve oxygen / mg • L^{-1}	Salinity	Amount of nitrogen / μ mol • l^{-1}	Amount of phosphorus / μ mol • l^{-1}	Luminous algae denseness / 100 • m^{-1}
1	22.9	7.06	30.3	0.4	0.54	1.77
2	23.1	7.5	30.4	0.56	0.39	470
3	23	7.44	30.6	0.81	0.18	440
4	23.2	7.54	30.5	0.52	0.07	180
5	23.4	7.62	30.4	0.88	0.07	160
6	23.4	7.54	29.5	0.23	0.43	60.4
7	22.9	7.56	30.8	0.83	0.21	23.7
8	24.2	7.83	30.5	0.14	0.4	8.28
9	22.5	6.97	30.4	0.52	0.56	7.6
10	24.7	7.56	30.2	0.32	0.32	91.5
11	23.2	7.31	30.4	0.73	0.26	467
12	23.1	7.12	30.2	0.17	0.4	5.99
13	23.5	7.38	30.3	0.31	0.47	4.04
14	23	7.06	30.3	0.4	0.54	2.8
15	23.7	7.36	30.5	2.05	0.36	260
16	23.3	7.22	30.4	0.72	0.1	530
17	23	7.14	30.3	0.27	0.43	7.56

3.2 Pretreatment of the data

First of all, standardize the data, in order to avoid the overflow of the data. The formula is:

$$\bar{x} = \frac{1}{n}\sum_{i=1}^{n} x_i$$

$$y_i = x_i - n\bar{x}$$

$$ees = [\frac{1}{n-1}\sum_{i=1}^{n}(y_i - \bar{x})^2]^{\frac{1}{2}}$$

$$x_i' = \frac{x_i}{n \cdot ees}$$

where, x_i refers to the original value of the sample, $\bar{x}$ is the average value of each longitudinal line of the sample, n refers to the number of the samples, ess is the variance and x_i' refers to the value after standardization .

The formula of standardization is:

$$x_i'' = 0.9 - \frac{0.9[\max(x_i') - x_i']}{[\max(x_i') - \min(x_i')]}$$

where, x_i'' is the standardized value. Max and min mean the maximum and minimum values.

The regulated data are shown in Table 2.

Tab. 2 Standardized data

Samples	Water temperature	Dissolve oxygen	Salinity	Amount of nitrogen	Amount of phosphorus	Luminous algae denseness
1	0.24545	0.18371	0.5923	0.2089	0.86733	0.1
2	0.31818	0.59302	0.65384	0.27592	0.62244	0.80915
3	0.28182	0.5372	0.77692	0.38063	0.27958	0.76369
4	0.35455	0.63023	0.71538	0.25916	0.1	0.36993
5	0.42727	0.70464	0.65384	0.40995	0.1	0.33964
6	0.42727	0.63023	0.1	0.1377	0.68775	0.18879
7	0.24545	0.64883	0.9	0.38901	0.32856	0.13321
8	0.71819	0.9	0.71538	0.1	0.63877	0.10986
9	0.1	0.1	0.65384	0.25916	0.9	0.10883
10	0.9	0.64883	0.53076	0.17539	0.50816	0.2359
11	0.35455	0.41628	0.65384	0.34712	0.4102	0.8046
12	0.31818	0.23953	0.53076	0.11256	0.63877	0.10639
13	0.46364	0.48139	0.5923	0.1712	0.75305	0.10344
14	0.28182	0.18371	0.5923	0.2089	0.86733	0.10156
15	0.53636	0.46279	0.71538	0.9	0.57346	0.49109
16	0.39091	0.33255	0.65384	0.34293	0.14896	0.9
17	0.28182	0.25814	0.5923	0.15445	0.68775	0.10877

The result calculated from the sample is that the best clustering number m = 3. Samples 1, 6, 9, 12, 13, 14, 17 belong to the first sort; samples 2 - 5, 11, 16 belong to the second sort; and samples 7, 8, 10, 15 belong to the third sort.

The matrix of the clustering center v_{ij}.

Tab. 3 Matrix of elementary values

Sorts	Input 1	Input 2	Input 3	Input 4	Input 5
1	0.6	0.66511	0.71538	0.3911	0.51224
2	0.3026	0.29667	0.52197	0.17898	0.77171
3	0.35455	0.53565	0.68461	0.33595	0.27686

3.3 Imitation and prediction of BF, RBF and neural network

According to the conclusion of reference [5], the MATLAB neural network box was adopted, and BP and RBF networks were separately constructed in this paper. The model parameters are as the following: there are three layers of BP network and the number of concealed nerve cells is 6; the training function is 'trainlm', the number of training process is 10 000; the parameter of RBF network is adopted as default value.

The result of imitation and prediction is shown in Fig. 2.

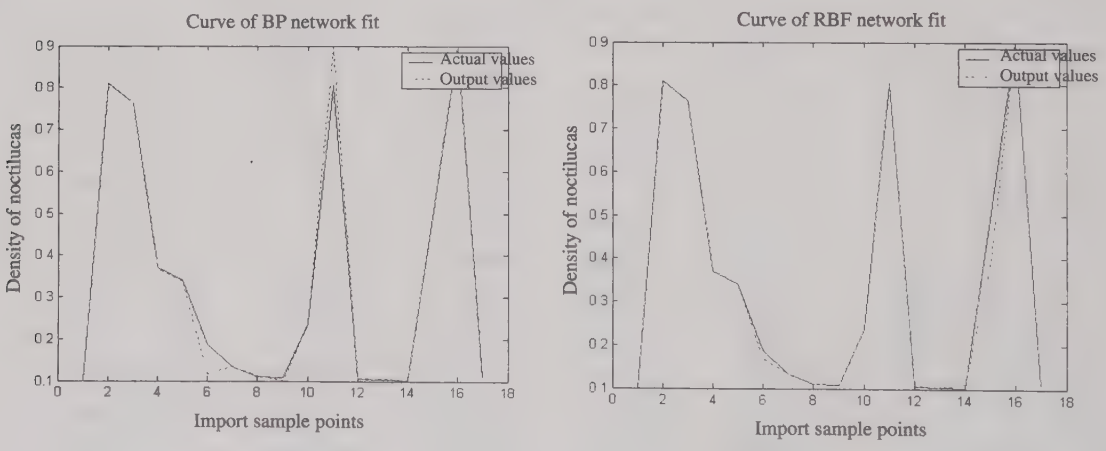

Fig. 2 a) Comparative curve of the actual values and the output value;
b) Comparative curve of the actual values and the output values of RBF

Comparing the above Table 3, Fig. 2-a and Fig. 2-b, we can conclude that as far as the training nodes used for imitation in the curve are concerned, the BP network is less precise than the RBF network. As far as the result of prediction is concerned, the result of the RBF network is more satisfying.

3.4 Imitation and prediction of the Fuzzy Neural Network (FNN)

Program and implement the network according to the reference [7] and the above structure parameters. The comparison of the result of the FNN with that of BP, RBF is shown in Fig. 3.

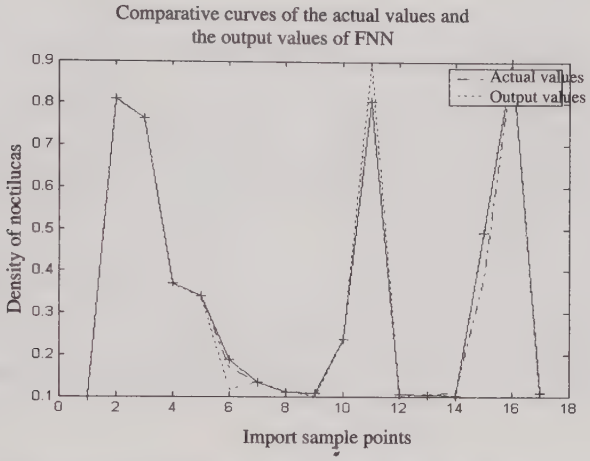

Fig. 3 Comparative curves of the actual values and the output values of FNN

The "+" in the figure refers to the values of the 17 samples of the fuzzy neural network. The following table shows the comparison of three values of prediction:

Tab. 4 Comparison of the actual values and the predicted values

Samples	Actual values	BP	RBF	FNN
6	0.18879	0.11712	0.16879	0.18877
14	0.10156	0.10163	0.10138	0.10159
15	0.49109	0.48938	0.48994	0.49134

According to the above comparison, it can be concluded that the prediction result of the fuzzy neural network is more precise. And the imitation result is more precise than those of BP and RBF networks.

4 Discussion and epilogue

(1) Fuzzy Neural Network overcomes the shortcomings of BP and RBF networks. The conversion of the input and output function of BP network (Sigmoid function) is too simple, and the approaching capability of single nerve cell is feeble. Moreover, it is difficult to confirm the number of nerve cells. There is some improvement about the RBF network, but there are still some problems in

selecting the center of the network. Fuzzy neural network confirms the center of the network using the clustering arithmetic, and the number of concealed nerve cells is confirmed with fuzzy rules. Thus the fuzzy clustering arithmetic is combined with the learning function of the neural network, so that both the speed and precision can be improved.

(2) The function of fuzzy subjection degree adopts the standard gauss function, so that the precision of both calculation and extrapolation can be improved. The shape of the gauss function within the center width is similar to that of radial function, and it has a better local characteristic. The shape of the function outside the center width is similar to that of Sigmoid function, and it has a better integrative characteristic. So the fuzzy neural network possesses both the quick constringency characteristic of RBF and the integrative characteristic of BP network.

(3) The result of the experiment shows that the model of fuzzy neural network can preferably reflect the nonlinear relationships between different physical -chemical factors and the denseness of red tide algae, and it is more precise. It is an efficient predicting method, and it provides some guidance for the prediction of red tide.

References

[1] Tan Ying. Neural-fuzzy system modeling and its application in forecasting. Tianjin university, graduate student essay, 1998.

[2] Shen F, Qu Y. The study on the prediction of artificial neural network for phytoplankton's density. ocean technology, 2005, 24(1): 44-47.

[3] Wu H, Chen W Q. Prediction of ups and downs of stock market by BP neural networks. Journal of Dalian University of Technology, 2001, 41(1): 9-15.

[4] Cai R Y. ArtificialNeural Network Predicting Model of NoctilucaSCientillans Density and Physicaland ChemicalParameters .*Fujian enviroment,* 2002, 18(3): 30-32.

[5] Yang J Q, Din D W. PreHmznary Study on Artificial Neural Network Method for Predcting Red Tide. Advances in marine science, 2003, 21(3): 318-323.

[6] Tang L B, Liao F Y, Luo J. The applycation of fuzzy neural net work in prediction Stock Price. *Systems Engineering*, 2004, 22(20): 107-109

[7] Wang S T. Fuzzy system fuzzy neural network and application program design. Shanghai: Shanghai Scientific and Technical Literature Publishing House.

基于模糊神经网络（FNN）的赤潮预警预测研究

张 容，阎 红，杜丽萍

（天津职业大学机械学院，天津 300402）

摘 要：为研究各种理化因子与赤潮藻类浓度间的非线性对应规律和有效预测赤潮藻类浓度，构建了基于BP算法的一个四层模糊神经网络模型。将模糊神经网络（FNN）技术引入赤潮预测研究，并与普通BP网络、RBF网络的结果作比较，结果表明，该模型能够较好地反演出各种理化因子与夜光藻密度的非线性对应变化规律，有更好的预测功能。

关键词：赤潮预测；模糊神经网络（FNN）；BP算法

Nontoxic Marine Anti-fouling Coating Containing Capsaicin

SHI Hang (史 航)*, WANG Lumin (王鲁民)

East China Sea Fisheries Research Institute, CAFS, Key and Open Laboratory of Marine and Estuarine Fisheries, Ministry of Agriculture, Shanghai 200090, *China*

Abstract: This paper summarizes a nontoxic Anti-fouling coating utilizing capsaicin as an anti-fouling agent. The capsaicin constituent used in the coating has a rating from about 100 000 to about 1 500 000 Scoville Heat Units. The capsaicin is mixed with a silicon dioxide and then solubilized into a free-flowing homogeneous liquid oleoresin composition by adding a solvent to increase solubility and facilitate mixing. The oleoresin capsaicin liquid solution is mixed with a suitable corrosion resistant epoxy resin, which is then mixed with a hardening catalyst and applied to the surface to be treated.

Keywords: antifouling coating; capsaicin; nontoxic; fishnet; marine fouling organism

Conventional anti-fouling agents used in marine anti-fouling coatings and paints include inorganic heavy-metal compounds such as mercury and copper, and various types of organic and organic-metallic compounds. However, the inorganic metal compounds loose their effectiveness rapidly in the seawater contaminated with hydrogen sulfide. Some of the organic anti-fouling agents are effective for preventing the attachment of only particular marine lives, but are not effective against others. Among the inorganic and organic compounds, there are many which may be effective for preventing the attachment of marine lives, but are not suited for practical use because they are toxic to the human body or other marine life, or will pollute the environment [1].

The antifouling coating containing the capsaicin constituent is nontoxic. The capsaicin is the main biological active ingredient and spicy ingredient in the capsicum. It was separated from the capsicum and named by Thres firstly. It is the vanillyl amine amide derivative and its chemical name is 8-methyl -6-decene vanillyl amine, the molecular formula is $C_{18}H_{27}NO_3$. Its chemical structural formula is H_3CO (HO) -C_6H_3-CH_2-NH-CO- $(CH_2)_4CH$=CHCH $(CH_3)_2$. As one kind of stable alkaloids, the capsaicin is not influenced by change of temperature and is antibacterial and lustrates marine fouling organisms. Furthermore, its superiority is that it does not pollute the environment and damage the natural ecology.

In the medicine domain, the capsaicin has been researched and applied in many aspects. For example, the extract of capsicum (EC) has been used to eliminate ache [2], and the capsaicin can be used

Received on Mar. 21, 2006

* Corresponding author. E-mail: 9yzj@sina.com

to therapy allergy rhinitis and so on [3].

1 Materials and methods

1.1 Experimental materials

In this experiment, the fishnets are made of nylon and copper brackets are used as experimental net materials. The capsaicin constituent used in the coating has a rating from about 100 000 to about 1 500 000 Scoville Heat Units. The capsaicin is mixed with a silicon dioxide and then solubilized into a free-flowing homogeneous liquid oleoresin composition by adding a solvent to increase solubility and facilitate mixing. The oleoresin capsaicin liquid solution is mixed with a suitable corrosion resistant epoxy resin, which is then mixed with a hardening catalyst and applied to the surfaces of the fishnets.

#1: contrast sample

#2: capsaicin antifouling fishnet

1.2 Experimental methods

Antifouling materials are hung in the test maritime space of Zhoushan in Zhejiang province. The depth of antifouling fishnet materials is lower than the sea surface by 2 - 3 meters. Interval distance is about 1.5 meters. Once a month the antifouling fishnet are checked on the degree on covered by fouling organisms, weighed and taken pictures.

2 Results and analysis

2.1 Physical and chemical conditions of the experimental sea area

In the experimental period, we carried out the survey under the seawater temperature and transparency. Fig. 1 is the change of temperature and transparency of the test maritime area.

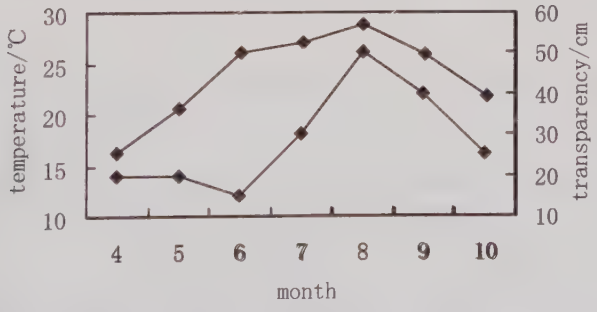

Fig. 1 Change of temperature and transparency in the test sea area

2.1 Main marine fouling organisms

According to the investigation results from April to October, 2002, main marine fouling organisms appear in the test sea area include *Caprella* sp., *Obelia* sp. and *Anthopleura pacifica*. The quantity of other marine fouling organisms is not high. The change of majority variety of antifouling organisms in the test sea area from April to October is shown in Table 1 [4].

Tab. 1 Change of majority variety of antifouling organisms in the test sea area from April to October, 2002

Majority variety	Apr.	May	Jun.	Jul.	Aug.	Sep.	Oct.
Caprella sp.	+	++	++	++	++	+	+
Obelia sp.	+	++	++	+	+	-	-
Anthopleura pacifica	-	-	-	+	++	++	+

Note: -: nil; +: a small amount; ++: prevailing

2.3 The effect of the antifouling fishnet

Once a month the antifouling fishnet is checked for the degree of attachment by fouling organisms, weighed and taken pictures. Fig. 2 is the percentage of the area covered by antifouling organisms during the testing period.

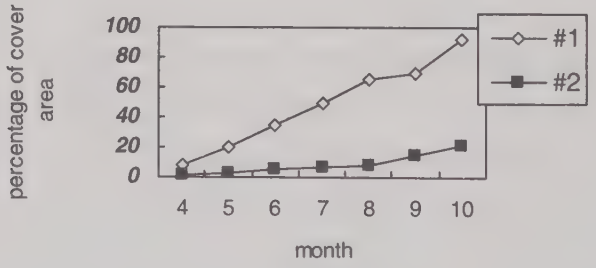

Fig.2 Percentage of the area covered by antifouling organisms during the testing period

Fig. 3 is the photographs of capsaicin antifouling net and contrast sample. #1a and #1b are the photographs of contrast sample hung for 180 d and 210 d respectively. #2a, #2b are the photographs of capsaicin antifouling fishnet of hung for 180 d and 210 d respectively.

Fig. 4 shows the growth in quantity of antifouling net material and contrast sample from April to October.

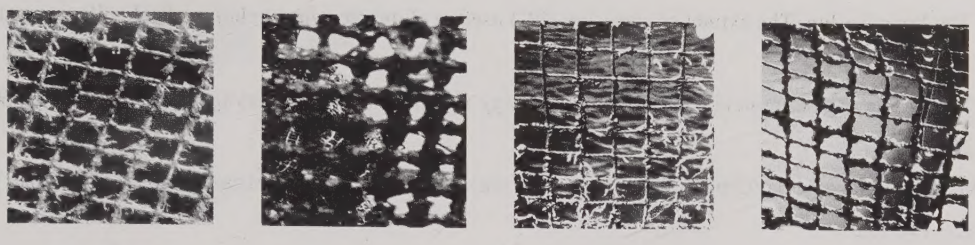

#1a #1b #2a #2b

Fig. 3 Photographs of capsaicin antifouling fishnet and contrast sample

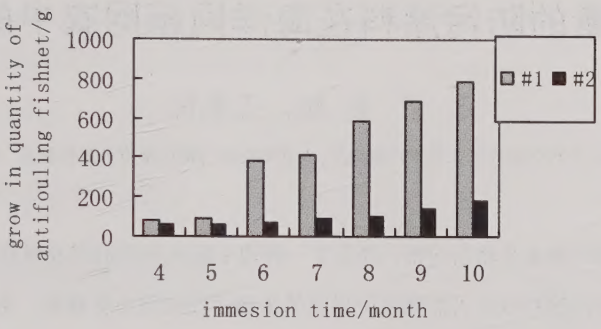

Fig. 4 Growth in quantity of antifouling net material and contrast sample between April and October in 2002

3 Discussions

The disadvantage of conventional anti-fouling agents used in marine anti-fouling coatings and paints is their toxicity to the human body or other marine life, or will pollute the environment. The difference between the capsaicin antifouling coating and the common antifouling coating lies in that the capsaicin is a kind of biological activity matter taken from the natural hot pepper and does not pollute the environment and destroy the marine life chain [5].

Acknowledgements

This work was supported by the National Key Scientific and Technological Project During the Tenth Five-Year Plan (No.2001BA505B0202).

References

[1] Sun Ping. The study on prevent marine fouling organism attachment. Dalian railroad institute journal, 2000, 1(2): 95.

[2] Yin Yong. Li Jun. The extract of capsicum (EC) used to eliminate ache. Anhui medical college journal, 2001, 36 (6): 430-431.

[3] Zhang Fanying. Capsaicin used to therapy allergy rhinitis. Chinese otolaryngology magazine 1999, 34 (4): 23.

[4] Xu Wenjun. Fishnet antifouling compound experiment. Shanghai fisheries university journal, 2003, 12 (2): 190-192

[5] Li Zhaolong. The application about the spicy compound. Chemical new material 1998, 1 (7): 24.

含辣椒素的防污涂料在海洋网箱网衣中的初步研究

史 航，王鲁民

（中国水产科学研究院东海水产研究所，农业部海洋与河口重点开放实验室 上海 200090）

摘 要：以辣椒素为海洋附着生物防污剂，开发了一种用于海水养殖的网衣材料中的防污期长、无毒且高效的防污涂料。辣椒素防污涂料以从天然辣椒中提取的生物活性物质为驱避剂，并不破坏海洋生物链。挂海防污实验证明涂有辣椒素防污涂料的网衣材料具有极佳的防污效果。并进一步讨论了防污涂料的防污效果及影响防污效果的诸多因素。

关键词：防污涂料；辣椒素；无毒；网衣材料；污损生物

海 洋 通 报（英文版）

HAIYANG TONGBAO

2006 年 5 月　第 8 卷　第 1 期

目次

3.0～2.0 MaBP 南海南部深海沉积物孢粉记录及其对全球气候变化的响应 …… 袁金红 等 (10)

黄河三角洲飞雁滩海岸的侵蚀与机理 …… 陈沈良 等 (21)

近岸流系与长江入海悬浮泥沙输移扩散 …… 李四海 等 (33)

甲醛对南美白对虾(*Penaeus vannamei*) β-N-乙酰-D-氨基葡萄糖苷酶的失活动力学研究 …… 谢晓兰 等 (45)

海洋沉积物中反硝化细菌的分离及去除硝酸盐氮的模拟试验 …… 全为民 等 (52)

虾池环境生物修复作用菌的生产发酵与菌体收集工艺优化 …… 李秋芬 等 (60)

利用卫星高度计风速资料研究海面粗糙度 …… 周良明 等 (67)

珠江口水域化学耗氧量(COD)的分布特征 …… 杨美兰 等 (74)

荧光法在赤潮图像分析中的应用 …… 王学民 等 (82)

基于模糊神经网络(FNN)的赤潮预警预测研究 …… 张 容 等 (91)

含辣椒素的防污涂料在海洋网箱网衣中的初步研究 …… 史 航 等 (96)

Marine Science Bulletin

Marine Science Bulletin publishes papers on marine science and technology including physical oceanography, chemical oceanography, marine biology, marine geology, environmental oceanography, estuarine & coastal sciences, marine technology, digital ocean, coastal zone management, ocean engineering, marine economics, etc., and aims to promote international academic exchange.

Editor-in-Chief: LIN Shaohua (林绍花)

Associate Editor-in-Chief: HE Guangshun (何广顺) YANG Ying (杨 鹰)

Executive Editor: LIN Baofa (林宝法) HE Xuewu (何学武) ZHANG Deshan (张德山)
ZHANG Xiaoxian (张潇娴) WANG Zhankun (王占坤)
CHENG Xiuchun (程秀春)

Marine Science Bulletin **(Vol. 8 No. 1 May 2006)**

Responsible Institution:
State Oceanic Administration of China
Edited and Published Semi-annually by:
National Marine Data and Information Service
Address: 93 Liuwei Road, Hedong District, Tianjin 300171, China
E-mail: msb@mail.nmdis.gov.cn

ISSN1000-9620
CN12-1271/N